JOHANNES KEPLER
UNIVERSITÄT LINZ
Netzwerk für Forschung, Lehre und Praxis

# Multigrid Solvers for 3D Multiharmonic Nonlinear Magnetic Field Computations

## Diplomarbeit

zur Erlangung des akademischen Grades

## Diplomingenieur

in der Studienrichtung

## Technische Mathematik

Angefertigt am *Institut für Numerische Mathematik*

Betreuung:

*O.Univ.Prof. Dipl.-Ing. Dr. U. Langer*

Eingereicht von:

*Florian Bachinger*

Linz, Oktober 2003

**Abstract**

This diploma thesis is concerned with the development and analysis of efficient numerical methods for the calculation of induction and eddy currents in electromagnetical problems. These results are important for reducing eddy current losses in electrical machines, for example, or contrariwise for the optimization of eddy current welding.

In both issues, interest is directed rather towards a steady state solution than to some device's response on closure of the electrical circuit. Consequently, it seems natural to analyze the unknown quantities in the frequency domain, what reduces the originally time-dependent problem to a problem in space.

A remarkable feature of eddy current problems is the generally nonlinear relation between magnetic field and induction. Furthermore, the matter of the extremely small penetration depth is worth to be mentioned: The magnetic field and the thereby generated eddy currents hardly penetrate into conducting materials and thus form a small layer of strong induction at the boundaries of this material. This peculiarity leads to difficulties in computations, because the skin depth has to be considered in the discretization.

In addition to some theoretical results – for example on unique solvability and on properties of the solution – we present an efficient solver for general eddy current problems. This solver handles the problem of the boundary layers by adaptive refinement and by an increase of the polynomial degree in the basis functions. The nonlinearity is dealt with by a Newton iteration.

The capacities of our solver are emphasized on the basis of several tests, even including the challenging problem of eddy current welding.

**Zusammenfassung**

Ziel der vorliegenden Diplomarbeit ist die Entwicklung effizienter numerischer Lösungsmethoden zur Berechnung von Induktion und Wirbelströmen in elektromagnetischen Problemstellungen. Diese Resultate werden zum Beispiel benötigt, um in elektrischen Maschinen die Wirbelstromverluste zu reduzieren, oder umgekehrt zur Optimierung des Schweißens durch Wirbelströme.

In beiden Fällen richtet sich das Interesse eher auf eine eingeschwungene Lösung als auf das Ansprechen eines Gerätes auf das Schließen des Stromkreises, weshalb es nahe liegt, die gesuchten Größen im Frequenzbereich zu analysieren. Dadurch wird das ursprünglich zeitabhängige Problem auf ein Problem im Ort übergeführt.

Besonders zu beachten sind bei Wirbelstromproblem zum einen der im allgemeinen nichtlineare Zusammenhang zwischen magnetischer Feldstärke und Induktion und zum anderen die Entstehung von Grenzschichten: Das Magnetfeld und die dadurch erzeugten Wirbelströme dringen in leitfähige Materialien kaum ein, wodurch sich am Rand dieses Materials eine dünne Schicht starker Induktion bildet. In der numerischen Lösung führt dieses Verhalten zu Schwierigkeiten, weil in der Diskretisierung die geringe Eindringtiefe berücksichtigt werden muss.

Neben theoretischen Resultaten – zum Beispiel zur eindeutigen Lösbarkeit und zu Eigenschaften der gesuchten Lösung – wird in dieser Arbeit auch ein effizienter Löser für allgemeine Wirbelstromprobleme präsentiert. Dieser bewältigt das Problem der Grenzschichten durch adaptive Verfeinerung und Erhöhung des Polynomgrads in den Ansatzfunktionen, während die Nichtlinearität durch eine Newton-Iteration behandelt wird.

Die Leistungsfähigkeit des Lösers wird anhand verschiedener Testbeispiele, zum Beispiel auch am anspruchsvollen praktischen Problem des Wirbelstromschweißens, verdeutlicht.

# Acknowledgements

First of all I would like to express my thanks to Prof. Dr. Ulrich Langer for giving me the possibility to work on this fascinating topic and to compose my diploma thesis about this subject.

My special thanks go to Dr. Joachim Schöberl (START project *hp-FEM*) for countless time-intensive discussions and vital hints during the development of this thesis, especially for his patience in answering all the questions that arose. Moreover, I highly appreciate his support concerning implementational details. In this context, I also thank his co-worker Dipl.-Ing. Sabine Zaglmayr for her assistance.

In addition, I would like to mention my colleague Clemens Pechstein, whose support and contributions have been of substantial value.

I also want to acknowledge the cooperation with Dr. Stefan Reitzinger (former co-worker in the FWF-project P14953) and Dr. Manfred Kaltenbacher (University of Erlangen), who originally initiated my work on electromagnetic problems.

Last but not least, I want to thank the Austrian Science Fund "Fonds zur Förderung der wissenschaftlichen Forschung (FWF)" for supporting the work on this diploma thesis under the grant P14953.

# Contents

**1 Introduction** **7**

**2 Problem Formulation and Analysis** **11**
2.1 Problem Description . . . 11
2.2 Vector Potential Formulation . . . 13
2.3 $\nu(|\boldsymbol{B}|)$ and the $\boldsymbol{B}$-$\boldsymbol{H}$-Curve . . . 14
2.4 Existence and Uniqueness . . . 15
2.4.1 Theoretical Background . . . 16
2.4.2 Some Results for Conducting and Non-Conducting Regions . . . 18
2.4.3 Application to Eddy Current Problems . . . 25

**3 Multiharmonic Ansatz** **29**
3.1 Steady State Solution . . . 30
3.2 Existence and Uniqueness . . . 31
3.3 Reduction to Odd Harmonics . . . 33
3.4 The Complex Problem . . . 34
3.4.1 Uniqueness over $\mathbb{C}$ . . . 34
3.4.2 Difficulties because of the Complex Notation . . . 35
3.5 Time Discretization by means of a Multiharmonic Ansatz . . . 37

**4 The Finite Element Method** **39**
4.1 Overview on the Method of Finite Elements . . . 39
4.2 Nédélec Elements for $\boldsymbol{H}(\mathbf{curl})$-Problems . . . 43
4.3 The Linear Problem . . . 44
4.3.1 Mixed Problems . . . 45
4.3.2 The Perturbed Problem . . . 47
4.3.3 Preconditioning . . . 50
4.4 Newton's Method for the Solution of the Nonlinear Problem . . . 53
4.4.1 Introduction . . . 53
4.4.2 The Fréchet Derivative . . . 54

**5 Multigrid** **58**
5.1 Introduction to Multigrid Methods . . . 58
5.1.1 Smoothing Effects of Classical Iterations . . . 58

5.1.2 Idea and Algorithm . . . . . . . . . . 59
5.1.3 Convergence of the Two-Grid Iteration . . . . . . . . . . 61
5.1.4 Convergence of the Multigrid V-Cycle . . . . . . . . . . 62
5.2 A Multigrid Method designed for Problems in $\boldsymbol{H}(\mathbf{curl})$ . . . . . . . . . . 63
5.2.1 Additive and Multiplicative Schwarz Smoothers . . . . . . . . . . 64
5.2.2 Decomposition of the Nédélec FE-Space . . . . . . . . . . 65

**6 Numerical Results** **67**
6.1 A Note on the Penetration Depth . . . . . . . . . . 67
6.2 Remarks Concerning Implementation . . . . . . . . . . 68
6.3 A Shielding Problem . . . . . . . . . . 69
6.4 Eddy Current Welding . . . . . . . . . . 78

**7 Conclusions** **83**

**Bibliography** **85**

# Chapter 1

# Introduction

This thesis deals with mathematical modeling and numerical simulation of electromagnetical problems, with a special focus on eddy current welding. In eddy current welding, a strong periodical magnetic field induces eddy currents in the material to weld. These currents in turn heat up the material and thus cause the process of welding (so the problem we are concerned with can be described as "inductive heating").
Obviously, this can only work if the material to weld is a good conductor, because otherwise the currents induced by the magnetic field would be fairly small and would not be able to raise the temperature by a considerable amount.
In real life application, eddy current welding is generally used to weld ferromagnetic materials such as iron or steel.

The goal of this work is to develop and analyze new efficient numerical methods for calculating the induction and the eddy currents for a realistic problem with given source current in a coil. In our modeling and calculations, we do not consider the thermic field, i.e. the rise of the temperature caused by the eddy currents.

We emphasize that the methods that we develop can of course be employed for the solution of all kinds of eddy current problems, not only for inductive heating problems such as eddy current welding.

**Characteristics of eddy current problems:**

Before going into detail, we would like to remark on some noteworthy features of the problem:
In general, the source is harmonic alternating current, what would imply the solution to be harmonic as well provided the problem was linear. Unfortunately, the magnetic reluctivity depends on the magnetic field in a nonlinear way, so the solution is usually not harmonic. However, both induced magnetic field and eddy currents will still be periodical and can be approximated by a multiharmonic function.

An interesting detail to point out is that the magnetic field does not penetrate very far into the material to weld, but forms a thin layer of strong induction and consequently strong eddy currents. Outside of this skin, both magnetic and electric field will be very small and disappear soon. Note that the penetration depth, i.e. the thickness of this layer, depends on the conductivity and magnetic permeability of the material and on the frequency of the current source. With one of these values increasing, the skin depth decreases and can in practice be as small as $10^{-4}$ meters or even less. That, of course, may cause problems with the discretization for the numerical solution; see below for the way we deal with this issue.

**The mathematical problem:**

Electromagnetic problems are described by Maxwell's equations, a system of partial differential equations relating magnetic (magnetic field and induction) to electric values (electric field, dielectric displacement and electric current density). Since in our case the frequency is fairly small, we can neglect the dielectric displacement. By introducing a vector potential, we simplify the equations further.

We solve the resulting nonlinear, time-dependent partial differential equation in the following way: Taking advantage of the expected periodicity of the solution, we reduce the problem to a space-dependent set of PDEs by applying a multiharmonic ansatz, i.e. by truncated Fourier expansion. This system of nonlinear equations is then solved by linearization, more precisely by Newton's method, where we use finite elements and a multigrid approach for solving the linear problem in each step.

For the finite element discretization and the multigrid algorithm we must be aware of the fact that we deal with a problem in $\boldsymbol{H}(\mathbf{curl})$: Firstly, this problem requires special finite elements (Nédélec elements [35]), and secondly, we will need a smart smoother for the multigrid method to be efficient, either the one proposed by Hiptmair [25] or the smoother by Arnold, Falk and Winther [3, 4].

When discretizing the thin layer of strong induction, the number of finite elements and consequently the size of the linear systems quickly increase. That is why we not only make use of adaptive refinement strategies, but also increase the polynomial degree in the elements. As a consequence, the total number of unknowns stays relatively small while we are able to reach sufficiently good approximation.

A fundamental and recommendable introduction to electromagnetic problems is provided by Ida and Bastos in [18]; they also give an overview on the finite element method in the same book. Other very good introductions to the finite element method can be found e.g. in [9, 11, 29].
Multigrid methods have been widely used for solving the linear systems arising from the finite element discretization. They have been established as among the most efficient solvers for discretized elliptic problems. Hackbusch covers a broad range of the theory in [22]; furthermore he provides a good explanation of the ideas and some applications. Other standard references on multigrid methods are for example [10, 13, 34, 51].

There are many works on the numerical solution of eddy current problems or more generally of electromagnetic problems via the finite element method, e.g. [19, 33, 42], but it has to be mentioned that most of them neglect the nonlinear behavior of the magnetic reluctivity and/or reduce the problem to two dimensions.
The simulation of electromagnetic devices in the frequency domain, i.e. by means of a harmonic or multiharmonic ansatz, has been pursued e.g. by Yamada and Bessho in [54] or Gyselinck et al. in [21]. Other works on this topic include for example [7, 19, 37, 52]. Whereas most of these works consider the problem in complex vector spaces, we propose a real scheme because of the easier linearization: The complex problem is not differentiable and thus cannot be linearized by the Newton method (cf. e.g. [19, 27]).

**The tasks of this thesis:**

Summarizing, the main problems we have to deal with in this thesis are the following:

- The magnetic reluctivity depends on the magnetic field in a nonlinear way.
- Since the source is periodical, the result will be periodical as well.
  However, due to the nonlinearity the result will in general *not* be harmonic, but can be approximated by a multiharmonic function.
- An $\boldsymbol{H}(\mathbf{curl})$-problem requires special finite elements and a particular smoother for the multigrid algorithm.
- For a realistic setup, the penetration depth of the magnetic field is very small. So the mesh for discretization has to meet special requirements.

**The organization of this thesis:**

- Chapter 2:
  We provide Maxwell's equations and introduce a vector potential for simplification. Moreover, some properties of the nonlinear reluctivity are quoted and a proof of existence and uniqueness of eddy current problems is given (with assumptions on the nonlinearity that are a direct consequence of the physical background).
- Chapter 3:
  After proving the existence of a unique periodic steady state solution, we derive some properties of this solution and characteristics of its representation as a Fourier series. Motivated by these results, we apply a multiharmonic ansatz to the original parabolic equation and derive the resulting space-dependent system of equations.

- Chapter 4:
  The principal concepts and results of the finite element method for linear elliptic problems are given, and we briefly remark on the peculiarities of edge elements used for discretizing $\boldsymbol{H}(\mathbf{curl})$-problems. Moreover, we dwell on the features of the linear problem and finally focus on the iterative solution of the nonlinear PDE.

- Chapter 5:
  We present the ideas behind multigrid plus the general algorithm. Some theoretical results are quoted, and eventually we describe the special smoothers that are required for edge element discretization.

- Chapter 6:
  Numerical results for a shielding problem and for a realistic setup for eddy current welding are depicted, including a presentation of the differences between low and high order finite element spaces as well as a comparison of the results with different numbers of harmonics in the multiharmonic ansatz. Moreover, we emphasize the advantages of nested iteration on the basis of several tests.

- Chapter 7:
  The presented models, theories and methods are reviewed and open problems are discussed.

### Notation

Concerning notation, we use boldface type for vectors, vector-valued functions, and spaces of vector-valued functions. Analogously, operators whose values are vector-valued functions are written in bold style as well.
Norm and scalar product in an arbitrary Hilbert space $V$ are denoted by $\|\cdot\|_V$ and $(\cdot,\cdot)_V$, respectively, where the subscript is sometimes omitted when the meaning is unambiguous due to the context.
For the duality product of $F \in V^*$ with $v \in V$ we use the notation $\langle F, v\rangle = \langle F, v\rangle_{V\times V^*}$.

# Chapter 2

# Problem Formulation and Analysis

## 2.1 Problem Description

One possible way of welding uses the effects of eddy currents, where a strong periodical magnetic field induces eddy currents in the material to weld. These currents raise the temperature in the material and thus cause the process of welding. Figure 2.1 shows an example of a setup used in practice, where a slitted tube is welded by the effects of eddy currents.

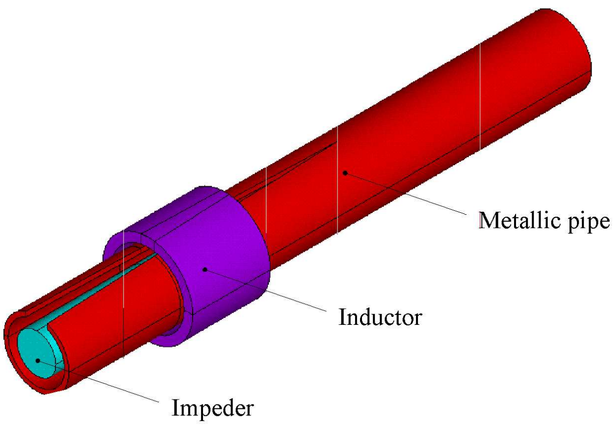


Figure 2.1: Example setup for eddy current welding.

As mentioned before, we disregard the thermic field in this thesis and consider only the problem of calculating the induction and the eddy currents.

For an introduction to electromagnetics and a detailed explanation of the meaning of the various quantities, we refer the reader to [18] or [31], for example.
Electromagnetic problems are described by Maxwell's equations (e.g. [18]) that specify the relations between magnetic field $\boldsymbol{H}$, magnetic flux density (induction) $\boldsymbol{B}$, electric field $\boldsymbol{E}$, electric flux density $\boldsymbol{D}$ and electric current density $\boldsymbol{J}$:

$$
\begin{aligned}
\mathbf{curl}\, \boldsymbol{H} &= \boldsymbol{J} + \frac{\partial \boldsymbol{D}}{\partial t}\,, && (2.1)\\
\mathbf{curl}\, \boldsymbol{E} &= -\frac{\partial \boldsymbol{B}}{\partial t}\,, && (2.2)\\
\operatorname{div} \boldsymbol{B} &= 0\,, && (2.3)\\
\operatorname{div} \boldsymbol{D} &= \rho\,, && (2.4)
\end{aligned}
$$

where $\rho$ is the electric charge density. These equations are joined by the material equations

$$
\begin{aligned}
\boldsymbol{B} &= \mu\, \boldsymbol{H}, && (2.5)\\
\boldsymbol{D} &= \epsilon\, \boldsymbol{E}, && (2.6)\\
\boldsymbol{J} &= \sigma\, \boldsymbol{E}, && (2.7)
\end{aligned}
$$

with the magnetic permeability $\mu$, electric permittivity $\epsilon$ and electric conductivity $\sigma$. Although in general $\mu$, $\epsilon$ and $\sigma$ are tensors, they are scalar in our case, since we consider only isotropic materials.
Note that these coefficients in general do not only depend on the coordinates in space, but also on the magnetic and/or electric field. For instance, the permeability is a function of the magnetic field ($\mu = \mu(|\boldsymbol{H}|)$), since we disregard the effects of hysteresis in this thesis.

We introduce another quantity, the reluctivity $\nu$, as the inverse of the permeability $\mu$. Then with

$$\nu(|\boldsymbol{B}|) = \frac{1}{\mu(|\boldsymbol{H}|)}, \tag{2.8}$$

we have the relation

$$\boldsymbol{H} = \nu(|\boldsymbol{B}|)\boldsymbol{B}. \tag{2.9}$$

Although Maxwell's equations are to be considered in the whole space $\mathbb{R}^3$, on calculations one mostly regards the problem only in a bounded region. Of course then one has to add appropriate boundary conditions.
For the numerical calculation of the eddy current problem that we are concerned with (cf. Figure 2.1), we also restrict the equations to a finite region $\Omega$. In this domain of consideration, we obviously include the iron tube, the impeder and the inductor, but we restrict the surrounding air to a finite box and add the boundary condition

$$\boldsymbol{B} \cdot \boldsymbol{n} = 0, \qquad \text{on } \Gamma = \partial\Omega. \tag{2.10}$$

This approximation to the real situation is justifiable, because both magnetic and electric field decrease very fast in the surrounding air and are almost equal to zero at some distance from the inductor.

## 2.2 Vector Potential Formulation

For the so-called "quasi-stationary" problem that we consider, the frequencies are relatively low. Therefore the displacement current is very small in comparison with the impressed currents and eddy currents, i.e.

$$\left|\frac{\partial \boldsymbol{D}}{\partial t}\right| \ll |\boldsymbol{J}|, \tag{2.11}$$

(cf. e.g. [18], page 44, [33], page 12, [42], page 15) and can thus be neglected.
Since $\boldsymbol{B}$ is divergence-free (see equation (2.3)), we can express this field in terms of a vector potential $\boldsymbol{A}$:

$$\boldsymbol{B} = \mathbf{curl}\,\boldsymbol{A}\,. \tag{2.12}$$

Obviously, $\boldsymbol{A}$ is not unique – any gradient field could be added, because its curl vanishes.
With the material relation (2.9) and the ansatz (2.12), equation (2.1) now reads as

$$\mathbf{curl}\,(\nu(|\mathbf{curl}\,\boldsymbol{A}|)\,\mathbf{curl}\,\boldsymbol{A}) = \boldsymbol{J}, \tag{2.13}$$

where we have neglected the displacement current due to (2.11).

We now consider equation (2.2): With the vector potential (2.12) this equation reads $\mathbf{curl}\,\boldsymbol{E} = -\mathbf{curl}\,\frac{\partial \boldsymbol{A}}{\partial t}$. Consequently the electric field can be expressed as

$$\boldsymbol{E} = -\frac{\partial \boldsymbol{A}}{\partial t} - \nabla\phi\,, \tag{2.14}$$

for some integration constant $\nabla\phi$.
The two terms on the right hand side of (2.14) and their contributions to the currents are treated separately. With Ohm's law (2.7) we get

$$\boldsymbol{J} = \boldsymbol{J}_s + \boldsymbol{J}_e \qquad \text{with} \quad \boldsymbol{J}_s = -\sigma\,\nabla\phi,\ \boldsymbol{J}_e = -\sigma\,\frac{\partial \boldsymbol{A}}{\partial t}, \tag{2.15}$$

where $\boldsymbol{J}_s$ are source and impressed currents and $\boldsymbol{J}_e$ are the eddy currents.
Using this splitting of the current (2.15) in (2.13) yields the following equation:

$$\mathbf{curl}\,(\nu(|\mathbf{curl}\,\boldsymbol{A}|)\,\mathbf{curl}\,\boldsymbol{A}) + \sigma\,\frac{\partial \boldsymbol{A}}{\partial t} = \boldsymbol{J}_s\,. \tag{2.16}$$

(In the following, we will use the letter $\boldsymbol{u}$ for $\boldsymbol{A}$ and $\boldsymbol{f}$ instead of $\boldsymbol{J}_s$.)

So the complete system including homogeneous Dirichlet boundary conditions and an initial condition (formally, i.e. neglecting interface conditions) reads as follows:

$$\begin{aligned}
&\text{Find } \boldsymbol{u}(\boldsymbol{x},t):\\
\sigma\,\frac{\partial \boldsymbol{u}}{\partial t} + \mathbf{curl}\,(\nu(|\mathbf{curl}\,\boldsymbol{u}|)\,\mathbf{curl}\,\boldsymbol{u}) &= \boldsymbol{f}, && \text{in } \Omega\times[0,T],\\
\boldsymbol{u}\times\boldsymbol{n} &= 0, && \text{on } \Gamma\times[0,T],\\
\boldsymbol{u} &= \boldsymbol{u}_0, && \text{on } \Omega\times\{0\}.
\end{aligned} \tag{2.17}$$

Here we suppose that $\Omega \subset \mathbb{R}^3$ be a bounded domain with sufficiently smooth boundary $\Gamma = \partial\Omega$. $\boldsymbol{n}$ denotes the outer unit normal vector to $\Gamma$.
The impressed currents $\boldsymbol{f}$ and the initial condition $\boldsymbol{u}_0$ are given and should both be divergence-free, i.e.

$$\operatorname{div} \boldsymbol{f} = 0 \quad \text{and} \quad \operatorname{div} \boldsymbol{u}_0 = 0.$$

*Remark* 2.1. The impressed currents $\boldsymbol{f}$ are given in the inductor; these are the currents we measure. Thus, $\boldsymbol{f}$ is the sum of currents produced by the applied voltage and those induced by the changing magnetic field in the inductor. (Note that the latter counteract the source current.)
Since the induced currents are already contained in $\boldsymbol{f}$, we assume the conductivity $\sigma$ in the coil to be zero; otherwise we would include these counteracting induced currents in our model twice.

## 2.3 $\nu(|\boldsymbol{B}|)$ and the $\boldsymbol{B}$-$\boldsymbol{H}$-Curve

One of the major tasks that we have to deal with in eddy current problems is the nonlinear relation between $\boldsymbol{B}$ and $\boldsymbol{H}$. In practical applications, this relation is given by a set of discrete data points that provide the connection between $|\boldsymbol{B}|$ and $|\boldsymbol{H}|$, cf. Figure 2.2. These data points are approximated [39] or interpolated [26] (e.g. by splines) to give the $\boldsymbol{B}$-$\boldsymbol{H}$-curve $|\boldsymbol{B}| = f(|\boldsymbol{H}|)$. Disregarding the effects of hysteresis, this curve is strictly monotone.

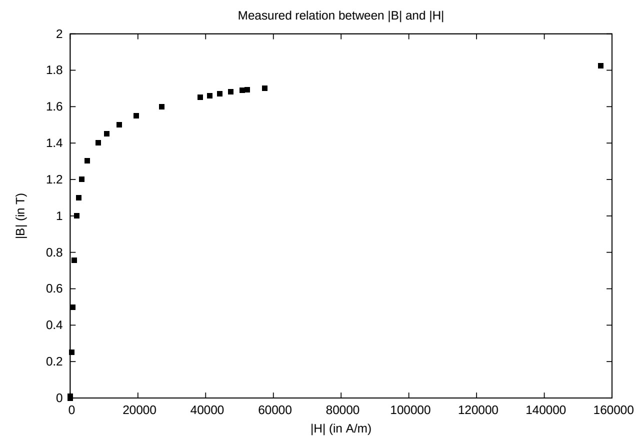


Figure 2.2: Example of measured data points for a $\boldsymbol{B}$-$\boldsymbol{H}$-curve.[1]

Obviously, $\nu$ can easily be calculated once you know the relation $|\boldsymbol{B}| = f(|\boldsymbol{H}|)$:

$$\nu(s) = \frac{f^{-1}(s)}{s}. \tag{2.18}$$

[1]The magnetic field intensity $|\boldsymbol{H}|$ is measured in Ampere/meter, the flux density $|\boldsymbol{B}|$ in Tesla.

Due to the physical background the function $\nu : \mathbb{R}_0^+ \to \mathbb{R}^+$ fulfills certain properties:

$$0 < \underline{\nu} \leq \nu(s) \leq \nu_0, \quad \forall\, s, \qquad (2.19)$$
$$\lim_{s\to\infty} \nu(s) = \nu_0,$$

where $\nu_0$ is the reluctivity in vacuum (cf. [39]).

Note that, since the $\boldsymbol{B}$-$\boldsymbol{H}$-curve is strictly monotone, also its inverse, i.e. the function $s \mapsto \nu(s) \cdot s$ is strictly monotone, what will be important in Section 2.4 to prove existence and uniqueness of a solution.
Furthermore $\nu$ can of course be assumed to be continuous (actually in our approximation, we have even $\nu \in C^1(\mathbb{R}_0^+)$).

For this thesis we use the function shown in Figure 2.3 that was approximated from measured data for iron according to [39]. As the figure clearly shows, the nonlinearity is strongest at a magnetic flux density of approximately 1.5 Tesla; for small and very big inductions $|\boldsymbol{B}|$ the reluctivity $\nu(|\boldsymbol{B}|)$ is almost constant.

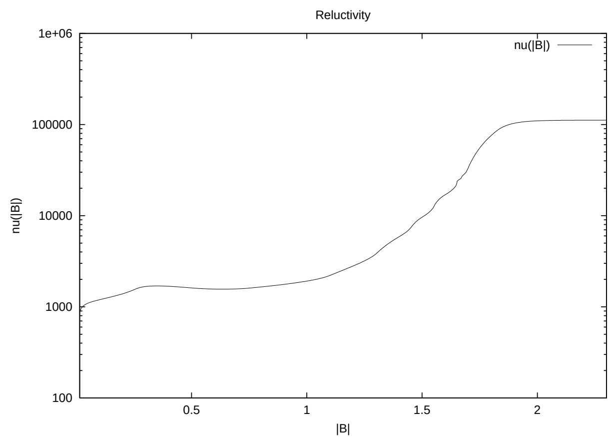


Figure 2.3: Reluctivity $\nu(|\boldsymbol{B}|)$ for a ferromagnetic material.

## 2.4 Existence and Uniqueness

In this section, we want to prove existence of a solution of problem (2.17). Furthermore, we show that the solution is unique in a certain sense.
For analyzing (2.17), we rewrite it in weak formulation and then apply theory of both linear and nonlinear variational equations to it. For this, we will need some basic understanding of Sobolev spaces and of functions mapping into a Banach space. Moreover we will require the notion of integrals and weak derivatives of Banach space valued functions. An introduction to these concepts can be found e.g. in [1, 16, 56, 57].

This section is arranged in three parts: First we quote some theoretical results that will be needed later on, then we show that problem (2.17) is uniquely solvable in both conducting and non-conducting regions. Finally we conclude that the eddy current problem we are concerned with is uniquely solvable.

### 2.4.1 Theoretical Background

Mostly, partial differential equations are treated in some subspace $V$ of the Sobolev space $H^1(\Omega)$. In variational form, a general (homogenized) linear problem reads as follows:

$$\text{Find } u \in V: \; a(u,v) = \langle F, v\rangle, \qquad \forall\, v \in V, \tag{2.20}$$

with some bilinear form $a(\cdot,\cdot)$ and a linear operator $F \in V^*$. Here, $\langle\cdot,\cdot\rangle = \langle\cdot,\cdot\rangle_{V^*\times V}$ denotes the duality product.
Linear elliptic problems are fully analyzed by the following fundamental theorem:

**Theorem 2.1 (Lax-Milgram [16]).** *Let $V$ be a real Hilbert space with scalar product $(\cdot,\cdot)$ and norm $\|\cdot\|$. If the bilinear form $a(\cdot,\cdot): V\times V \to \mathbb{R}$ is*

1. *elliptic, i.e. there is a constant $\mu_1 > 0$ such that*

$$a(v,v) \geq \mu_1 \|v\|^2, \qquad \forall\, v \in V.$$

2. *continuous = bounded, i.e. for some $\mu_2 > 0$ we have*

$$|a(u,v)| \leq \mu_2 \|u\|\|v\|, \qquad \forall\, u,v \in V.$$

*and the linear form $F: V \to \mathbb{R}$ is continuous, i.e. there is a constant $c > 0$ such that*

$$|\langle F, v\rangle| \leq c\|v\|, \qquad \forall\, v \in V,$$

*then there exists a unique $u \in V$ which solves* (2.20).

Let us now turn to the analysis of nonlinear variational problems of the form

$$\text{Find } u \in V: \; \langle A(u), v\rangle = \langle F, v\rangle, \qquad \forall\, v \in V, \tag{2.21}$$

with some operator $A: V \to V^*$.
Before we can quote the main theorem on existence and uniqueness, we need some basic definitions.

**Definition 2.1 ([57]).** Let $V$ be a real Banach space with norm $\|\cdot\|$ and let $A: V \to V^*$ be an operator. Then:

- $A$ is called *monotone* iff

$$\langle A(u) - A(v), u - v\rangle \geq 0, \qquad \forall\, u,v \in V.$$

- $A$ is called *strictly monotone* iff

$$\langle A(u) - A(v), u - v \rangle > 0, \qquad \forall\, u, v \in V,\, u \neq v.$$

- $A$ is called *strongly monotone* iff there is a $c > 0$ such that

$$\langle A(u) - A(v), u - v \rangle > c\, \|u - v\|^2, \qquad \forall\, u, v \in V.$$

- $A$ is called *coercive* iff

$$\lim_{\|u\| \to \infty} \frac{\langle A(u), u \rangle}{\|u\|} = \infty.$$

- $A$ is said to be *hemicontinuous* iff the real function

$$t \mapsto \langle A(u + tv), w \rangle$$

  is continuous on $[0, 1]$ for all $u, v, w \in V$.

**Theorem 2.2 (Browder-Minty [57]).** *Let $A : V \to V^*$ be a monotone, coercive and hemicontinuous operator on the real, reflexive Banach space $V$. Then the following assertions hold:*

1. *For each $F \in V^*$, the equation* (2.21) *has a solution. The solution set of* (2.21) *is bounded, convex and closed.*
2. *If in addition $A$ is strictly monotone, then equation* (2.21) *is uniquely solvable in $V$.*

In order to obtain existence theorems for parabolic differential equations, we will need the notion of an *evolution triple* and the concept of Banach space valued functions. The latter is required because we think of a function $(\boldsymbol{x}, t) \mapsto \boldsymbol{u}(\boldsymbol{x}, t)$ as a function from a time interval to a Banach space, i.e. $t \mapsto (\boldsymbol{x} \mapsto \boldsymbol{u}(\boldsymbol{x}, t))$. In our context, the spaces $L_2((0, T), V)$ and $L_2((0, T), V^*)$ (for some Banach space $V$) are sufficient. (See e.g. [56, 57]).

In the following, we want to analyze (nonlinear) initial value problems of the form

$$u'(t) + A(u(t)) = b(t), \quad \text{for almost all } t \in (0, T), \tag{2.22a}$$

$$u(0) = u_0 \in H, \tag{2.22b}$$

$$u \in L_2((0, T), V),\ u' \in L_2((0, T), V^*), \tag{2.22c}$$

with the (possibly nonlinear) operator $A : V \to V^*$. We suppose furthermore that for each $t \in (0, T)$, we have $b(t) \in V^*$.
The initial condition (2.22b) is meaningful, because the embedding $\{u \in L_2((0, T), V) : u' \in L_2((0, T), V^*)\} \subset C([0, T], H)\}$ is continuous if $V \subset H \subset V^*$ is an evolution triple as defined below, cf. [56].

**Definition 2.2 ([56]).** We understand an *evolution triple*

$$V \subset H \subset V^*$$

to be the following:

1. $V$ is a real, separable and reflexive Banach space.
2. $H$ is a real, separable Hilbert space.
3. The embedding $V \subset H$ is continuous, i.e.

$$\|v\|_H \leq \text{const}\, \|v\|_V, \qquad \forall\, v \in V,$$

   and $V$ is dense in $H$.

We can now state the main theorem on existence and uniqueness of nonlinear parabolic problems:

**Theorem 2.3 ([57]).** *Let $V \subset H \subset V^*$ be an evolution triple and let $A : V \to V^*$ be a hemicontinuous, monotone and coercive operator. Suppose furthermore that $A$ is bounded, i.e.*

$$\exists\, c > 0 : \; \|A(\boldsymbol{u})\|_{V^*} \leq c\|\boldsymbol{u}\|_V, \qquad \forall\, \boldsymbol{u} \in V.$$

*Let $u_0 \in H$ and $b \in L_2((0,T), V^*)$ (with $0 < T < \infty$) be given.*
*Then the initial value problem* (2.22) *has a unique solution.*

### 2.4.2 Some Results for Conducting and Non-Conducting Regions

In electromagnetic problems, one often deals with conducting ($\sigma > 0$) and non-conducting ($\sigma = 0$) regions, for example in the case of some conducting part surrounded by air. The problem that we consider has a significantly different structure in these two cases. For non-conducting regions, equation (2.17) is a stationary and elliptic problem:

$$\begin{aligned} &\text{Find } \boldsymbol{u}(\boldsymbol{x}) : \\ \mathbf{curl}\,(\nu\, \mathbf{curl}\, \boldsymbol{u}) &= \boldsymbol{f}, && \text{in } \Omega, \\ \boldsymbol{u} \times \boldsymbol{n} &= \boldsymbol{g}, && \text{on } \Gamma. \end{aligned} \tag{2.23}$$

For conductors, on the other hand, we face a parabolic problem:

$$\begin{aligned} &\text{Find } \boldsymbol{u}(\boldsymbol{x}, t) : \\ \sigma \frac{\partial \boldsymbol{u}}{\partial t} + \mathbf{curl}\,(\nu\, \mathbf{curl}\, \boldsymbol{u}) &= \boldsymbol{f}, && \text{in } \Omega \times [0,T], \\ \boldsymbol{u} \times \boldsymbol{n} &= \boldsymbol{g}, && \text{on } \Gamma \times [0,T], \\ \boldsymbol{u} &= \boldsymbol{u}_0, && \text{on } \Omega \times \{0\}. \end{aligned} \tag{2.24}$$

In general, the relation between the magnetic field $\boldsymbol{H}$ and the induction $\boldsymbol{B}$ could be nonlinear in both conducting and non-conducting regions. In our case, however, for the non-conducting part, i.e. in the inductor[2], the impeder and the surrounding air, we have a linear relation between $\boldsymbol{B}$ and $\boldsymbol{H}$, so there $\nu = \nu(\boldsymbol{x})$.
In the conducting region, i.e. in the iron tube, $\nu(|\mathbf{curl}\,\boldsymbol{u}|)$ is given by the $\boldsymbol{B}$-$\boldsymbol{H}$-curve, cf. Section 2.3.

We will now prove that both problems are solvable and that the solution is unique in a certain sense. For this task, we consider the weak formulation of these equations.

### Non-Conducting Regions

Let us start out with further analysis of the problem in the non-conducting area:
The weak formulation of (2.23) yields the variational equation

$$\underbrace{\int_\Omega \nu\,\mathbf{curl}\,\boldsymbol{u}\cdot\mathbf{curl}\,\boldsymbol{v}\,\mathrm{d}\boldsymbol{x}}_{=:a(\boldsymbol{u},\boldsymbol{v})} = \underbrace{\int_\Omega \boldsymbol{f}\,\boldsymbol{v}\,\mathrm{d}\boldsymbol{x}}_{=:\langle F,\boldsymbol{v}\rangle}, \qquad \forall\,\boldsymbol{v}\in\boldsymbol{V}, \tag{2.25}$$

with $\boldsymbol{V} = \boldsymbol{H}_0(\mathbf{curl},\Omega) = \{\boldsymbol{v}\in\boldsymbol{H}(\mathbf{curl},\Omega) : \boldsymbol{v}\times\boldsymbol{n} = 0 \text{ on } \Gamma\}$.
We are looking for a solution $\boldsymbol{u}$ in the linear manifold $\tilde{\boldsymbol{g}}+\boldsymbol{V}$, where $\tilde{\boldsymbol{g}}\in\boldsymbol{H}(\mathbf{curl})$ should meet the boundary condition $\tilde{\boldsymbol{g}}\times\boldsymbol{n} = \boldsymbol{g}$ on $\Gamma$. Of course, we can homogenize the problem, what leads to

$$\text{Find } \boldsymbol{u}\in\boldsymbol{V}: \quad a(\boldsymbol{u},\boldsymbol{v}) = \langle\tilde{F},\boldsymbol{v}\rangle, \qquad \forall\,\boldsymbol{v}\in\boldsymbol{V}, \tag{2.26}$$

with $\langle\tilde{F},\boldsymbol{v}\rangle := \langle F,\boldsymbol{v}\rangle - a(\tilde{\boldsymbol{g}},\boldsymbol{v})$. The linear form $F\in\boldsymbol{V}^*$ and the bilinear form $a(\cdot,\cdot):\boldsymbol{H}(\mathbf{curl})\times\boldsymbol{H}(\mathbf{curl})\to\mathbb{R}$ are those defined in (2.25).

For gradient fields $\boldsymbol{v}$, the left hand side of (2.25) = (2.26) equals zero, so clearly the sources $\boldsymbol{f}$ have to be weakly divergence-free in order to ensure solvability. This means $\int_\Omega \boldsymbol{f}\cdot\mathbf{grad}\,\phi\,\mathrm{d}\boldsymbol{x} = 0$, for all $\phi\in H_0^1(\Omega)$, is a necessary condition for existence of a solution.

*Remark* 2.2. Later on, we will consider only divergence-free test functions. With this reduced set of test functions, *no additional conditions for solvability* are required, since the space $\boldsymbol{V}$ then does not contain any gradient fields.
The following considerations will motivate this reduction to solenoidal functions:

Since the curl of a gradient field vanishes, we can add $\mathbf{grad}\,\phi$ (for arbitrary $\phi\in H_0^1(\Omega)$) to $\boldsymbol{u}$ in (2.26) without changing anything:

$$\int_\Omega \nu\,\mathbf{curl}\,\boldsymbol{u}\cdot\mathbf{curl}\,\boldsymbol{v}\;\mathrm{d}\boldsymbol{x} = \int_\Omega \nu\,\mathbf{curl}\,(\boldsymbol{u}+\mathbf{grad}\,\phi)\cdot\mathbf{curl}\,\boldsymbol{v}\;\mathrm{d}\boldsymbol{x}. \tag{2.27}$$

Consequently, the problem is not uniquely solvable; however, we can hope to find a unique divergence-free, i.e. solenoidal solution. As we will see, this is actually the case.

[2]See Remark 2.1 for the reason why we assume the inductor to have zero conductivity.

In general, the domain $\Omega$ can be multiply connected[3], and in that case, we can add an even larger set of gradient fields without changing the equation.
For multiply connected domains, we denote the $p \geq 1$ components of the boundary $\partial\Omega$ by $\Gamma_i$, $1 \leq i \leq p$. In this general case, the equality (2.27) still holds for arbitrary $\phi \in H^1(\Omega)$ with $\phi$ constant on each boundary component, i.e. $\phi = c_i$ on $\Gamma_i$, $1 \leq i \leq p$. This gives rise to the definition

$$\boldsymbol{W}(\Omega) := \boldsymbol{W} := \{\boldsymbol{w} = \mathbf{grad}\,\phi : \phi \in H^1(\Omega) \text{ and } \phi = c_i \text{ on } \Gamma_i,\ 1 \leq i \leq p\}. \tag{2.28}$$

Since each solution $\boldsymbol{u}$ of problem (2.26) yields a set of solutions $\boldsymbol{u} + \boldsymbol{W}$, we factor the space $\boldsymbol{V}$ by $\boldsymbol{W}$ for proving uniqueness, and restrict equation (2.26) to this factor space

$$\bar{\boldsymbol{V}} := \boldsymbol{V}/\boldsymbol{W} \simeq \{\boldsymbol{v} \in \boldsymbol{V} : (\boldsymbol{v}, \boldsymbol{w})_{L_2} = 0,\ \forall\, \boldsymbol{w} \in \boldsymbol{W}\}. \tag{2.29}$$

So the problem that we deal with now reads as follows:

$$\text{Find } \boldsymbol{u} \in \bar{\boldsymbol{V}} : \quad a(\boldsymbol{u}, \boldsymbol{v}) = \langle \tilde{F}, \boldsymbol{v} \rangle, \qquad \forall\, \boldsymbol{v} \in \bar{\boldsymbol{V}}. \tag{2.30}$$

We will see that this variational equation is uniquely solvable by the Lax-Milgram theorem (Thm. 2.1). For proving existence and uniqueness, we need an important result on norm equivalence in the space $\boldsymbol{H}(\mathbf{curl}, \Omega) \cap \boldsymbol{H}(\mathrm{div}, \Omega)$ for multiply connected domains $\Omega$.

**Lemma 2.4 ([2]).** *Let $\Omega$ be multiply connected with Lipschitz boundary and boundary components $\Gamma_i$, $1 \leq i \leq p$, let $X(\Omega) := \boldsymbol{H}(\mathbf{curl}, \Omega) \cap \boldsymbol{H}(\mathrm{div}, \Omega)$ with the norm $\|\boldsymbol{v}\|^2_{X(\Omega)} = \|\boldsymbol{v}\|^2_{\boldsymbol{L}_2(\Omega)} + \|\mathbf{curl}\,\boldsymbol{v}\|^2_{\boldsymbol{L}_2(\Omega)} + \|\mathrm{div}\,\boldsymbol{v}\|^2_{L_2(\Omega)}$.*
*Then on the space $X_N(\Omega) = \{\boldsymbol{v} \in X(\Omega) : \boldsymbol{v} \times \boldsymbol{n} = 0 \text{ on } \partial\Omega\}$, the seminorm*

$$\boldsymbol{v} \mapsto \|\mathbf{curl}\,\boldsymbol{v}\|_{\boldsymbol{L}_2(\Omega)} + \|\mathrm{div}\,\boldsymbol{v}\|_{L_2(\Omega)} + \sum_{i=1}^{p} |\langle \boldsymbol{v} \cdot \boldsymbol{n}, 1 \rangle_{\Gamma_i}|$$

*is equivalent to the norm $\|\cdot\|_{X(\Omega)}$.*

*Remark* 2.3. As can easily be seen, in $\bar{\boldsymbol{V}}$ we have that both $\mathrm{div}\,\boldsymbol{v}$ in the domain and $\boldsymbol{v} \cdot \boldsymbol{n}$ on each boundary component are zero: By the definition of $\bar{\boldsymbol{V}} = \boldsymbol{V}/\boldsymbol{W}$, we have $\int_\Omega \boldsymbol{v} \cdot \mathbf{grad}\,\phi \,\mathrm{d}\boldsymbol{x} = 0$ for all functions $\phi \in H^1(\Omega)$ that are constant on all components of the boundary. Integration by parts yields

$$-\int_\Omega \mathrm{div}\,\boldsymbol{v} \cdot \phi \,\mathrm{d}\boldsymbol{x} + \sum_i c_i(\phi) \int_{\Gamma_i} \boldsymbol{v} \cdot \boldsymbol{n} \,\mathrm{ds} = 0.$$

Since this equality is satisfied for all $\phi \in H^1_0(\Omega)$, $\mathrm{div}\,\boldsymbol{v}$ equals zero almost everywhere, and thus also $\boldsymbol{v} \cdot \boldsymbol{n}$ on each boundary component.

[3]In our problem, for example, we face a multiply connected non-conducting domain, since we consider the whole region of air, inductor and impeder without the iron tube. (Cf. Figure 2.1)

Consequently, Lemma 2.4 provides

$$\|\boldsymbol{v}\|_{\boldsymbol{L}_2} \leq c \cdot \|\mathbf{curl}\, \boldsymbol{v}\|_{\boldsymbol{L}_2} \text{ on } \bar{\boldsymbol{V}},$$

and thus the much-needed equivalence between the full $\boldsymbol{H}(\mathbf{curl})$-norm and the semi-norm $|\boldsymbol{u}|^2 = \int_\Omega |\mathbf{curl}\, \boldsymbol{u}|^2$.

**Lemma 2.5.** *For $\nu \in L_\infty(\Omega)$ with $0 < \underline{\nu} \leq \nu(\boldsymbol{x}) \leq \overline{\nu}$ almost everywhere (a.e.) in $\Omega$, there is a unique $\boldsymbol{u} \in \bar{\boldsymbol{V}}$ which solves*

$$a(\boldsymbol{u}, \boldsymbol{v}) = \langle \tilde{F}, \boldsymbol{v} \rangle, \qquad \forall\, \boldsymbol{v} \in \bar{\boldsymbol{V}}. \tag{2.30}$$

*Proof.* By Thm. 2.1, it suffices to show that $a(\cdot,\cdot)$ is bilinear, $\bar{\boldsymbol{V}}$-elliptic and $\bar{\boldsymbol{V}}$-continuous and that $\tilde{F} \in \bar{\boldsymbol{V}}^*$.
Bilinearity is obvious, the same with linearity of $\tilde{F}$. $\bar{\boldsymbol{V}}$-ellipticity and $\bar{\boldsymbol{V}}$-continuity of $a(\cdot,\cdot)$ follow immediately from the assumptions on $\nu$ and the norm equivalence stated in Lemma 2.4 and Remark 2.3. This norm equivalence also implies boundedness of $\tilde{F}$. $\square$

*Remark* 2.4. Problem (2.30) is uniquely solvable for nonlinear reluctivity $\nu = \nu(|\mathbf{curl}\, \boldsymbol{u}|)$ as well, if $\nu$ fulfills certain assumptions. For example, $s \mapsto \nu(s)s$ being strictly monotone and $0 < \underline{\nu} \leq \nu(s) \leq \overline{\nu}$, $\forall\, s$ suffices for proving existence and uniqueness by Browder's and Minty's theorem (Thm. 2.2).

### Conducting Regions

We continue by analyzing the parabolic problem in the conducting area:
The weak formulation of (2.24) yields the variational equation

$$\int_\Omega \sigma \frac{\partial \boldsymbol{u}}{\partial t} \boldsymbol{v} + \underbrace{\int_\Omega \nu(|\mathbf{curl}\, \boldsymbol{u}|)\, \mathbf{curl}\, \boldsymbol{u} \cdot \mathbf{curl}\, \boldsymbol{v}}_{=:\langle A(\boldsymbol{u}), \boldsymbol{v}\rangle} = \underbrace{\int_\Omega \boldsymbol{f}\, \boldsymbol{v}}_{=:\langle F, \boldsymbol{v}\rangle}, \qquad \forall\, \boldsymbol{v} \in \boldsymbol{V}, \tag{2.31}$$

almost everywhere in $(0, T)$, with $\boldsymbol{V} = \boldsymbol{H}_0(\mathbf{curl}, \Omega) = \{\boldsymbol{v} \in \boldsymbol{H}(\mathbf{curl}, \Omega) : \boldsymbol{v} \times \boldsymbol{n} = 0 \text{ on } \Gamma\}$ as above.

The main differences between this problem and the one considered in the part on non-conducting regions are the following:

1. The nonlinear reluctivity entails a nonlinear operator $A : \boldsymbol{V} \to \boldsymbol{V}^*$.
2. Due to the time-dependence, we will embark on a slightly different strategy for our proof.

However, the first steps are the same, that is we homogenize the problem as before. Furthermore, we also restrict our equation to the factor space $\bar{\boldsymbol{V}}$ as defined in (2.29), at least at first. Later on, we will see that we get a unique solution in $\boldsymbol{V} = \boldsymbol{H}_0(\mathbf{curl})$, not only in $\bar{\boldsymbol{V}}$.

So almost everywhere in $(0,T)$ the problem we are concerned with reads as follows:

$$\text{Find } \boldsymbol{u} \in \bar{\boldsymbol{V}}: \quad (\sigma \frac{\partial \boldsymbol{u}}{\partial t}, \boldsymbol{v})_{L_2} + \langle A(\boldsymbol{u}), \boldsymbol{v}\rangle = \langle \tilde{F}, \boldsymbol{v}\rangle, \qquad \forall\, \boldsymbol{v} \in \bar{\boldsymbol{V}}. \tag{2.32}$$

Here, $A : \bar{\boldsymbol{V}} \to \bar{\boldsymbol{V}}^*$ is the operator defined in (2.31), and $\tilde{F}$ results from the homogenization: If we have $\tilde{\boldsymbol{g}}(t)$ fulfilling the boundary conditions, we get $\langle \tilde{F}, \boldsymbol{v}\rangle := \langle F, \boldsymbol{v}\rangle - (\sigma \frac{\partial \tilde{\boldsymbol{g}}}{\partial t}, \boldsymbol{v})_{L_2} - \langle A(\tilde{\boldsymbol{g}}), \boldsymbol{v}\rangle$ with $F$ as in (2.31).

All this was for a fixed moment in time $t$. Let us now consider $\boldsymbol{u}$ as a function $\boldsymbol{u} : [0,T] \to \bar{\boldsymbol{V}}, t \mapsto \boldsymbol{u}(\cdot,t)$ and define the operators $\bar{A} : L_2((0,T), \bar{\boldsymbol{V}}) \to L_2((0,T), \bar{\boldsymbol{V}}^*)$ and $\bar{F} \in L_2((0,T), \bar{\boldsymbol{V}}^*)$ as follows:

$$\begin{aligned}
\langle \bar{A}(\boldsymbol{u})(t), \boldsymbol{v}\rangle &:= \int_\Omega \nu(|\mathbf{curl}\,\boldsymbol{u}(t)|)\,\mathbf{curl}\,\boldsymbol{u}(t) \cdot \mathbf{curl}\,\boldsymbol{v}\ \mathrm{d}\boldsymbol{x}, \\
&\qquad\qquad \forall\, \boldsymbol{v} \in \bar{\boldsymbol{V}},\ \boldsymbol{u} \in L_2((0,T), \bar{\boldsymbol{V}}), \qquad (2.33) \\
\langle \bar{F}(t), \boldsymbol{v}\rangle &:= \int_\Omega \boldsymbol{f}(t) \cdot \boldsymbol{v}\ \mathrm{d}\boldsymbol{x} - \int_\Omega \sigma \frac{\partial \tilde{\boldsymbol{g}}(t)}{\partial t} \cdot \boldsymbol{v}\ \mathrm{d}\boldsymbol{x} - \langle \bar{A}(\tilde{\boldsymbol{g}})(t), \boldsymbol{v}\rangle, \\
&\qquad\qquad \forall\, \boldsymbol{v} \in \bar{\boldsymbol{V}}. \qquad (2.34)
\end{aligned}$$

Here we require $\tilde{\boldsymbol{g}} \in L_2((0,T), \boldsymbol{H}(\mathbf{curl}))$ with $\frac{\partial \tilde{\boldsymbol{g}}}{\partial t} \in L_2((0,T), \boldsymbol{H}(\mathbf{curl})^*)$ for the definition of $\bar{F}$. This prerequisite is met by any reasonable function $\boldsymbol{g}(t)$ in the boundary condition, e.g. for $\boldsymbol{g} \in L_2((0,T), \boldsymbol{H}^{\frac{1}{2}}(\Gamma))$ with $\frac{\partial \boldsymbol{g}}{\partial t} \in L_2((0,T), \boldsymbol{H}^{\frac{1}{2}}(\Gamma))$.

With the above definitions, equation (2.32) together with the initial condition $\boldsymbol{u}(\boldsymbol{x},0) = \boldsymbol{u}_0(\boldsymbol{x})$, i.e. the original equation (2.24) in its weak formulation, can be written as an operator equation in $L_2((0,T), \bar{\boldsymbol{V}}^*)$:

Find $\boldsymbol{u} \in L_2((0,T), \bar{\boldsymbol{V}})$ with $\dot{\boldsymbol{u}} \in L_2((0,T), \bar{\boldsymbol{V}}^*)$ such that

$$\sigma\,\dot{\boldsymbol{u}} + \bar{A}(\boldsymbol{u}) = \bar{F}, \tag{2.35a}$$

$$\boldsymbol{u}(0) = \boldsymbol{u}_0, \tag{2.35b}$$

with $\boldsymbol{u}_0 \in \boldsymbol{L}_2(\Omega)$.
Note that the initial condition (2.35b) is meaningful, because the Banach space valued functions $\{\boldsymbol{u} \in L_2((0,T), \bar{\boldsymbol{V}}) : \dot{\boldsymbol{u}} \in L_2((0,T), \bar{\boldsymbol{V}}^*)\}$ can be continuously embedded into $C([0,T], L_2(\Omega))$, see [56].

We will see that the operator equation (2.35) is uniquely solvable by Zeidler's theorem on nonlinear monotone operators in parabolic equations (Thm. 2.3), as we state in the following lemma.

**Lemma 2.6.** *Let $s \mapsto \nu(s)$ be continuous, $0 < \underline{\nu} \leq \nu(s) \leq \overline{\nu}$, $\forall\, s \in \mathbb{R}_0^+$ and let the function $s \mapsto \nu(s)s$ be monotone.*
*Let moreover $\boldsymbol{u}_0 \in \boldsymbol{L}_2(\Omega)$, $\boldsymbol{f} \in L_2((0,T), \bar{\boldsymbol{V}}^*)$ and $\tilde{\boldsymbol{g}} \in L_2((0,T), \boldsymbol{H}(\mathbf{curl}))$ with $\frac{\partial \tilde{\boldsymbol{g}}}{\partial t} \in L_2((0,T), \boldsymbol{H}(\mathbf{curl})^*)$ be given, and suppose $\sigma \in L_\infty$ to be strictly positive.*
*Then we have a unique $\boldsymbol{u} \in L_2((0,T), \bar{\boldsymbol{V}})$ with $\dot{\boldsymbol{u}} \in L_2((0,T), \bar{\boldsymbol{V}}^*)$ which solves* (2.35), *i.e.*

$$\begin{aligned} \sigma\, \dot{\boldsymbol{u}} + \bar{A}(\boldsymbol{u}) &= \bar{F}, \\ \boldsymbol{u}(0) &= \boldsymbol{u}_0. \end{aligned}$$

*Proof.* We show that the assumptions of Thm. 2.3 are fulfilled:

- *Evolution triple.* $\bar{\boldsymbol{V}} \subset \boldsymbol{L}_2 \subset \bar{\boldsymbol{V}}^*$ is obvious. Clearly, $\bar{\boldsymbol{V}}$ is separable and reflexive, the embedding $\bar{\boldsymbol{V}} \subset \boldsymbol{L}_2$ is continuous and $\bar{\boldsymbol{V}}$ is dense in $\boldsymbol{L}_2$.

- *Monotonicity.* As can easily be seen, the operator $A : \bar{\boldsymbol{V}} \to \bar{\boldsymbol{V}}^*$ as defined in (2.31), i.e. $\langle A(\boldsymbol{u}), \boldsymbol{v}\rangle = \int_\Omega \nu(|\mathbf{curl}\,\boldsymbol{u}|)\,\mathbf{curl}\,\boldsymbol{u} \cdot \mathbf{curl}\,\boldsymbol{v}$, is monotone: The function $s \mapsto \nu(s)s$ being monotone implies

$$\langle A(\boldsymbol{u}) - A(\boldsymbol{v}), \boldsymbol{u} - \boldsymbol{v}\rangle \geq 0, \qquad \forall\, \boldsymbol{u}, \boldsymbol{v} \in \bar{\boldsymbol{V}}.$$

- *Coerciveness.* The norm equivalence in $\bar{\boldsymbol{V}}$ (Lemma 2.4) and the fact that $\nu$ is strictly positive bring about coerciveness of $A$, more precisely there is $c > 0$ such that

$$\langle A(\boldsymbol{u}), \boldsymbol{u}\rangle \geq c\, \|\boldsymbol{u}\|_{\bar{\boldsymbol{V}}}^2, \qquad \forall\, \boldsymbol{u} \in \bar{\boldsymbol{V}}.$$

- *Boundedness.* Since $\nu$ is bounded from above and because of the norm equivalence (Lemma 2.4), we have

$$\exists\, c > 0 : \ \|A(\boldsymbol{u})\|_{\bar{\boldsymbol{V}}^*} \leq c\, \|\boldsymbol{u}\|_{\bar{\boldsymbol{V}}}, \qquad \forall\, \boldsymbol{u} \in \bar{\boldsymbol{V}}.$$

Furthermore, $A$ is continuous, and the given data also meets the prerequisites of Thm. 2.3. Consequently, we have a unique solution $\boldsymbol{u} \in \bar{\boldsymbol{V}}$ of problem (2.35). ☐

**Uniqueness in $\boldsymbol{H}_0(\mathbf{curl})$:** Our next issue is to show that under certain assumptions the solution given by Lemma 2.6 is unique in the whole space $\boldsymbol{V} = \boldsymbol{H}_0(\mathbf{curl})$. For this task we consider equation (2.35) with an arbitrary test function $\boldsymbol{w} \in \boldsymbol{W}$:

$$\begin{aligned} &\int_\Omega \sigma\, \frac{\partial \boldsymbol{u}}{\partial t}\, \boldsymbol{w} + \int_\Omega \nu(|\mathbf{curl}\,\boldsymbol{u}|)\,\mathbf{curl}\,\boldsymbol{u} \cdot \mathbf{curl}\,\boldsymbol{w} \\ &\qquad = \int_\Omega \boldsymbol{f}\, \boldsymbol{w} - \int_\Omega \sigma\, \frac{\partial \tilde{\boldsymbol{g}}}{\partial t}\, \boldsymbol{w} - \int_\Omega \nu(|\mathbf{curl}\,\tilde{\boldsymbol{g}}|)\,\mathbf{curl}\,\boldsymbol{u} \cdot \mathbf{curl}\,\boldsymbol{w}. \end{aligned} \tag{2.36}$$

Suppose now, that $\boldsymbol{f}(t)$ is divergence-free for all $t$, i.e.

$$\int_\Omega \boldsymbol{f}(t)\cdot\boldsymbol{w} = 0, \qquad \forall\, t\in[0,T],\ \forall\,\boldsymbol{w}\in\boldsymbol{W},$$

where $\boldsymbol{W} = \{\boldsymbol{w} = \mathbf{grad}\,\phi : \phi \in H^1(\Omega) \text{ and } \phi = c_i \text{ on } \Gamma_i,\ 1\le i\le p\}$ as defined in (2.28). Assume moreover that the same holds for $\sigma\frac{\partial\tilde{\boldsymbol{g}}}{\partial t}(t)$. Then the right hand side in (2.36) equals zero, what implies

$$\int_\Omega \sigma\,\frac{\partial\boldsymbol{u}}{\partial t}\,\boldsymbol{w} = 0, \qquad \forall\,\boldsymbol{w}\in\boldsymbol{W}, \tag{2.37}$$

since the curl of a gradient field $\boldsymbol{w}\in\boldsymbol{W}$ vanishes.
In other words, for constant conductivity $\sigma$, the time derivative of the function we are looking for is divergence-free for all moments in time. This means that – provided the initial solution $\boldsymbol{u}_0$ is solenoidal as well – all possible solutions $\boldsymbol{u}(t)$ are divergence-free and thus lie in $\bar{\boldsymbol{V}}$, where we have already shown existence and uniqueness in Lemma 2.6.
We summarize these ideas in the following lemma:

**Lemma 2.7.** *Suppose that the functions $\boldsymbol{f}(t)$ and $\sigma\frac{\partial\tilde{\boldsymbol{g}}}{\partial t}(t)$ are defined for all $t\in[0,T]$ and divergence-free in the following weak sense:*

$$\begin{aligned}\int_\Omega \boldsymbol{f}(t)\cdot\boldsymbol{w} &= 0, \qquad \forall\, t\in[0,T],\ \forall\,\boldsymbol{w}\in\boldsymbol{W},\\ \int_\Omega \sigma\frac{\partial\tilde{\boldsymbol{g}}}{\partial t}(t)\cdot\boldsymbol{w} &= 0, \qquad \forall\, t\in[0,T],\ \forall\,\boldsymbol{w}\in\boldsymbol{W}.\end{aligned}$$

*Assume moreover that $\sigma\boldsymbol{u}_0$ is divergence-free as well, i.e.*

$$\int_\Omega \sigma\boldsymbol{u}_0\cdot\boldsymbol{w} = 0, \qquad \forall\,\boldsymbol{w}\in\boldsymbol{W}.$$

*Then, if there is a solution $\boldsymbol{u}$ of* (2.35) *that is defined for all $t$, we have*

$$\int_\Omega \sigma\,\boldsymbol{u}(t)\cdot\boldsymbol{w} = 0, \qquad \forall\, t\in[0,T],\ \forall\,\boldsymbol{w}\in\boldsymbol{W}.$$

*Proof.* We have already shown this in the discussion preceding this lemma. ☐

For constant conductivity in the whole domain $\Omega$, we immediately get the following consequence:

**Corollary 2.8.** *Let the assumptions of the Lemmata 2.6 and 2.7 be satisfied. Suppose furthermore that $\sigma = \mathrm{const}$.*
*Then there exists a unique $\boldsymbol{u}\in L_2((0,T),\boldsymbol{V})$ with $\dot{\boldsymbol{u}}\in L_2((0,T),\boldsymbol{V}^*)$ such that*

$$\begin{aligned}\sigma\,\dot{\boldsymbol{u}} + \bar{A}(\boldsymbol{u}) &= \bar{F},\\ \boldsymbol{u}(0) &= \boldsymbol{u}_0,\end{aligned}$$

*and this solution $\boldsymbol{u}$ is divergence-free for almost all $t$.*

### 2.4.3 Application to Eddy Current Problems

Taking advantage of the knowledge we have gained in the previous paragraphs, we can now prove the main result of this section, to wit existence of a solution of the eddy current problem and its uniqueness in a certain sense.
The Lemmata 2.5 and 2.6 provide existence and uniqueness of the solution in non-conducting and conducting regions, respectively. However, we have not treated the case of domains consisting of parts with positive conductivity and of regions with $\sigma = 0$ yet.
As we know, the domain of the whole eddy current welding problem (2.17) is such a mixed domain, because the iron tube $\Omega_1 = \Omega_{Fe}$ is a conductor, and we have $\sigma = 0$ in $\Omega_2 = \Omega \setminus \overline{\Omega}_1$, i.e. in the inductor, the impeder and the surrounding air. We sketch the situation of a simple two-dimensional problem in Figure 2.4.

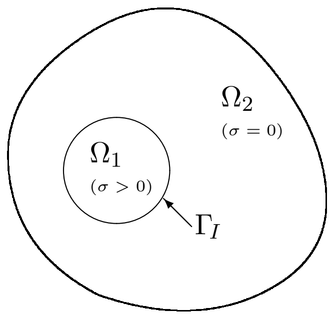


Figure 2.4: Sketch of the domain $\overline{\Omega} = \overline{\Omega}_1 \cup \overline{\Omega}_2$.

Consequently, our task in the following paragraph consists in assembling the previous results to the desired theorem.

Let us first consider some fixed moment in time $t$.
For joining the solutions in the respective domains, we need an interface condition on $\Gamma_I = \overline{\Omega}_1 \cap \overline{\Omega}_2$: The tangential component of the joined solution should be continuous, i.e. we should have

$$\boldsymbol{u}_1 \times \boldsymbol{n}_1 = -\boldsymbol{u}_2 \times \boldsymbol{n}_2, \qquad \text{on } \Gamma_I, \tag{2.38}$$

where $\boldsymbol{u}_1$ and $\boldsymbol{u}_2$ are the solutions in $\Omega_1$ and $\Omega_2$ at the fixed time $t$, and $\boldsymbol{n}_i$ are the respective outer unit normal vectors at the interface $\Gamma_I$.
Suppose we knew the solution $\boldsymbol{u}_1$ in the conducting region. Then the *interface condition* (2.38) together with the original boundary condition

$$\boldsymbol{u} \times \boldsymbol{n} = 0, \qquad \text{on } \Gamma = \partial\Omega,$$

provide the necessary boundary conditions for the equation in the non-conducting part (2.23). So by Lemma 2.5 we have a unique divergence-free solution $\boldsymbol{u}_2 \in \tilde{\boldsymbol{g}} + \bar{\boldsymbol{V}}_2$, where $\tilde{\boldsymbol{g}} \in \boldsymbol{H}(\mathbf{curl}, \Omega_2)$ satisfies the boundary conditions, and $\bar{\boldsymbol{V}}_2$ is the factor space of divergence-free functions as in (2.29).

In other words, the solution in the conducting domain $\Omega_1$ uniquely determines the solution in the non-conducting region $\Omega_2$.
We summarize these considerations in the following lemma:

**Lemma 2.9.** *Let $\overline{\Omega} = \overline{\Omega}_1 \cup \overline{\Omega}_2$ with $\Omega_1 \cap \Omega_2 = \emptyset$ and let $\Omega_2$ be multiply connected. Assume $\nu \in L_\infty(\Omega_2)$ with $0 < \underline{\nu} \le \nu(\boldsymbol{x}) \le \overline{\nu}$ a.e. in $\Omega_2$.*
*Let $\boldsymbol{V} = \{\boldsymbol{v} \in \boldsymbol{H}(\mathbf{curl}, \Omega_2) : \boldsymbol{v} \times \boldsymbol{n} = 0$ on $\partial\Omega_2\}$ and $\boldsymbol{W} = \boldsymbol{W}(\Omega_2)$ as in (2.28). Define $\bar{\boldsymbol{V}} := \boldsymbol{V}/\boldsymbol{W}$ and let $\boldsymbol{f} \in \bar{\boldsymbol{V}}^*$ be given.*
*Then for each $\boldsymbol{u}_1 \in \boldsymbol{H}(\mathbf{curl}, \Omega_1)$ exists exactly one function $\boldsymbol{u}_2 \in \tilde{\boldsymbol{g}} + \bar{\boldsymbol{V}}$ such that $\boldsymbol{u}_2$ is the weak solution of*

$$\begin{aligned} \mathbf{curl}\,(\nu\, \mathbf{curl}\, \boldsymbol{u}_2) &= \boldsymbol{f}, && \text{in } \Omega_2, \\ \boldsymbol{u}_2 \times \boldsymbol{n} &= 0, && \text{on } \partial\Omega \cap \partial\Omega_2, \\ \boldsymbol{u}_2 \times \boldsymbol{n} &= \boldsymbol{u}_1 \times \boldsymbol{n}, && \text{on } \partial\Omega_1 \cap \partial\Omega_2, \end{aligned} \tag{2.39}$$

*where $\boldsymbol{n}$ is the outer unit normal vector to $\partial\Omega_2$ and $\tilde{\boldsymbol{g}} \in \boldsymbol{H}(\mathbf{curl}, \Omega_2)$ satisfies the boundary conditions.*

Lemma 2.9 shows that $\boldsymbol{u}_2 = \boldsymbol{U}(\boldsymbol{u}_1)$ for some function $\boldsymbol{U} : \boldsymbol{H}(\mathbf{curl}, \Omega_1) \to \boldsymbol{H}(\mathbf{curl}, \Omega_2)$, i.e. the solution in $\Omega_2$ is uniquely defined by the solution in $\Omega_1$. We point out that the eddy current problem is uniquely solvable in the conducting region $\Omega_1$ (Lemma 2.6). Consequently, the idea to take advantage of the relation $\boldsymbol{u}_2 = \boldsymbol{U}(\boldsymbol{u}_1)$ for proving unique solvability of the whole eddy current problem seems obvious.

For our proof, we define a space $\tilde{\boldsymbol{V}}$ which contains arbitrary divergence-free functions in $\Omega_1$, but only those functions in the non-conducting domain $\Omega_2$ that are determined by the function $\boldsymbol{U} : \boldsymbol{H}(\mathbf{curl}, \Omega_1) \to \boldsymbol{H}(\mathbf{curl}, \Omega_2)$. Moreover, we impose homogeneous Dirichlet boundary conditions as usual:

$$\begin{aligned} \tilde{\boldsymbol{V}} := \{\boldsymbol{v} \in \boldsymbol{H}(\mathbf{curl}, \Omega) : \;& \boldsymbol{v}_{|\Omega_1} \in \boldsymbol{H}(\mathbf{curl}, \Omega_1), \\ & \boldsymbol{v}_{|\Omega_2} = \boldsymbol{U}(\boldsymbol{v}_{|\Omega_1}), \\ & (\boldsymbol{v}, \boldsymbol{w})_{\boldsymbol{L}_2} = 0, \; \forall\, \boldsymbol{w} \in \boldsymbol{W}(\Omega_1), \\ & \boldsymbol{v} \times \boldsymbol{n} = 0, \; \text{on } \Gamma = \partial\Omega\}, \end{aligned} \tag{2.40}$$

where $\boldsymbol{W}(\Omega_1)$ are the gradient fields on $\Omega_1$ as defined in (2.28).

Obviously, $\tilde{\boldsymbol{V}}$ is just another representation of the divergence-free $\boldsymbol{H}(\mathbf{curl})$-functions in $\Omega_1$ with zero tangential component on the boundary $\tilde{\Gamma} := \partial\Omega \cap \partial\Omega_1$, i.e. $\tilde{\boldsymbol{V}} \simeq \boldsymbol{H}_{\tilde{\Gamma}}(\mathbf{curl}, \Omega_1)/\boldsymbol{W}(\Omega_1)$. Since in $\Omega_1$ we deal with the nonlinear parabolic problem (2.35), and since this equation is uniquely solvable by Lemma 2.6, we may hope that the whole eddy current problem restricted to $\tilde{\boldsymbol{V}}$ is uniquely solvable as well. As we see in the following main theorem on unique solvability of eddy current problems, this is actually the case.

**Theorem 2.10.** *Let $s \mapsto \nu_1(s)$ be continuous, $0 < \underline{\nu}_1 \le \nu_1(s) \le \overline{\nu}_1$, $\forall\, s \in \mathbb{R}_0^+$ and let the function $s \mapsto \nu_1(s)s$ be monotone. Assume furthermore $\nu_2 \in L_\infty(\Omega_2)$ with $0 < \underline{\nu}_2 \le \nu_2(\boldsymbol{x}) \le \overline{\nu}_2$ a.e. in $\Omega_2$.*

*Let moreover* $\boldsymbol{u}_0 \in \boldsymbol{L}_2(\Omega)$ *and* $\boldsymbol{f} \in L_2((0,T), \tilde{\boldsymbol{V}}^*)$ *be given, and suppose* $\sigma \in L_\infty$ *to be strictly positive.*

*Then there is a unique* $\boldsymbol{u} \in L_2((0,T), \tilde{\boldsymbol{V}})$ *with* $\dot{\boldsymbol{u}} \in L_2((0,T), \tilde{\boldsymbol{V}}^*)$ *such that* $\boldsymbol{u}$ *is the weak solution of* (2.17)*, more precisely of*

$$
\begin{aligned}
\sigma \frac{\partial \boldsymbol{u}}{\partial t} + \mathbf{curl}\,(\nu_1(|\mathbf{curl}\,\boldsymbol{u}|)\,\mathbf{curl}\,\boldsymbol{u}) &= \boldsymbol{f}, && \textit{in } \Omega_1 \times [0,T],\\
\mathbf{curl}\,(\nu_2\,\mathbf{curl}\,\boldsymbol{u}) &= \boldsymbol{f}, && \textit{in } \Omega_2 \times [0,T],\\
\boldsymbol{u} \times \boldsymbol{n} &= 0, && \textit{on } \Gamma \times [0,T],\\
\boldsymbol{u} &= \boldsymbol{u}_0, && \textit{on } \Omega \times \{0\},
\end{aligned}
$$

*with a continuos tangential component along the interface* $\overline{\Omega}_1 \cap \overline{\Omega}_2$*.*
*This means that we have a unique* $\boldsymbol{u} \in L_2((0,T), \tilde{\boldsymbol{V}})$ *with* $\dot{\boldsymbol{u}} \in L_2((0,T), \tilde{\boldsymbol{V}}^*)$ *solution of*

$$
\begin{aligned}
\sigma \dot{\boldsymbol{u}} + A_1(\boldsymbol{u}) &= F, && \textit{in } \Omega_1, && (2.41a)\\
A_2 \boldsymbol{u} &= F, && \textit{in } \Omega_2, && (2.41b)\\
\boldsymbol{u}_0 &= \boldsymbol{u}_0, && && (2.41c)
\end{aligned}
$$

*with the operators* $A_1$*,* $A_2$ *and* $F$ *as in* (2.25) *and* (2.31)*, respectively.*

*Proof.* By the choice of the space $\tilde{\boldsymbol{V}}$, i.e. by Lemma 2.9, equation (2.41b) is fulfilled for any $\boldsymbol{u} \in L_2((0,T), \tilde{\boldsymbol{V}})$.
Remains to show that equation (2.41a) with the initial condition (2.41c) is uniquely solvable. We have already proven this fact in Lemma 2.6 for the space $\bar{\boldsymbol{V}}$ instead of $\tilde{\boldsymbol{V}}$. However, since $\tilde{\boldsymbol{V}}$ is nothing more than another representation of $\bar{\boldsymbol{V}}$, the result can be carried over to $\tilde{\boldsymbol{V}}$ one-to-one.
Thus we have proven that (2.41) is uniquely solvable. □

*Remark* 2.5. We mention that no solvability condition for the sources $\boldsymbol{f}$ is required (cf. Remark 2.2), since the space of test functions does not contain any gradient fields. Moreover, we stress that the condition $\boldsymbol{f} \in L_2((0,T), \tilde{\boldsymbol{V}}^*)$ is satisfied for any reasonable right hand side. For example, $\boldsymbol{f} \in L_2((0,T), \boldsymbol{L}_2(\Omega))$ is clearly sufficient.

Under certain assumptions, the solution is not only unique among the divergence-free functions, but even in the space

$$
\begin{aligned}
\hat{\boldsymbol{V}} = \{\boldsymbol{v} \in \boldsymbol{H}(\mathbf{curl}, \Omega) : \boldsymbol{v}_{|\Omega_1} &\in \boldsymbol{H}(\mathbf{curl}, \Omega_1),\\
\boldsymbol{v}_{|\Omega_2} &= \boldsymbol{U}(\boldsymbol{v}_{|\Omega_1}),\\
\boldsymbol{v} \times \boldsymbol{n} &= 0, \text{ on } \Gamma = \partial\Omega\}.
\end{aligned}
\tag{2.42}
$$

This means the solution is unique among those $\boldsymbol{H}(\mathbf{curl})$-functions that are divergence-free in the non-conducting region $\Omega_2$ and arbitrary in $\Omega_1$.
We summarize this result, which is an immediate consequence of Theorem 2.10 and Corollary 2.8, in the following corollary:

**Corollary 2.11.** *Let the assumptions of Thm. 2.10 be satisfied and suppose that* $\sigma =$ const. *Let furthermore* $\boldsymbol{f}(t)$ *be defined for all* $t$ *and* $\boldsymbol{f}(t)$ *and* $\boldsymbol{u}_0$ *be divergence-free in* $\Omega_1$*, i.e.*

$$\begin{aligned} \int_{\Omega_1} \boldsymbol{f}(t) \cdot \boldsymbol{w} &= 0, \qquad \forall\, t \in [0,T],\, \forall\, \boldsymbol{w} \in \boldsymbol{W}(\Omega_1), \\ \int_{\Omega_1} \boldsymbol{u}_0 \cdot \boldsymbol{w} &= 0, \qquad \forall\, \boldsymbol{w} \in \boldsymbol{W}(\Omega_1). \end{aligned}$$

*Moreover, let* $\hat{\boldsymbol{V}}$ *be defined as in* (2.42).
*Then there exists a unique* $\boldsymbol{u} \in L_2((0,T), \hat{\boldsymbol{V}})$ *with* $\dot{\boldsymbol{u}} \in L_2((0,T), \hat{\boldsymbol{V}}^*)$ *solving* (2.41)*, and this solution is divergence-free for almost all* $t$*.*

# Chapter 3

# Multiharmonic Ansatz

We recall that we are engaged in the solution of the problem

$$\mathbf{curl}\,(\nu\,\mathbf{curl}\,\boldsymbol{u}) + \sigma\frac{\partial \boldsymbol{u}}{\partial t} = \boldsymbol{f}, \tag{2.17}$$

with Dirichlet boundary conditions and an initial condition. In order to solve this equation numerically, we need a discretization in time and space. Instead of semi-discretizing the equation in space and solving the resulting ODE by a time-stepping method, we take advantage of the periodicity of the source current and thus the expected solution: Since the right hand side of (2.17) is a harmonic current of the form $\hat{\boldsymbol{f}} \cdot \cos(\omega t)$, the ansatz

$$\boldsymbol{u}(\boldsymbol{x}, t) = \boldsymbol{u}^c(\boldsymbol{x}) \cdot \cos(\omega t) + \boldsymbol{u}^s(\boldsymbol{x}) \cdot \sin(\omega t)$$

seems to be manifest. This would reduce equation (2.17) to an equation for the coefficients $\boldsymbol{u}^c(\boldsymbol{x})$ and $\boldsymbol{u}^s(\boldsymbol{x})$ that only depend on the space coordinates.
In the linear case (i.e. for $\nu$ independent of $\mathbf{curl}\,\boldsymbol{u}$), the solution can be expressed in terms of the same base frequency $\omega$ as the given current source. Due to the nonlinearity, however, the solution depends on higher harmonics as well, but will still be periodical and can consequently be approximated by a multiharmonic ansatz.
This ansatz – a truncated Fourier expansion – reduces the original time-dependent problem (2.17) to a system of equations for the Fourier coefficients.

This chapter is arranged as follows: First, we define the notion of a periodic steady state solution and then we show the existence and uniqueness of such a solution by means of Fourier series expansion.
Obviously, the Fourier series $\sum\,[\boldsymbol{u}_k^c \cos(k\omega t) + \boldsymbol{u}_k^s \sin(k\omega t)]$ can be written in complex notation as $\mathrm{Re}\sum \hat{\boldsymbol{u}}_k e^{ik\omega t}$ with $\hat{\boldsymbol{u}}_k = \boldsymbol{u}_k^c - i\boldsymbol{u}_k^s$ as well. Taking advantage of some properties of the ansatz, we can show that in this notation the projector Re can be skipped without losing unique solvability. This would allow to rewrite the problem as a system of complex equations, as is done in [7, 19, 54], for example, or in [27, 33, 37], where only the base harmonic is considered. Anyhow, we prefer to stay with the real

problem because dealing with the complex problem leads to complications with the linearization. We will describe these difficulties in Section 3.4.2.
In Section 3.5, we finally write down the system of equations in space that arises from the multiharmonic ansatz.

## 3.1 Steady State Solution

In many eddy current problems, we are not so much interested in some device's response on closure of the electrical circuit, but more on its behavior under a harmonic current for the time $t \to \infty$. So what we really want to calculate is a steady state solution, i.e. a solution of the original problem (2.17) without the initial condition:

**Definition 3.1.** The function $\boldsymbol{u}(\boldsymbol{x}, t)$ is called a *periodic steady state solution* of equation (2.17), if

1. $\boldsymbol{u}$ satisfies (2.17) (but not necessarily the initial condition),
2. $\boldsymbol{u}$ is periodic, i.e. $\exists\, T\, \forall\, t : \boldsymbol{u}(\boldsymbol{x}, t) = \boldsymbol{u}(\boldsymbol{x}, t + T)$.

For our eddy current problem, we are actually looking for a periodic steady state solution as defined in Definition 3.1.

Let the right hand side be given as $\boldsymbol{f}(\boldsymbol{x}, t) = \hat{\boldsymbol{f}}(\boldsymbol{x}) \cdot \cos(\omega t)$, and suppose we knew a periodic solution $\boldsymbol{u}$ with the same period $T = \frac{2\pi}{\omega}$. Then we could of course rewrite it as a Fourier series

$$\boldsymbol{u}(\boldsymbol{x}, t) = \sum_{k=0}^{\infty} \boldsymbol{u}_k^c \cdot \cos(k\omega t) + \boldsymbol{u}_k^s \cdot \sin(k\omega t). \tag{3.1}$$

Hence, the magnetic field $\boldsymbol{H} = \boldsymbol{H}(\mathbf{curl}\, \boldsymbol{u})$ is periodic as well and can be written in the form

$$\boldsymbol{H}(\mathbf{curl}\, \boldsymbol{u}) = \sum_{k=0}^{\infty} \boldsymbol{H}_k^c(\mathbf{curl}\, \boldsymbol{u}) \cdot \cos(k\omega t) + \boldsymbol{H}_k^s(\mathbf{curl}\, \boldsymbol{u}) \cdot \sin(k\omega t). \tag{3.2}$$

We consider equation (2.17) in its weak formulation, i.e.

$$\underbrace{\int_0^T \int_\Omega \boldsymbol{H}(\mathbf{curl}\, \boldsymbol{u}) \cdot \mathbf{curl}\, \boldsymbol{v} + \sigma \frac{\partial \boldsymbol{u}}{\partial t} \cdot \boldsymbol{v}\, \mathrm{d}\boldsymbol{x}\, \mathrm{dt}}_{=:\langle A(\boldsymbol{u}), \boldsymbol{v}\rangle} = \underbrace{\int_0^T \int_\Omega \boldsymbol{f} \cdot \boldsymbol{v}\, \mathrm{d}\boldsymbol{x}\, \mathrm{dt}}_{=:\langle F, \boldsymbol{v}\rangle}, \quad \forall\, \boldsymbol{v}. \tag{3.3}$$

Apparently, using (3.1) and (3.2) as ansatz for the solution, the problem consists in calculating the Fourier coefficients $\boldsymbol{u}_k^c$ and $\boldsymbol{u}_k^s$. This means that we regard the nonlinear operator $A$ as defined in (3.3) as

$$A : l_*^2(\boldsymbol{V}) \to \left(l_*^2(\boldsymbol{V})\right)^*, \tag{3.4}$$

where $\boldsymbol{V} = \boldsymbol{H}_0(\mathbf{curl})^2$ and

$$l_*^2(\boldsymbol{V}) := \left\{ \boldsymbol{u} \in \boldsymbol{V}^{\mathbb{N}} : \left\{ k \,\|\boldsymbol{u}_k\|_{\boldsymbol{V}} = k \left( \|\boldsymbol{u}_k^c\|^2_{\boldsymbol{H}(\mathbf{curl})} + \|\boldsymbol{u}_k^s\|^2_{\boldsymbol{H}(\mathbf{curl})} \right)^{\frac{1}{2}} \right\}_{k\in\mathbb{N}} \in l^2 \right\}. \tag{3.5}$$

The condition $\{k \,\|\boldsymbol{u}_k\|_{\boldsymbol{V}}\}_{k\in\mathbb{N}} \in l^2$ in the definition of $l_*^2(\boldsymbol{V})$ implies

$$\int_0^T \int_\Omega \left| \frac{\partial \boldsymbol{u}}{\partial t} \right|^2 \mathrm{d}\boldsymbol{x}\, \mathrm{d}t = \frac{T}{2} \omega^2 \sum_{k=0}^{\infty} k^2 \int_\Omega |\boldsymbol{u}_k^c|^2 + |\boldsymbol{u}_k^s|^2 \,\mathrm{d}\boldsymbol{x} < \infty,$$

so the operator $A$ is well-defined on the space $l_*^2(\boldsymbol{V})$.
Obviously, $l_*^2(\boldsymbol{V})$ is a Hilbert space with scalar product

$$(\boldsymbol{u}, \boldsymbol{v})_{l_*^2(\boldsymbol{V})} = \sum_{k=0}^{\infty} (\boldsymbol{u}_k^c, \boldsymbol{v}_k^c)_{\boldsymbol{H}(\mathbf{curl})} + (\boldsymbol{u}_k^s, \boldsymbol{v}_k^s)_{\boldsymbol{H}(\mathbf{curl})}, \tag{3.6}$$

and norm $\|\boldsymbol{u}\|_{l_*^2(\boldsymbol{V})} = (\boldsymbol{u}, \boldsymbol{u})^{\frac{1}{2}}_{l_*^2(\boldsymbol{V})}$.

## 3.2 Existence and Uniqueness

With these considerations, we are now able to show the existence of a uniquely defined periodic steady state solution of the eddy current problem (2.17).

As in Section 2.4, we factor the space $\boldsymbol{V} = \boldsymbol{H}_0(\mathbf{curl})^2$ by the irrotational fields and restrict the problem to the space $\bar{\boldsymbol{V}} = \boldsymbol{V}/\boldsymbol{W}^2$, with $\boldsymbol{W} = \boldsymbol{W}(\Omega)$ defined as in (2.28). Consequently, for $\boldsymbol{u} = (\boldsymbol{u}^c, \boldsymbol{u}^s)^T \in \bar{\boldsymbol{V}}$ we have the norm equivalence

$$\|\boldsymbol{u}^c\|^2_{\boldsymbol{H}(\mathbf{curl})} + \|\boldsymbol{u}^s\|^2_{\boldsymbol{H}(\mathbf{curl})} \simeq \int_\Omega |\mathbf{curl}\,\boldsymbol{u}^c|^2 + |\mathbf{curl}\,\boldsymbol{u}^s|^2 \,\mathrm{d}\boldsymbol{x}, \tag{3.7}$$

cf. Lemma 2.4 and Remark 2.3.
This allows us to prove the following theorem on existence and uniqueness of a periodic steady state solution:

**Theorem 3.1.** *Let $\sigma \in L_\infty$ and let the reluctivity $\nu$ be strongly monotone and continuous. Suppose the source current $\boldsymbol{f} = \sum_{k=0}^{\infty} \boldsymbol{f}_k^c \cdot \cos(k\omega t) + \boldsymbol{f}_k^s \cdot \sin(k\omega t)$ satisfies $\boldsymbol{f}_k \in \bar{\boldsymbol{V}}^*$, $\forall\, k$.*
*Then $F$ as defined in* (3.3) *is in $l_*^2(\bar{\boldsymbol{V}})^*$ and the problem*

$$\langle A(\boldsymbol{u}), \boldsymbol{v} \rangle = \langle F, \boldsymbol{v} \rangle, \quad \forall\, \boldsymbol{v} \in l_*^2(\bar{\boldsymbol{V}}),$$

*with $A : l_*^2(\bar{\boldsymbol{V}}) \to l_*^2(\bar{\boldsymbol{V}})^*$ as in* (3.3)*, is uniquely solvable, i.e. there exists a unique divergence-free periodic steady state solution of* (2.17)*.*
*If moreover we have*

$$\sum_{k=0}^{\infty} \boldsymbol{u}_k^c = \boldsymbol{u}_0,$$

*this periodic steady state solution satisfies the initial condition and thus is the unique solenoidal solution of* (2.17)*.*

*Proof.* By Browder's and Minty's Theorem (Thm. 2.2) it suffices to show that $A$ is strictly monotone, coercive and hemicontinuous.
Due to the assumptions on $\nu$ we know that

$$[\boldsymbol{H}(\boldsymbol{B}_1) - \boldsymbol{H}(\boldsymbol{B}_2)]^T [\boldsymbol{B}_1 - \boldsymbol{B}_2] \geq c\, |\boldsymbol{B}_1 - \boldsymbol{B}_2|^2, \tag{3.8}$$

for all inductions $\boldsymbol{B}_1, \boldsymbol{B}_2$ and the magnetic field $\boldsymbol{H}(\boldsymbol{B}) = \nu(|\boldsymbol{B}|) \cdot \boldsymbol{B}$.
We first show strict monotonicity and coerciveness of $A$ by proving strong monotonicity and then deducing the required properties:

$$\begin{aligned}
&\langle A(\boldsymbol{u}) - A(\boldsymbol{v}), \boldsymbol{u} - \boldsymbol{v}\rangle = \\
&\quad \int_0^T \int_\Omega \big[\boldsymbol{H}(\mathbf{curl}\, \boldsymbol{u}(t)) - \boldsymbol{H}(\mathbf{curl}\, \boldsymbol{v}(t))\big]^T \big[\mathbf{curl}\, \boldsymbol{u}(t) - \mathbf{curl}\, \boldsymbol{v}(t)\big] + \\
&\quad + \sigma \left[\frac{\partial}{\partial t}(\boldsymbol{u}(t) - \boldsymbol{v}(t))\right]^T \big[\boldsymbol{u}(t) - \boldsymbol{v}(t)\big]\, \mathrm{d}\boldsymbol{x}\, \mathrm{dt} \geq \\
&\quad \overset{(3.8),(3.10)}{\geq} \int_0^T \int_\Omega \big|\mathbf{curl}\, \boldsymbol{u}(t) - \mathbf{curl}\, \boldsymbol{v}(t)\big|^2\, \mathrm{d}\boldsymbol{x}\, \mathrm{dt}.
\end{aligned} \tag{3.9}$$

Here we use our knowledge about the strongly monotone $\boldsymbol{B}$-$\boldsymbol{H}$-curve (3.8) and the readily identifiable fact that the time derivative of any $\boldsymbol{u} = \sum \boldsymbol{u}_k^c \cos(k\omega t) + \boldsymbol{u}_k^s \sin(k\omega t)$ is orthogonal to the original function:

$$\int_0^T \frac{\partial \boldsymbol{u}}{\partial t} \cdot \boldsymbol{u} = 0. \tag{3.10}$$

Since we have

$$\begin{aligned}
&\int_0^T \int_\Omega \big|\mathbf{curl}\, \boldsymbol{u}(t) - \mathbf{curl}\, \boldsymbol{v}(t)\big|^2\, \mathrm{d}\boldsymbol{x}\, \mathrm{dt} = \\
&\quad = \int_0^T \int_\Omega \left|\sum_{k=0}^{\infty} \big[\mathbf{curl}\,(\boldsymbol{u}_k^c - \boldsymbol{v}_k^c) \cos(k\omega t) + \mathbf{curl}\,(\boldsymbol{u}_k^s - \boldsymbol{v}_k^s) \sin(k\omega t)\big]\right|^2 \mathrm{d}\boldsymbol{x}\, \mathrm{dt} = \\
&\quad = \frac{T}{2} \sum_{k=0}^{\infty} \int_\Omega \big|\mathbf{curl}\,(\boldsymbol{u}_k^c - \boldsymbol{v}_k^c)\big|^2 + \big|\mathbf{curl}\,(\boldsymbol{u}_k^s - \boldsymbol{v}_k^s)\big|^2\, \mathrm{d}\boldsymbol{x},
\end{aligned} \tag{3.11}$$

strong monotonicity is proved with (3.9), the norm equivalence (3.7) and the definition of the norm in $l_*^2(\bar{\boldsymbol{V}})$ (3.6).
Strict monotonicity follows easily, and coerciveness is an immediate consequence as well:

$$\langle A(\boldsymbol{u}), \boldsymbol{u}\rangle = \langle A(\boldsymbol{u}) - A(0), \boldsymbol{u}\rangle + \langle A(0), \boldsymbol{u}\rangle \geq c\|\boldsymbol{u}\|^2 - \|A(0)\| \cdot \|\boldsymbol{u}\|$$

$$\Longrightarrow \lim_{\|\boldsymbol{u}\| \to \infty} \frac{\langle A(\boldsymbol{u}), \boldsymbol{u}\rangle}{\|\boldsymbol{u}\|} = \infty.$$

So, since continuity of $\nu$ obviously implies hemicontinuity of $A$, we gain existence and uniqueness due to Browder's and Minty's Theorem.
Clearly, if we have $\sum \boldsymbol{u}_k^c = \boldsymbol{u}_0$, this unique divergence-free periodic steady state solution satisfies the initial condition and consequently is the unique divergence-free solution of (2.17). □

## 3.3 Reduction to Odd Harmonics

Theorem 3.1 states that for given current source $\boldsymbol{f}$, there is exactly one periodic steady state solution $\boldsymbol{u} \in l_*^2(\bar{\boldsymbol{V}})$ for the factor space $\bar{\boldsymbol{V}}$ as defined in the previous section. In the following, we will use this result to show that we do not require the even coefficients in the Fourier series for $\boldsymbol{u}$.
In order to keep notation simple, we use $\boldsymbol{u}$ to denote the sequence of Fourier coefficients and $\boldsymbol{u}(t)$ to signify the periodic function that is determined by these coefficients according to (3.1), and similarly for $\boldsymbol{f}$.

Since odd modes $\cos((2k+1)\omega t)$, $\sin((2k+1)\omega t)$, $k \in \mathbb{N}$, change the sign when shifted by half a period, the condition

$$\boldsymbol{v}\big(t + \frac{\pi}{\omega}\big) = -\boldsymbol{v}(t), \quad \forall\, t, \tag{3.12}$$

obviously is an equivalent characterization of the property $\boldsymbol{v}_{2k}^c = \boldsymbol{v}_{2k}^s = 0$, $\forall\, k \in \mathbb{N}$, for any function $\boldsymbol{v} = \sum \boldsymbol{v}_k^c \cos(k\omega t) + \boldsymbol{v}_k^s \sin(k\omega t)$. The current source $\boldsymbol{f} = \hat{\boldsymbol{f}} \cdot \cos(\omega t)$ apparently satisfies (3.12).

Due to the unique solvability of (2.17) in the space of divergence-free functions, it is fairly easy to see that $\boldsymbol{f}$ satisfying (3.12) implies the same property for the periodic steady state solution:
For a given right hand side $\boldsymbol{f}(\cdot)$, we get the unique solution $\boldsymbol{u}$. Shifting the right hand side to $\tilde{\boldsymbol{f}}(\cdot) = \boldsymbol{f}\left(\cdot + \frac{\pi}{\omega}\right)$, we obtain the solution $\tilde{\boldsymbol{u}}$. On the other hand, $\bar{\boldsymbol{f}} = -\boldsymbol{f}$ leads to the result $\bar{\boldsymbol{u}}$.
Note that, since $\boldsymbol{f}\left(\cdot + \frac{\pi}{\omega}\right) = -\boldsymbol{f}(\cdot)$, we have $\tilde{\boldsymbol{u}} = \bar{\boldsymbol{u}}$.

Clearly, $\boldsymbol{u}\left(\cdot + \frac{\pi}{\omega}\right)$ is a periodic steady state solution of (2.17) with right hand side $\tilde{\boldsymbol{f}}$. Because of Thm. 3.1, we have $\tilde{\boldsymbol{u}}(\cdot) = \boldsymbol{u}\left(\cdot + \frac{\pi}{\omega}\right)$.
On the other hand, $-\boldsymbol{u}$ apparently solves (2.17) with right hand side $\bar{\boldsymbol{f}}$ and so $-\boldsymbol{u} = \bar{\boldsymbol{u}}$ because of the uniqueness.

Consequently,

$$\boldsymbol{u}\big(\,\cdot + \frac{\pi}{\omega}\big) = \tilde{\boldsymbol{u}}(\cdot) = \bar{\boldsymbol{u}}(\cdot) = -\boldsymbol{u}(\cdot),$$

i.e. $\boldsymbol{u}$ satisfies (3.12) and can thus be described by odd harmonics.

We summarize this discussion in the following theorem.

**Theorem 3.2.** *Let the current source $\boldsymbol{f}$ satisfy* (3.12). *Then the unique periodic steady state solution of* (2.17) *with right hand side $\boldsymbol{f}$ satisfies* (3.12) *as well and can accordingly be entirely represented by odd harmonics, i.e.*

$$\boldsymbol{u}(\boldsymbol{x},t) = \sum_{k=0}^{\infty} \left[ \boldsymbol{u}^c_{2k+1}(\boldsymbol{x}) \cdot \cos((2k+1)\omega t) + \boldsymbol{u}^s_{2k+1}(\boldsymbol{x}) \cdot \sin((2k+1)\omega t) \right].$$

*Remark* 3.1. Since the solution $\boldsymbol{u}(\boldsymbol{x},t)$ depends only on odd harmonics, the magnetic field $\boldsymbol{H}(\mathbf{curl}\,\boldsymbol{u})$ has the same property:

$$\begin{aligned}\boldsymbol{H}\big(t+\frac{\pi}{\omega}\big) &= \nu\big(\big|\mathbf{curl}\,\boldsymbol{u}\big(t+\frac{\pi}{\omega}\big)\big|\big) \cdot \mathbf{curl}\,\boldsymbol{u}\big(t+\frac{\pi}{\omega}\big) = \\ &= \nu(|-\mathbf{curl}\,\boldsymbol{u}(t)|) \cdot (-\mathbf{curl}\,\boldsymbol{u}(t)) = -\boldsymbol{H}(t).\end{aligned}$$

## 3.4 The Complex Problem

Clearly, the Fourier series (3.1) can also be written in complex notation as

$$\boldsymbol{u}(\boldsymbol{x},t) = \mathrm{Re} \sum_{k=0}^{\infty} \hat{\boldsymbol{u}}_k \cdot e^{ik\omega t}, \tag{3.13}$$

with $\hat{\boldsymbol{u}}_k = \boldsymbol{u}^c_k - i\boldsymbol{u}^s_k$.
In this section, we show that the problem can be regarded as a complex one, i.e. that the projector Re can be skipped without losing unique solvability. Furthermore, we point out the difficulties that arise when complex Fourier coefficients $\hat{\boldsymbol{u}}_k$ are considered and the problem is regarded in complex vector spaces.

### 3.4.1 Uniqueness over $\mathbb{C}$

We are concerned with the equation

$$\mathbf{curl}\,(\nu\,\mathbf{curl}\,\boldsymbol{u}) + \sigma \frac{\partial \boldsymbol{u}}{\partial t} = \boldsymbol{f}. \tag{2.17}$$

By Fourier series expansion of the desired periodic steady state solution, we can rewrite it as

$$\mathrm{Re}\left( \mathbf{curl} \sum_{k=0}^{\infty} \hat{\boldsymbol{H}}_k(\mathbf{curl}\,\boldsymbol{u}) \cdot e^{ik\omega t} + i\omega\sigma \sum_{k=0}^{\infty} k\hat{\boldsymbol{u}}_k \cdot e^{ik\omega t} \right) = \mathrm{Re} \sum_{k=0}^{\infty} \hat{\boldsymbol{f}}_k \cdot e^{ik\omega t}, \tag{3.14}$$

where we know that the coefficients $\hat{\boldsymbol{f}}_k$, $\hat{\boldsymbol{u}}_k$ and $\hat{\boldsymbol{H}}_k$ are zero for even $k$.
In (3.14) we have expressed the magnetic field $\boldsymbol{H}$ and the right hand side $\boldsymbol{f}$ as complex Fourier series, just like we did for $\boldsymbol{u}$ in (3.13).

We show now that the projector Re is injective for these Fourier series and can thus be skipped without losing unique solvability.

**Lemma 3.3.** *For Fourier series* $\boldsymbol{u} = \sum_{k\geq 0} \hat{\boldsymbol{u}}_k \cdot e^{ik\omega t}$ *with* $\hat{\boldsymbol{u}}_0 = 0$*, the projector* Re *is injective, i.e.*

$$\operatorname{Re} \boldsymbol{u} = 0 \implies \hat{\boldsymbol{u}}_k = 0,\ \forall\, k.$$

*Proof.* We have

$$\operatorname{Re} \boldsymbol{u} = \sum_{k=1}^{\infty} \operatorname{Re} \hat{\boldsymbol{u}}_k \cos(k\omega t) - \operatorname{Im} \hat{\boldsymbol{u}}_k \sin(k\omega t),$$

and the functions $\{\cos(k\omega t), \sin(k\omega t)\}_{k\geq 1}$ are linearly independent. □

Consequently, the complex problem

$$\mathbf{curl} \sum_{k=0}^{\infty} \hat{\boldsymbol{H}}_k(\mathbf{curl}\, \boldsymbol{u}) \cdot e^{ik\omega t} + i\omega\sigma \sum_{k=0}^{\infty} k\hat{\boldsymbol{u}}_k \cdot e^{ik\omega t} = \sum_{k=0}^{\infty} \hat{\boldsymbol{f}}_k \cdot e^{ik\omega t}, \tag{3.15}$$

i.e. problem (3.14) without the projector Re, is uniquely solvable as well:

**Lemma 3.4.** *Under the assumptions of Theorem 3.1 and Theorem 3.2, equation* (3.15) *with Dirichlet boundary conditions*

$$\hat{\boldsymbol{u}}_k \times \boldsymbol{n} = 0, \quad \forall\, k,$$

*is uniquely solvable in the space* $l^2_*(\bar{\boldsymbol{V}})$.

*Proof.* Since Re is injective (Lemma 3.3), any solution of (3.14) with homogeneous Dirichlet boundary conditions solves equation (3.15). Uniqueness is guaranteed by the unique solvability of (3.14) (provided by Theorem 3.1) and again by Lemma 3.3. □

### 3.4.2 Difficulties because of the Complex Notation

Although some might prefer to regard equation (3.3) in complex vector spaces, we will consider the real problem in the rest of this thesis, because the solution of (3.15) leads to some complications:

Denote by $\hat{\boldsymbol{u}} = (\hat{\boldsymbol{u}}_1, \hat{\boldsymbol{u}}_3, \ldots)$ the sequence of complex Fourier coefficients of $\boldsymbol{u}(\boldsymbol{x}, t)$, where we exploit the knowledge that $\hat{\boldsymbol{u}}_{2k} = 0$, $\forall\, k \in \mathbb{N}$ according to Theorem 3.2. We introduce the notation

$$\boldsymbol{H}_{\mathbf{curl}\,\boldsymbol{u}}(\mathbf{curl}\, \boldsymbol{w}) = \nu(|\mathbf{curl}\, \boldsymbol{u}|) \cdot \mathbf{curl}\, \boldsymbol{w}.$$

Accordingly, let $\hat{\boldsymbol{H}}_{k,\mathbf{curl}\,\boldsymbol{u}}(\mathbf{curl}\, \boldsymbol{w})$ be the $k$-th Fourier coefficient of $\boldsymbol{H}_{\mathbf{curl}\,\boldsymbol{u}}(\mathbf{curl}\, \boldsymbol{w})$ and let $\hat{\boldsymbol{H}}_{\mathbf{curl}\,\boldsymbol{u}}(\mathbf{curl}\, \boldsymbol{w})$ denominate the sequence of these coefficients.

Consider the nonlinear operator

$$\begin{aligned}\langle A_{\hat{\boldsymbol{u}}}(\hat{\boldsymbol{w}}), \hat{\boldsymbol{v}}\rangle = & \int_0^T \int_\Omega \sum_{k\in\mathbb{N}_{odd}} \hat{\boldsymbol{H}}_{k,\mathbf{curl}\,\boldsymbol{u}(t)}(\mathbf{curl}\,\boldsymbol{w}(t))\, e^{ik\omega t} \cdot \overline{\mathbf{curl} \sum_{l\in\mathbb{N}_{odd}} \hat{\boldsymbol{v}}_l\, e^{il\omega t}} + \\ & + i\omega\sigma \sum_{k\in\mathbb{N}_{odd}} k\hat{\boldsymbol{u}}_k\, e^{ik\omega t} \cdot \overline{\sum_{l\in\mathbb{N}_{odd}} \hat{\boldsymbol{v}}_l\, e^{il\omega t}}\, \mathrm{d}\boldsymbol{x}\, \mathrm{dt} = \\ = & T \int_\Omega \hat{\boldsymbol{H}}_{\mathbf{curl}\,\boldsymbol{u}(t)}(\mathbf{curl}\,\boldsymbol{w}(t)) \cdot \overline{\mathbf{curl}\,\hat{\boldsymbol{v}}} + i\omega\sigma \boldsymbol{D}\hat{\boldsymbol{u}} \cdot \overline{\hat{\boldsymbol{v}}}\, \mathrm{d}\boldsymbol{x},\end{aligned} \tag{3.16}$$

with the linear operator $\boldsymbol{D}$ defined by $\boldsymbol{D}\hat{\boldsymbol{u}} = (\hat{\boldsymbol{u}}_1, 3\hat{\boldsymbol{u}}_3, \ldots, k\hat{\boldsymbol{u}}_k, \ldots)$, and where by $\mathbb{N}_{odd}$ we mean the set of all odd numbers.

The usual approach for solving a nonlinear problem

$$\langle A_{\hat{\boldsymbol{u}}}(\hat{\boldsymbol{u}}), \hat{\boldsymbol{v}}\rangle = \langle F, \hat{\boldsymbol{v}}\rangle, \quad \forall\, \hat{\boldsymbol{v}}, \tag{3.17}$$

would be linearization. However, here this leads to the following difficulties:

- The operator $A : \hat{\boldsymbol{u}} \mapsto A_{\hat{\boldsymbol{u}}}(\hat{\boldsymbol{u}})$ is not differentiable, so we cannot apply the Newton method for the solution of (3.17). This method is locally superlinearly convergent (cf. Lemma 4.10) and thus would be the preferred way to solve the nonlinear problem.

- Another idea is the solution by means of a fixed point iteration. This seems well suited for our problem, since equation (2.17) is quasi-linear. Unfortunately, $A$ is not quasi-linear, and so the natural "linearization" $A_{\hat{\boldsymbol{u}}}(\hat{\boldsymbol{w}})$ is not linear in $\boldsymbol{w}$:

  The Fourier coefficient $\hat{\boldsymbol{H}}_{k,\mathbf{curl}\,\boldsymbol{u}}(\mathbf{curl}\,\boldsymbol{w})$ can be calculated by

  $$\hat{\boldsymbol{H}}_{k,\mathbf{curl}\,\boldsymbol{u}}(\mathbf{curl}\,\boldsymbol{w}) = \frac{1}{T}\int_0^T \nu(|\mathbf{curl}\,\boldsymbol{u}(t)|)\,\mathbf{curl}\,\boldsymbol{w}(t) \cdot e^{ik\omega t}\,\mathrm{dt}.$$

  This expression is not linear in the coefficients $\hat{\boldsymbol{w}}$, since for $\lambda \in \mathbb{C}$ with $\operatorname{Im}\lambda \neq 0$ we have

  $$\begin{aligned}&\int_0^T \nu(|\mathbf{curl}\,\boldsymbol{u}(t)|)\,\mathbf{curl}\,\mathrm{Re}\left(\sum_l (\lambda\hat{\boldsymbol{w}}_l)\, e^{il\omega t}\right) \cdot e^{ik\omega t}\,\mathrm{dt} \\ &\qquad\neq \lambda \int_0^T \nu(|\mathbf{curl}\,\boldsymbol{u}(t)|)\,\mathbf{curl}\,\mathrm{Re}\left(\sum_l \hat{\boldsymbol{w}}_l\, e^{il\omega t}\right) \cdot e^{ik\omega t}\,\mathrm{dt}.\end{aligned}$$

For these reasons, we prefer the notation with real coefficients $\boldsymbol{u}_k^c$ and $\boldsymbol{u}_k^s$. We will now derive the space-dependent equations that arise from this ansatz:

## 3.5 Time Discretization by means of a Multiharmonic Ansatz

For numerical calculations, we do not use the whole Fourier series, but only a finite sum

$$\boldsymbol{u}(\boldsymbol{x},t) \sim \sum_{k=0}^{N} \big[\boldsymbol{u}_k^c(\boldsymbol{x}) \cdot \cos(k\omega t) + \boldsymbol{u}_k^s(\boldsymbol{x}) \cdot \sin(k\omega t)\big]. \tag{3.18}$$

We use this so-called *multiharmonic ansatz* for the current source $\boldsymbol{f}$ and for the magnetic field $\boldsymbol{H}(\mathbf{curl}\,\boldsymbol{u})$ as well, i.e. we truncate the Fourier series expansion at the $N$-th coefficient. Consequently, the problem that we deal with reads

$$\begin{aligned}\mathbf{curl} \sum_{k=0}^{N} \big[\boldsymbol{H}_k^c(\mathbf{curl}\,\boldsymbol{u}) \cdot \cos(k\omega t) + \boldsymbol{H}_k^s(\mathbf{curl}\,\boldsymbol{u}) \cdot \sin(k\omega t)\big] + \\ + \omega\sigma \sum_{k=0}^{N} k\big[\boldsymbol{u}_k^s \cdot \cos(k\omega t) - \boldsymbol{u}_k^c \cdot \sin(k\omega t)\big] = \sum_{k=0}^{N} \big[\boldsymbol{f}_k^c \cdot \cos(k\omega t) + \boldsymbol{f}_k^s \cdot \sin(k\omega t)\big].\end{aligned} \tag{3.19}$$

We test this equation with $\cos(m\omega t)$ and $\sin(m\omega t)$ and integrate by $t$, taking advantage of the orthogonality

$$\begin{aligned}\frac{\omega}{\pi}\int_0^{\frac{2\pi}{\omega}} \cos(k\omega t)\cos(m\omega t)\,\mathrm{dt} &= \delta_{km},\\ \frac{\omega}{\pi}\int_0^{\frac{2\pi}{\omega}} \cos(k\omega t)\sin(m\omega t)\,\mathrm{dt} &= 0,\\ \frac{\omega}{\pi}\int_0^{\frac{2\pi}{\omega}} \sin(k\omega t)\sin(m\omega t)\,\mathrm{dt} &= \delta_{km}.\end{aligned}$$

Together with the fact that all even harmonics are zero (cf. Theorem 3.2), this leads to the following system of equations in space:

$$
\frac{\omega}{\pi}\int_0^{\frac{2\pi}{\omega}} (3.19) \cdot \begin{Bmatrix} \cos(m\omega t) \\ \sin(m\omega t) \end{Bmatrix} dt \Longrightarrow
$$

$$
\begin{aligned}
&\mathbf{curl} \begin{pmatrix} \boldsymbol{H}_1^c(\mathbf{curl}\,\boldsymbol{u}) \\ \boldsymbol{H}_1^s(\mathbf{curl}\,\boldsymbol{u}) \\ \vdots \\ \boldsymbol{H}_{2n+1}^c(\mathbf{curl}\,\boldsymbol{u}) \\ \boldsymbol{H}_{2n+1}^s(\mathbf{curl}\,\boldsymbol{u}) \end{pmatrix} + \\
&+ \omega\sigma \underbrace{\begin{pmatrix} 0 & 1 & & & \\ -1 & 0 & & & \\ & & \ddots & & \\ & & & 0 & 2n+1 \\ & & & -(2n+1) & 0 \end{pmatrix}}_{=:\boldsymbol{D}} \begin{pmatrix} \boldsymbol{u}_1^c \\ \boldsymbol{u}_1^s \\ \vdots \\ \boldsymbol{u}_{2n+1}^c \\ \boldsymbol{u}_{2n+1}^s \end{pmatrix} = \begin{pmatrix} \boldsymbol{f}_1^c \\ \boldsymbol{f}_1^s \\ \vdots \\ \boldsymbol{f}_{2n+1}^c \\ \boldsymbol{f}_{2n+1}^s \end{pmatrix},
\end{aligned} \tag{3.20}
$$

where we assume $N = 2n + 1$.
For the sake of better readability, we introduce the abbreviation $\boldsymbol{H} = (\boldsymbol{H}_1^c, \boldsymbol{H}_1^s, \ldots, \boldsymbol{H}_{2n+1}^s)^T$ for the Fourier coefficients of the magnetic field, and analogously we write $\boldsymbol{u}$ for $(\boldsymbol{u}_1^c, \ldots, \boldsymbol{u}_{2n+1}^s)^T$ and $\boldsymbol{f}$ for $(\boldsymbol{f}_1^c, \ldots, \boldsymbol{f}_{2n+1}^s)^T$. Now the problem that we have to solve, i.e. (3.20) together with homogeneous Dirichlet boundary conditions, can be written in a more compact way:

$$
\begin{aligned}
\mathbf{curl}\,\boldsymbol{H}(\mathbf{curl}\,\boldsymbol{u}) + \omega\sigma\,\boldsymbol{D}\,\boldsymbol{u} &= \boldsymbol{f}, && \text{in } \Omega, \\
\boldsymbol{u} \times \boldsymbol{n} &= 0, && \text{on } \Gamma,
\end{aligned} \tag{3.21}
$$

with the matrix $\boldsymbol{D}$ from (3.20).

# Chapter 4

# The Finite Element Method

The finite element method (FEM) is a powerful method for the numerical solution of partial differential equations.
In this chapter we summarize the main results of finite element analysis that will be needed for mathematical modeling of the inductive heating problem that we are concerned with. To give some ideas, we start with FEM for linear elliptic problems.
After that, we point out the most important properties of the edge-based Nédélec elements that we need for approximating $\boldsymbol{H}(\mathbf{curl})$.
The interested reader will find a more detailed introduction to the finite element method in [9, 11, 14, 29], for example.

After this part that deals with the discretization of the eddy current problem, we analyze the corresponding harmonic linear problem. Whereas the original variational equation is uniquely solvable only in the factor space of divergence-free functions,[1] we show that a slightly perturbed problem is uniquely solvable in the whole space $\boldsymbol{H}(\mathbf{curl})$. As a consequence, we solve the perturbed problem in our numerical calculations.

Finally, we turn to the nonlinear multiharmonic problem and show how to calculate the derivative of the nonlinear operator that we need for Newton's iteration.

## 4.1 Overview on the Method of Finite Elements

The finite element method is used to approximate the solution of boundary and initial value problems that are given in variational formulation over a space $V$. Because of this weak formulation, the solution appears in the integral of a quantity over a domain. This is a crucial property, because the integral of a measurable function over an arbitrary domain can be broken up into the sum of integrals over disjoint subdomains whose union is the original domain. Consequently, the analysis of a problem can be done locally.

[1]Compare the results of Chapter 2, notably Lemma 2.5 and Theorem 2.10.

On sufficiently small subdomains, the so-called finite elements, the solution is approximated by polynomial functions. Apparently, the quality of the approximation is enhanced with decreasing mesh size and with increasing degree of the polynomials. Accordingly, there are different ways for improving approximation: Whereas traditional theory mostly analyzes convergence on refinement of the mesh for a constant polynomial degree ($h$ version) (e.g. [9, 14]), there have been published many results on the augmentation of local refinement with ansatz functions of higher order ($hp$-FEM) in recent years (e.g. [5, 6, 36, 48, 49]).

**The weak formulation** Let $\Omega \subset \mathbb{R}^d$ be a sufficiently smooth domain. We assume a given problem in weak formulation, which is already homogenized, i.e. the Dirichlet boundary conditions are homogeneous. The problem can be stated in abstract form as follows:

$$\text{Find } u \in V: \quad a(u,v) = \langle F, v\rangle, \quad \forall\, v \in V. \tag{4.1}$$

For second-order problems, the space $V$ often is some subspace of $H^1(\Omega)$ that includes the homogeneous Dirichlet boundary conditions.[2] In our case the variational problem is defined in $\boldsymbol{H}(\mathbf{curl})$, and we have $\boldsymbol{V} = \{\boldsymbol{v} \in \boldsymbol{H}(\mathbf{curl}, \Omega) : \boldsymbol{v} \times \boldsymbol{n} = 0 \text{ on } \partial\Omega\} = \boldsymbol{H}_0(\mathbf{curl}, \Omega)$.

If $a(\cdot,\cdot)$ is bilinear, elliptic and continuous and if $F \in V^*$, existence and uniqueness of the solution of (4.1) is guaranteed by the Lax-Milgram theorem (Thm. 2.1).

**Discretization by the Galerkin method** The Galerkin method for approximating the solution of a variational problem consists in defining similar problems in finite-dimensional spaces $V_h$.
We only consider so-called *conforming* methods, i.e. methods where the discrete problem is stated in a subspace $V_h \subset V$.
The subscript $h$ is the discretization parameter and denotes that with $h \to 0$ we want to achieve convergence of the approximate solution $u_h \in V_h$ against the exact solution $u \in V$.

We state the discrete problem in $V_h \subset V$ as

$$\text{Find } u_h \in V_h: \quad a(u_h, v_h) = \langle F, v_h\rangle, \quad \forall\, v_h \in V_h. \tag{4.2}$$

Since we have $V_h \subset V$, Lax' and Milgram's theorem still holds for the discrete problem, i.e. there is a unique $u_h \in V_h$ solving (4.2).

We choose a basis $(p^{(i)})_{i\in\omega_h}$ of $V_h$ and can thus represent $u_h \in V_h$ by the linear combination

$$u_h = \sum_{i\in\omega_h} u^{(i)} p^{(i)}, \tag{4.3}$$

with $u^{(i)} \in \mathbb{R}$ (or $u^{(i)} \in \mathbb{C}$, if $V$ is a space over $\mathbb{C}$).

[2]For instance in the Poisson problem $-\Delta u = f$ in $\Omega$, $u = 0$ on $\partial\Omega$, we would have $V = H_0^1(\Omega)$.

Obviously, since $a(\cdot,\cdot)$ and $F$ are linear, the discrete problem (4.2) is fulfilled, if we have $a(u_h, p^{(j)}) = \langle F, p^{(j)}\rangle$ for all $j \in \omega_h$.
This leads to the *Galerkin system*

$$\text{Find } \underline{u}_h = (u^{(i)})_{i\in\omega_h} \in \mathbb{R}^{N_h} : K_h\,\underline{u}_h = \underline{f}_h, \tag{4.4}$$

with $N_h = \#\omega_h = \dim V_h$, $K_{h,ij} = a(p^{(j)}, p^{(i)})$, $\forall\, i,j \in \omega_h$ and $\underline{f}_{h,j} = \langle F, p^{(j)}\rangle$, $\forall\, j \in \omega_h$.

*Cea's Lemma* answers the natural question how well the solution of the discrete problem approximates the solution of the continuous problem: it states that the discretization error can be bounded by the approximation error, to wit by the distance between the function $u \in V$ and the subspace $V_h \subset V$.

**Lemma 4.1 (Cea [9]).** *Let $F \in V^*$ and suppose $a(\cdot,\cdot)$ is bilinear, elliptic and bounded:*

$$a(v,v) \geq \mu_1\|v\|^2,\ \forall\, v \in V \qquad \text{and} \qquad a(u,v) \leq \mu_2\|u\|\|v\|,\ \forall\, u,v \in V.$$

*Assume furthermore that $u \in V$ is the solution of* (4.1) *and $u_h \in V_h \subset V$ its approximation satisfying* (4.2).
*Then we have*

$$\|u - u_h\|_V \leq \frac{\mu_2}{\mu_1} \inf_{v_h \in V_h} \|u - v_h\|_V.$$

We have estimated the *discretization error* of the variational problem by the *best approximation error* to the continuous solution $u$. The next step is to find some estimate for the approximation error. This question can be decided by properties of the space $V_h$ and additional knowledge about the smoothness of the true solution.

**Finite element subspaces** The finite element method is a special case of the Galerkin method, i.e. a special choice of the subspaces $V_h$. The construction of the space $V_h$ is characterized by the following three basic aspects:

- First, a *triangulation* $\mathcal{T}_h$ is established over the given domain $\Omega \subset \mathbb{R}^d$, i.e. $\overline{\Omega}$ is written as a finite union of subdomains (called elements) $T \in \mathcal{T}_h$, in such a way that some properties are satisfied:

  1. $\forall\, T \in \mathcal{T}_h : T = \overline{T}$, $\mathring{T} \neq \emptyset$ and connected,
  2. $\forall\, T \in \mathcal{T}_h : \partial T$ is Lipschitz-continuous,
  3. $\bigcup\limits_{T\in\mathcal{T}_h} = \overline{\Omega}$,
  4. $\forall\, T_1, T_2 \in \mathcal{T}_h :\ T_1 \neq T_2 \ \Rightarrow\ T_1 \cap T_2 = \begin{cases} \emptyset, \\ \text{vertex}, \\ \text{edge}, \\ \text{face (if } d = 3). \end{cases}$

- Secondly, the functions $v_h \in V_h$ are *piecewise polynomials*, i.e. for each $T \in \mathcal{T}_h$, the spaces $P_T = \{v_{h|_T} : v_h \in V_h\}$ consist of polynomials.

- Thirdly, there should exist a basis in the space $V_h$ whose functions have *small supports.*

Many approximation estimates depend on properties of the triangulation such as *shape regularity.*

**Definition 4.1.** A family of triangulations $\{\mathcal{T}_h\}_h$ is called *shape regular* if there exists $\kappa > 0$ such that each $T \in \bigcup_h \mathcal{T}_h$ contains a sphere of radius $\rho_T$ with

$$\frac{h_T}{\rho_T} \leq \kappa,$$

where $h_T$ is the diameter of $T$.
A family of triangulations $\{\mathcal{T}_h\}_h$ is *quasi-uniform* if it is shape regular and there is a constant $\nu$ such that for all $\mathcal{T}_h$ we have

$$\frac{h}{h_T} \leq \nu, \quad \forall\, T \in \mathcal{T}_h,$$

where the mesh size $h$ is defined as $h = \max_{T\in\mathcal{T}_h} h_T$.

The following theorem provides estimates for the approximation error in the case of a smooth solution $u$ and for a shape regular triangulation. So together with Cea's Lemma (Lemma 4.1) it ensures convergence for $h \to 0$.

**Theorem 4.2 ([9]).** *Let $t \geq 2$ and $\mathcal{T}_h$ a shape regular triangulation of $\Omega$. Suppose $u \in H^t(\Omega)$. Then there exists a constant $c = c(\Omega, \kappa, t)$ such that*

$$\|u - I_h u\|_{m,h} \leq c \cdot h^{t-m} |u|_{t,\Omega}, \quad 0 \leq m \leq t, \tag{4.5}$$

*where $I_h : H^t(\Omega) \to V_h$ denotes the interpolation by piecewise polynomials of degree $t-1$ and the mesh dependent norm $\|\cdot\|_{m,h}$ is defined as follows:*

$$\|v\|_{m,h} := \sqrt{\sum_{T\in\mathcal{T}_h} \|v\|_{m,T}}. \tag{4.6}$$

*Example.* If we deal with a problem in $V = H_0^1(\Omega)$ with smooth solution $u \in H^2(\Omega)$, Theorem 4.2 and Cea's Lemma provide the estimate

$$\|u - u_h\|_1 \leq c \inf_{v_h\in V_h} \|u - v_h\|_1 \leq c\|u - I_h u\|_{1,h} \leq \tilde{c}h|u|_2,$$

for interpolation with piecewise linear functions. That means, if we choose polynomials of at least degree 1 as ansatz functions in the finite element space $V_h$, convergence is ensured.

Our case is slightly more difficult, because the problem that we are concerned with is defined in $\boldsymbol{H}(\mathbf{curl})$. Consequently, we need estimates for

$$\inf_{\boldsymbol{v}_h \in \boldsymbol{V}_h} \|\boldsymbol{u} - \boldsymbol{v}_h\|_{\boldsymbol{V}} = \inf_{\boldsymbol{v}_h \in \boldsymbol{V}_h} \left[ (\boldsymbol{u} - \boldsymbol{v}_h, \boldsymbol{u} - \boldsymbol{v}_h)^2_{\boldsymbol{L}_2} + (\mathbf{curl}\,(\boldsymbol{u} - \boldsymbol{v}_h), \mathbf{curl}\,(\boldsymbol{u} - \boldsymbol{v}_h))^2_{\boldsymbol{L}_2} \right]^{\frac{1}{2}}.$$

For this task we require the interpolation operator $\boldsymbol{\Pi}_h$ mapping adequately smooth functions into the Nédélec finite element space, which will be introduced in Section 4.2. Then we have the following result for a sufficiently smooth solution $\boldsymbol{u}$:

**Lemma 4.3.** *Let $\boldsymbol{u} \in \boldsymbol{H}^1(\Omega)$ with $\mathbf{curl}\,\boldsymbol{u} \in \boldsymbol{H}(\mathrm{div})$, suppose we have a shape regular triangulation $\mathcal{T}_h$ of $\Omega$. Then*

$$\|\boldsymbol{u} - \boldsymbol{\Pi}_h \boldsymbol{u}\|_{\boldsymbol{L}_2} \leq c \cdot h \, \|\boldsymbol{u}\|_{\boldsymbol{H}^1}.$$

*If moreover $\mathbf{curl}\,\boldsymbol{u} \in \boldsymbol{H}^1$, we have*

$$\|\mathbf{curl}\,(\boldsymbol{u} - \boldsymbol{\Pi}_h \boldsymbol{u})\|_{\boldsymbol{L}_2} \leq c \cdot h \, \|\mathbf{curl}\,\boldsymbol{u}\|_{\boldsymbol{H}^1}.$$

*Proof.* The proof can be found in [4], or – for the case of a Clément-type quasi interpolation operator – in [45]. □

## 4.2 Nédélec Elements for $\boldsymbol{H}(\mathbf{curl})$-Problems

Finally, we go into more detail and describe the finite element space $\boldsymbol{V}_h$ that we use to approximate $\boldsymbol{H}(\mathbf{curl}, \Omega)$.
One important property of $\boldsymbol{H}(\mathbf{curl})$, that will immediately give rise to ideas for discretization, is the following: If we have two adjacent domains $\Omega_1$ and $\Omega_2$ and a vector $\boldsymbol{p} \in \boldsymbol{H}(\mathbf{curl}, \Omega_1 \cup \Omega_2)$, then the tangential component of $\boldsymbol{p}$ is continuous along the interface between the two domains (e.g. [35]). Consequently, the degrees of freedom in the finite element space are exactly the tangential components of edges and faces (as well as interior moments for higher order elements).
Nédélec introduced these edge elements in [35]; see also [24] for the connection between conforming spaces for discretization of $\boldsymbol{H}(\mathbf{curl})$ and $\boldsymbol{H}(\mathrm{div})$ and differential forms.

Suppose we have a triangulation of $\Omega \subset \mathbb{R}^3$ consisting of closed tetrahedra, and fix an integer $k \geq 0$. We define $\boldsymbol{V}_h$ to be the Nédélec edge discretization of $\boldsymbol{H}(\mathbf{curl}, \Omega)$ of index $k$. That means, restricted to a tetrahedron $T$, the elements of $\boldsymbol{V}_h$ are functions of the form $\boldsymbol{p}(\boldsymbol{x}) + \boldsymbol{r}(\boldsymbol{x})$ with $\boldsymbol{p} \in \boldsymbol{\mathcal{P}}_k(T)$ and $\boldsymbol{r} \in \boldsymbol{\mathcal{P}}_{k+1}(T)$ such that $\boldsymbol{r} \cdot \boldsymbol{x} \equiv 0$.
The degrees of freedom of $\boldsymbol{v}_h \in \boldsymbol{V}_h$ are

- the moments of $\boldsymbol{v}_h \cdot \boldsymbol{s}$ of order at most $k$ on each edge, where $\boldsymbol{s}$ denotes the unit tangent vector to the edge,
- the moments of $\boldsymbol{v}_h \times \boldsymbol{n}$ of order at most $k-1$ on each face, where $\boldsymbol{n}$ is the normal to the face,

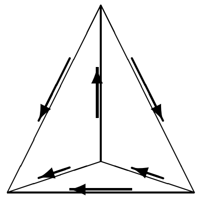

Figure 4.1: Degrees of freedom for the Nédélec edge discretization in the case $k = 0$.

- the moments of $\boldsymbol{v}_h$ of order at most $k-2$ on each tetrahedron.

In the lowest order case $k = 0$, the degrees of freedom for the space $\boldsymbol{V}_h$ are the tangential components of the edges, cf. Figure 4.1.
The finite element space $\boldsymbol{V}_h$ corresponding to the Nédélec edge discretization is conforming in the space $\boldsymbol{H}(\mathbf{curl})$ [35].

## 4.3 The Linear Problem

For the numerical solution of equation (3.21), we discretize the problem using the method of finite elements and solve the resulting system of nonlinear equations by means of Newton's method.
However, before we turn to the nonlinear problem, we will discuss the main features of the corresponding linear problem. For the sake of simplicity, we restrict ourselves to one harmonic in this section, i.e. we apply the ansatz

$$\boldsymbol{u}(\boldsymbol{x},t) = \boldsymbol{u}^c(\boldsymbol{x}) \cdot \cos(\omega t) + \boldsymbol{u}^s(\boldsymbol{x}) \cdot \sin(\omega t),$$

to the problem

$$\mathbf{curl}\,(\nu\,\mathbf{curl}\,\boldsymbol{u}) + \sigma \frac{\partial \boldsymbol{u}}{\partial t} = \boldsymbol{f},$$

with homogeneous Dirichlet boundary conditions. We suppose that the reluctivity $\nu = \nu(\boldsymbol{x})$ does not depend on the induction $\boldsymbol{B} = \mathbf{curl}\,\boldsymbol{u}$.
As we have seen in Chapter 3, this leads to the following equation:

$$\int_\Omega \nu\,\mathbf{curl}\,(\boldsymbol{v}^c,\boldsymbol{v}^s)\mathbf{curl}\begin{pmatrix}\boldsymbol{u}^c\\ \boldsymbol{u}^s\end{pmatrix} + \omega\sigma(\boldsymbol{v}^c,\boldsymbol{v}^s)\begin{pmatrix}0 & 1\\ -1 & 0\end{pmatrix}\begin{pmatrix}\boldsymbol{u}^c\\ \boldsymbol{u}^s\end{pmatrix}\,\mathrm{d}\boldsymbol{x} = \\ = \int_\Omega (\boldsymbol{v}^c,\boldsymbol{v}^s)\begin{pmatrix}\boldsymbol{f}^c\\ \boldsymbol{f}^s\end{pmatrix}\mathrm{d}\boldsymbol{x}, \quad \forall \begin{pmatrix}\boldsymbol{v}^c\\ \boldsymbol{v}^s\end{pmatrix} \in \boldsymbol{H}_0(\mathbf{curl})^2. \tag{4.7}$$

In Theorem 3.1 we have shown that there exists a unique divergence-free periodic steady state solution of the eddy current problem (2.17). Since for linear problems and harmonic source current, this solution obviously depends only on the base frequency, equation (4.7) is uniquely solvable in the space of divergence-free functions.
Anyhow, we will show existence and uniqueness of this linear problem again by employing the knowledge about mixed finite element methods and saddle point problems.

### 4.3.1 Mixed Problems

Mixed finite element methods are concerned with the solution of problems of the following form:

$$\begin{aligned}
&\text{Find } (u,\phi) \in V \times W: \\
&a(u,v) + b(v,\phi) = \langle F, v\rangle, \qquad \forall\, v \in V, \\
&b(u,\psi) = \langle G, \psi\rangle, \qquad \forall\, \psi \in W.
\end{aligned} \tag{4.8}$$

We introduce the space

$$V_b := \{v \in V : b(v,\psi) = 0,\ \forall\, \psi \in W\}. \tag{4.9}$$

*Remark* 4.1. Note that, if a pair $(u,\phi)$ satisfies (4.8) with $G = 0$, then the first argument $u$ obviously is a solution of the variational problem

$$\text{Find } u \in V_b: \ a(u,v) = \langle F, v\rangle, \quad \forall\, v \in V_b. \tag{4.10}$$

The following theorem answers the question about unique solvability of the mixed problem (4.8):

**Theorem 4.4 ([12]).** *Suppose that the bilinear form $a(\cdot,\cdot)$ is continuous on $V \times V$ and $V_b$-elliptic, i.e.*

$$\exists\, \alpha > 0: \ a(v,v) \geq \alpha \|v\|_V^2, \quad \forall\, v \in V_b.$$

*Assume moreover that the bilinear form $b(\cdot,\cdot)$ is continuous on $V \times W$ and that it satisfies the so-called* inf-sup-condition

$$\exists\, \beta > 0: \ \inf_{\psi \in W,\, \psi \neq 0} \ \sup_{v \in V,\, v \neq 0} \frac{b(v,\psi)}{\|v\|_V \|\psi\|_W} \geq \beta.$$

*Then, for each $F \in V^*$ and $G \in W^*$, problem* (4.8) *has a unique solution.*

We now want to rewrite the variational equation (4.7) as an equivalent saddle point problem. For this task, we define $\boldsymbol{V} := \boldsymbol{H}_0(\mathbf{curl})^2$ and, as in Chapter 2, the space of all gradient fields in the general multiply connected domain $\Omega$:[3]

$$\tilde{\boldsymbol{W}} := \{\boldsymbol{w} = \mathbf{grad}\,\phi : \phi \in H^1(\Omega) \text{ and } \phi = c_i \text{ on } \Gamma_i,\ 1 \leq i \leq p\}, \tag{4.11}$$

$$\boldsymbol{W} := \tilde{\boldsymbol{W}}^2. \tag{4.12}$$

If we define the bilinear form $b(\cdot,\cdot)$ as

$$b(\boldsymbol{v},\boldsymbol{\phi}) := \int_\Omega (\boldsymbol{v}^c, \boldsymbol{v}^s) \begin{pmatrix} \boldsymbol{\phi}^c \\ \boldsymbol{\phi}^s \end{pmatrix} \mathrm{d}\boldsymbol{x}, \quad \forall\, \boldsymbol{v} \in \boldsymbol{V},\ \boldsymbol{\phi} \in \boldsymbol{W}, \tag{4.13}$$

the space $\boldsymbol{V}_b$ (4.9) introduced for the analysis of mixed finite element methods equals exactly the space of all weakly divergence-free functions in $\boldsymbol{V} = \boldsymbol{H}_0(\mathbf{curl})^2$. As we

[3]Compare the definition (2.28) on page 20 (Chapter 2).

have seen in the discussion about existence and uniqueness in Chapter 2, this space is essential for eddy current problems, since in non-conducting regions uniqueness can only be guaranteed up to the set of gradient fields.

Let us now define

$$a(\boldsymbol{u}, \boldsymbol{v}) := \int_\Omega \nu \,\mathbf{curl}\,(\boldsymbol{v}^c, \boldsymbol{v}^s)\,\mathbf{curl} \begin{pmatrix} \boldsymbol{u}^c \\ \boldsymbol{u}^s \end{pmatrix} + \omega\sigma(\boldsymbol{v}^c, \boldsymbol{v}^s) \begin{pmatrix} 0 & 1 \\ -1 & 0 \end{pmatrix} \begin{pmatrix} \boldsymbol{u}^c \\ \boldsymbol{u}^s \end{pmatrix} \mathrm{d}\boldsymbol{x}, \tag{4.14}$$

for $\boldsymbol{u}, \boldsymbol{v} \in \boldsymbol{V}$, and consider the mixed formulation

$$\begin{aligned} a(\boldsymbol{u}, \boldsymbol{v}) + b(\boldsymbol{v}, \boldsymbol{\phi}) &= \int_\Omega (\boldsymbol{v}^c, \boldsymbol{v}^s) \begin{pmatrix} \boldsymbol{f}^c \\ \boldsymbol{f}^s \end{pmatrix} \mathrm{d}\boldsymbol{x}, && \forall\, \boldsymbol{v} \in \boldsymbol{V}, \\ b(\boldsymbol{u}, \boldsymbol{\psi}) &= 0, && \forall\, \boldsymbol{\psi} \in \boldsymbol{W}. \end{aligned} \tag{4.15}$$

For the following, we denote the right hand side of the first equation, $\int \boldsymbol{v}^T \boldsymbol{f}$, by $\langle F, \boldsymbol{v} \rangle$.

By Remark 4.1 we know that, if the pair $(\boldsymbol{u}, \boldsymbol{\phi}) \in \boldsymbol{V} \times \boldsymbol{W}$ satisfies (4.15), $\boldsymbol{u}$ is a solution of equation (4.7) with test functions $\boldsymbol{v} \in \boldsymbol{V}_b$. However, since the source current is divergence-free, i.e. $(\boldsymbol{f}, \boldsymbol{\psi})_{\boldsymbol{L}_2} = 0$, $\forall\, \boldsymbol{\psi} \in \boldsymbol{W}$, $\boldsymbol{u}$ also satisfies equation (4.7) for gradient fields as test functions, as can easily be seen.
On the other hand, if we have a divergence-free solution $\boldsymbol{u}$ of (4.7), obviously the pair $(\boldsymbol{u}, 0)$ solves problem (4.15).
In this sense, the mixed problem (4.15) and the equation (4.7) (in the space of solenoidal functions $\boldsymbol{V}_b$) are equivalent.

Finally, we will show that the assumptions of Theorem 4.4 are fulfilled, i.e. that equation (4.15) is uniquely solvable.

**Lemma 4.5.** *The mixed problem* (4.15) *has a unique solution* $(\boldsymbol{u}, \boldsymbol{\phi}) \in \boldsymbol{V} \times \boldsymbol{W}$*, where moreover, we have* $\boldsymbol{u} \in \boldsymbol{V}_b$*, i.e.* $\boldsymbol{u}$ *is divergence-free, and* $\boldsymbol{\phi} = 0$*.*

*Proof.* The proof splits in two parts: First, we show the assumptions of Thm. 4.4, and secondly, we prove the additional properties of the solution.

1. *Existence and uniqueness.*
   Obviously, $a(\cdot, \cdot)$ is bilinear and continuous. $\boldsymbol{V}_b$ - ellipticity follows from the norm equivalence $\int |\mathbf{curl}\,\cdot|^2 \simeq \|\cdot\|^2_{\boldsymbol{H}(\mathbf{curl})}$ in the space of divergence-free functions $\boldsymbol{V}_b$ (cf. Lemma 2.4 and Remark 2.3).

   Remains to show the inf-sup-condition:
   Let $\boldsymbol{\psi} \in \boldsymbol{W}$ be given. We have to find $\boldsymbol{v} \in \boldsymbol{V}$ such that

   $$b(\boldsymbol{v}, \boldsymbol{\psi}) = \int_\Omega \boldsymbol{v}^T \boldsymbol{\psi}\, \mathrm{d}\boldsymbol{x} \leq \beta \|\boldsymbol{v}\|_{\boldsymbol{V}} \|\boldsymbol{\psi}\|_{\boldsymbol{W}}.$$

   Choose $\boldsymbol{v} = \boldsymbol{\psi}$. This choice is possible because $\boldsymbol{\psi} \in \boldsymbol{H}_0(\mathbf{curl})^2 = \boldsymbol{V}$: Firstly, $\mathbf{curl}\,\boldsymbol{\psi} = 0$ and thus $\boldsymbol{\psi} \in \boldsymbol{H}(\mathbf{curl})^2$, and secondly, since $\boldsymbol{\psi} = \mathbf{grad}\,(\phi^1, \phi^2)^T$

with $\phi^j = c_i^j$ on $\Gamma_i$, the tangential component $\boldsymbol{\psi} \times \boldsymbol{n}$ obviously equals zero on $\Gamma_i$, what implies $\boldsymbol{\psi} \in \boldsymbol{V}$. Finally we have

$$\|\boldsymbol{\psi}\|_{\boldsymbol{V}} \|\boldsymbol{\psi}\|_{\boldsymbol{W}} = \left(\|\boldsymbol{\psi}\|_{\boldsymbol{L}_2}^2 + \|\mathbf{curl}\,\boldsymbol{\psi}\|_{\boldsymbol{L}_2}^2\right)^{\frac{1}{2}} \|\boldsymbol{\psi}\|_{\boldsymbol{L}_2} = \|\boldsymbol{\psi}\|_{\boldsymbol{L}_2}^2 = b(\boldsymbol{\psi}, \boldsymbol{\psi}),$$

thus the inf-sup-condition is fulfilled with $\beta = 1$.

2. *Additional properties.*
The second part of (4.15), $b(\boldsymbol{u}, \boldsymbol{\psi}) = 0,\ \forall\, \boldsymbol{\psi} \in \boldsymbol{W}$, is the defining equation of $\boldsymbol{u} \in \boldsymbol{V}_b$, so this property is clear.

It is easy to see that $(\boldsymbol{u}, 0)$ solves (4.15). Consequently, due to the uniqueness, we have $\boldsymbol{\phi} = 0$.

□

By the discussion on equivalence between the mixed problem (4.15) and the variational equation (4.7), we have the following corollary:

**Corollary 4.6.** *Problem* (4.7) *is uniquely solvable in the space of weakly divergence-free functions $\boldsymbol{V}_b$, even with test functions $\boldsymbol{v} \in \boldsymbol{V} = \boldsymbol{H}_0(\mathbf{curl})^2$.*

### 4.3.2 The Perturbed Problem

For the numerical solution of the variational equation (4.7), one can try to tackle the problem in the factor space $\boldsymbol{V}/\boldsymbol{W}$, or work with the saddle point problem (4.15).
However, we prefer to follow a different approach: We slightly perturb the problem by introducing a small regularization parameter $\epsilon > 0$ in the non-conducting regions, more precisely by replacing the conductivity coefficient $\sigma$ by

$$\sigma_\epsilon(\boldsymbol{x}) = \max\{\sigma(\boldsymbol{x}), \epsilon\}. \tag{4.16}$$

This perturbed problem is uniquely solvable not only in $\boldsymbol{V}_b = \boldsymbol{H}_0(\mathbf{curl})^2/\boldsymbol{W}$, but the solution is unique in the whole space $\boldsymbol{H}_0(\mathbf{curl})^2$. Of course, we expect this uniqueness by the discussion and results on conducting regions in Chapter 2 (cf. Corollary 2.8 and 2.11), but naturally we will prove this property of the linear problem (4.7) arising from the harmonic ansatz.
First, though, we point out that the perturbed problem is close to the original equation and that its solution converges to the original solution for $\epsilon \to 0$. In order to clarify this proposition, we define the bilinear form

$$a_\epsilon(\boldsymbol{u}, \boldsymbol{v}) := \int_\Omega \nu\, \mathbf{curl}\,(\boldsymbol{v}^c, \boldsymbol{v}^s)\, \mathbf{curl} \begin{pmatrix} \boldsymbol{u}^c \\ \boldsymbol{u}^s \end{pmatrix} + \omega \sigma_\epsilon (\boldsymbol{v}^c, \boldsymbol{v}^s) \begin{pmatrix} 0 & 1 \\ -1 & 0 \end{pmatrix} \begin{pmatrix} \boldsymbol{u}^c \\ \boldsymbol{u}^s \end{pmatrix} \mathrm{d}\boldsymbol{x}. \tag{4.17}$$

The perturbed problem

$$\begin{array}{lcll} \text{Find } (\boldsymbol{u}_\epsilon, \boldsymbol{\phi}_\epsilon) \in \boldsymbol{V} \times \boldsymbol{W} : & & & \\ a_\epsilon(\boldsymbol{u}_\epsilon, \boldsymbol{v}) + b(\boldsymbol{v}, \boldsymbol{\phi}_\epsilon) & = & \langle F, \boldsymbol{v} \rangle, & \forall\, \boldsymbol{v} \in \boldsymbol{V}, \\ b(\boldsymbol{u}_\epsilon, \boldsymbol{\psi}) & = & 0, & \forall\, \boldsymbol{\psi} \in \boldsymbol{W}, \end{array} \tag{4.18}$$

with the linear form $F$ as in (4.15), satisfies the assumptions of Theorem 4.4 and thus is well posed in $\boldsymbol{H}_0(\mathbf{curl})^2 \times \boldsymbol{W}$, just like the original problem (4.15).

For elliptic variational problems, the situation of a perturbed bilinear form is covered by Strang's Lemmata on variational crimes [50]. These can be generalized to mixed problems, what provides an estimate of the error $\|\boldsymbol{u} - \boldsymbol{u}_\epsilon\|$:

**Lemma 4.7.** *Suppose that both the problem* (4.8) *and the problem*

$$\begin{array}{lcll} a_\epsilon(u_\epsilon, v) + b(v, \phi_\epsilon) & = & \langle F, v\rangle, & \forall\, v \in V, \\ b(u_\epsilon, \psi) & = & 0, & \forall\, \psi \in W, \end{array} \tag{4.19}$$

*with a perturbed bilinear form $a_\epsilon(\cdot,\cdot)$ satisfy the assumptions of Theorem 4.4. Then there exists a constant $C$ such that*

$$\|u - u_\epsilon\|_V \le C \inf_{v \in V_b} \left( \|u - v\|_V + \sup_{w \in V_b} \frac{a(v,w) - a_\epsilon(v,w)}{\|w\|_V} \right),$$

*where $u$ is the solution of* (4.8) *and $u_\epsilon$ the solution of* (4.19).

*Proof.* By the assumptions, we know

$$a_\epsilon(v,v) \ge \alpha_\epsilon \|v\|_V^2, \quad \forall\, v \in V_b, \tag{4.20}$$

for some $\alpha_\epsilon > 0$, and

$$a(u,v) \le \mu \|u\|_V \|v\|_V, \quad \forall\, u, v \in V,$$

for a constant $\mu$. Obviously,

$$\|u - u_\epsilon\|_V \le \|u - v\|_V + \|v - u_\epsilon\|_V, \tag{4.21}$$

for arbitrary $v \in V_b$. Define $w := u_\epsilon - v \in V_b$. Then we have

$$\begin{aligned} \alpha_\epsilon \|u_\epsilon - v\|_V^2 &\le a_\epsilon(u_\epsilon - v, w) = \\ &= \underbrace{a_\epsilon(u_\epsilon, w)}_{=\langle F,w\rangle} - a_\epsilon(v,w) + a(u - v, w) - \underbrace{a(u,w)}_{=\langle F,w\rangle} + a(v,w) \le \\ &\le a(v,w) - a_\epsilon(v,w) + \mu \|u - v\|_V \|w\|_V. \end{aligned}$$

Dividing by $\|w\| = \|u_\epsilon - v\|$ and $\alpha_\epsilon$ and taking the supremum over all $w \in V_b$ leads to

$$\|u_\epsilon - v\|_V \le \frac{\mu}{\alpha_\epsilon} \|u - v\|_V + \frac{1}{\alpha_\epsilon} \sup_{w \in V_b} \frac{a(v,w) - a_\epsilon(v,w)}{\|w\|_V}, \quad \forall\, v \in V_b. \tag{4.22}$$

The combination of (4.21) and (4.22) yields the desired result

$$\|u - u_\epsilon\| \le \inf_{v \in V_b} \left( (1 + \frac{\mu}{\alpha_\epsilon}) \|u - v\|_V + \frac{1}{\alpha_\epsilon} \sup_{w \in V_b} \frac{a(v,w) - a_\epsilon(v,w)}{\|w\|_V} \right),$$

so the lemma is proved with $C = \max\{(1 + \frac{\mu}{\alpha_\epsilon}), \frac{1}{\alpha_\epsilon}\}$. ∎

*Remark* 4.2. The constant $C$ in Lemma 4.7 depends on $\alpha_\epsilon$, the $V_b$-ellipticity constant of the perturbed bilinear form $a_\epsilon(\cdot,\cdot)$ (4.20). We emphasize that in our case, i.e. with $a_\epsilon(\cdot,\cdot)$ as defined in (4.17), $\alpha_\epsilon$ does not depend on $\epsilon$, since we have

$$\begin{aligned} a_\epsilon(\boldsymbol{v},\boldsymbol{v}) &= \int_\Omega \nu\,|\mathbf{curl}\,\boldsymbol{v}|^2 + \omega\sigma_\epsilon(\boldsymbol{v}^c\boldsymbol{v}^s - \boldsymbol{v}^s\boldsymbol{v}^c)\,\mathrm{d}\boldsymbol{x} = \\ &= \int_\Omega \nu\,|\mathbf{curl}\,\boldsymbol{v}|^2\,\mathrm{d}\boldsymbol{x} \geq c\,\|\boldsymbol{v}\|_{\boldsymbol{V}}^2, \qquad \forall\,\boldsymbol{v}\in\boldsymbol{V}_b. \end{aligned} \tag{4.23}$$

Indeed, in the space of divergence-free functions $\boldsymbol{V}_b$ we have equivalence between the seminorm $\|\mathbf{curl}\,\boldsymbol{v}\|_{\boldsymbol{L}_2}$ and the full norm $\|\boldsymbol{v}\|_{\boldsymbol{V}} = \left(\|\boldsymbol{v}\|_{\boldsymbol{L}_2}^2 + \|\mathbf{curl}\,\boldsymbol{v}\|_{\boldsymbol{L}_2}^2\right)^{\frac{1}{2}}$ according to Lemma 2.4 and Remark 2.3. Since $\nu$ is assumed to be bounded from below, i.e. $\nu(\boldsymbol{x}) \geq \underline{\nu} > 0$ almost everywhere, the estimate (4.23) holds.

*Remark* 4.3. As a consequence, the solution of the corresponding variational problem

$$\text{Find } \boldsymbol{u}_\epsilon \in \boldsymbol{V}_b: \quad a_\epsilon(\boldsymbol{u}_\epsilon,\boldsymbol{v}) = \langle F,\boldsymbol{v}\rangle, \quad \forall\,\boldsymbol{v}\in\boldsymbol{V} = \boldsymbol{H}(\mathbf{curl})^2,$$

converges to the solution of (4.7) for $\epsilon \to 0$.
This is due to the fact that the difference between perturbed and original bilinear form can be easily estimated in the following way:

$$\begin{aligned} |a(\boldsymbol{v},\boldsymbol{w}) - a_\epsilon(\boldsymbol{v},\boldsymbol{w})| &= \left|\int_\Omega \omega(\sigma-\sigma_\epsilon)(\boldsymbol{v}^c,\boldsymbol{v}^s)\begin{pmatrix} 0 & 1 \\ -1 & 0 \end{pmatrix}\begin{pmatrix}\boldsymbol{w}^c \\ \boldsymbol{w}^s\end{pmatrix}\mathrm{d}\boldsymbol{x}\right| \leq \\ &\leq \epsilon\omega\,\|\boldsymbol{v}\|_{\boldsymbol{L}_2}\,\|\boldsymbol{w}\|_{\boldsymbol{L}_2}. \end{aligned}$$

With this estimate and the knowledge that $\boldsymbol{u}\in\boldsymbol{V}_b$ (cf. Lemma 4.5), we have

$$\begin{aligned} \|\boldsymbol{u}-\boldsymbol{u}_\epsilon\|_{\boldsymbol{V}} &\leq C\inf_{\boldsymbol{v}\in\boldsymbol{V}_b}\left(\|\boldsymbol{u}-\boldsymbol{v}\|_{\boldsymbol{V}} + \sup_{\boldsymbol{w}\in\boldsymbol{V}_b}\frac{\epsilon\omega\,\|\boldsymbol{v}\|_{\boldsymbol{L}_2}\,\|\boldsymbol{w}\|_{\boldsymbol{L}_2}}{\|\boldsymbol{w}\|_{\boldsymbol{V}}}\right) \leq \\ &\leq \epsilon\,\omega\,C\|\boldsymbol{u}\|_{\boldsymbol{L}_2}, \end{aligned}$$

according to Lemma 4.7, so convergence for $\epsilon \to 0$ is ensured.

Ultimately, we show that the perturbed problem is uniquely solvable in $\boldsymbol{H}(\mathbf{curl})^2$:

**Lemma 4.8.** *There exists a unique solution $\boldsymbol{u}_\epsilon\in\boldsymbol{V}$ of the variational equation*

$$a_\epsilon(\boldsymbol{u}_\epsilon,\boldsymbol{v}) = \langle F,\boldsymbol{v}\rangle, \quad \forall\,\boldsymbol{v}\in\boldsymbol{V}, \tag{4.24}$$

*and $\boldsymbol{u}_\epsilon$ is divergence-free, i.e. $\boldsymbol{u}_\epsilon\in\boldsymbol{V}_b$.*

*Proof.* Existence of a solution $\boldsymbol{u}_\epsilon\in\boldsymbol{V}_b$ and uniqueness in $\boldsymbol{V}_b$ is guaranteed by the equivalence with the mixed problem. Suppose now that $\tilde{\boldsymbol{u}} = \boldsymbol{u}_\epsilon + \boldsymbol{w}$ solves (4.24) for some $\boldsymbol{w}\in\boldsymbol{W}$. Then we have

$$0 = a_\epsilon(\boldsymbol{u}_\epsilon+\boldsymbol{w},\boldsymbol{v}) - \langle F,\boldsymbol{v}\rangle = a_\epsilon(\boldsymbol{u}_\epsilon,\boldsymbol{v}) + a_\epsilon(\boldsymbol{w},\boldsymbol{v}) - \langle F,\boldsymbol{v}\rangle = a_\epsilon(\boldsymbol{w},\boldsymbol{v}), \quad \forall\,\boldsymbol{v}\in\boldsymbol{V}.$$

For gradient fields $\boldsymbol{w} \in \boldsymbol{W}$, $a_\epsilon(\boldsymbol{w}, \boldsymbol{v})$ reduces to

$$\int_\Omega \omega\sigma_\epsilon(\boldsymbol{w}^c\boldsymbol{v}^s - \boldsymbol{w}^s\boldsymbol{v}^c)\,\mathrm{d}\boldsymbol{x}.$$

Since $\omega \neq 0$ and $\sigma_\epsilon(\boldsymbol{x}) \neq 0$, $\forall\,\boldsymbol{x}$,

$$a_\epsilon(\boldsymbol{w}, \boldsymbol{v}) = 0, \quad \forall\,\boldsymbol{v} \in \boldsymbol{V},$$

implies $\boldsymbol{w} = 0$. Consequently, $\boldsymbol{u}_\epsilon$ is unique in $\boldsymbol{V} = \boldsymbol{H}_0(\mathbf{curl})^2$. □

The results of this section, especially the Lemmata 4.7 and 4.8, motivate and justify our procedure of solving a perturbed problem with conductivity $\sigma_\epsilon$ instead of $\sigma$.

### 4.3.3 Preconditioning

For some given finite element space $\boldsymbol{V}_h$, the discretization of the perturbed linear harmonic problem leads to a system of the form

$$\underbrace{\begin{pmatrix} A & M \\ -M & A \end{pmatrix}}_{=:K} \begin{pmatrix} u^c \\ u^s \end{pmatrix} = \begin{pmatrix} f^c \\ f^s \end{pmatrix}. \tag{4.25}$$

Here the matrix $A = A_h$ is the discretization of the operator

$$\langle A\boldsymbol{u}, \boldsymbol{v}\rangle = \int_\Omega \nu\,\mathbf{curl}\,\boldsymbol{v}^T\mathbf{curl}\,\boldsymbol{u}\,\mathrm{d}\boldsymbol{x},$$

and $M = M_h$ results from

$$\langle M\boldsymbol{u}, \boldsymbol{v}\rangle = \int_\Omega \omega\sigma_\epsilon\,\boldsymbol{v}^T\boldsymbol{u}\,\mathrm{d}\boldsymbol{x},$$

where in (4.25) as well as in the sequel we omit the subscript $h$.
By $u^c \in \mathbb{R}^n$ we mean the discretization of $\boldsymbol{u}^c$, and analogously for $u^s$, $f^c$ and $f^s$.

Before we remark on the solution of the system (4.25), we point out that on refinement of the discretization, the condition number of the matrix $K$ in (4.25) deteriorates: We have

$$\kappa(K) = \mathcal{O}(h^{-2}),$$

where $h$ is the mesh size and the condition number is defined as $\kappa(K) := \|K\| \cdot \|K^{-1}\|$ with an arbitrary (fixed) matrix norm $\|\cdot\|$ in $\mathbb{R}^{2n\times 2n}$.

For the solution of large linear systems, iterative solvers seem to be most appropriate. Their convergence speed, however, depends strongly on the spectrum of the system matrix.
In the case of a symmetric system, the condition number $\kappa$ reveals the essential structure of the spectrum and consequently provides information about the convergence of

an iterative solver. The issue is more complicated for non-symmetric matrices, since they generally have complex eigenvalues, wherefore the condition number is not fully sufficient to illustrate the distribution of the eigenvalues.
Anyhow, even for non-symmetric problems, the condition number hints on the convergence properties of iterative solvers.

Since the dimension of the finite element space and consequently the condition number $\kappa(K)$ can be fairly large, *preconditioning* is vital in order to keep the number of steps in the iterative solution at an acceptable level.
The essence of preconditioning is to construct a matrix $C$ such that the operation

$$w = C^{-1}d \tag{4.26}$$

can be carried out at low computational costs, and such that at the same time $C$ approximates the system matrix $K$: We want to achieve

$$\kappa(C^{-1}K) = \text{const},$$

or even better, the eigenvalues of $C^{-1}K$ should cluster around 1.

In this context, the question arises how to choose $C$. Multigrid methods (cf. Chapter 5) have proven to yield good preconditioners, while the computational work in their application (4.26) is of optimal order, namely proportional to the number of unknowns. Since multigrid theory mostly deals with symmetric problems, we prefer to apply a multigrid iteration to a symmetric system and by this means construct a preconditioner for the non-symmetric system $K$ as defined in (4.25).
More precisely, we propose to choose $C$ by

$$C^{-1} = \frac{1}{2}\begin{pmatrix} (A+M)^{-1} & 0 \\ 0 & (A+M)^{-1} \end{pmatrix}\begin{pmatrix} I & I \\ I & -I \end{pmatrix}, \tag{4.27}$$

where the inverse of $A+M$ is approximated by a symmetric multigrid iteration (e.g. [28, 30]).

This choice is justified because we can show that for exact inversion of $A+M$, the condition number is bounded by 2.

**Lemma 4.9.** *With $K \in \mathbb{R}^{2n\times 2n}$ defined as in* (4.25) *and $C^{-1}$ as in* (4.27)*, we have*

$$\kappa(C^{-1}K) \leq 2,$$

*if we choose the vector norm in $\mathbb{R}^{2n}$ by $\|u\|_{A+M} = \|(u^c, u^s)^T\|_{A+M} := \big[\big((A+M)u^c, u^c\big) + \big((A+M)u^s, u^s\big)\big]^{\frac{1}{2}}$.*

*Proof.* In the following, we refer to $(u^c, u^s)^T \in \mathbb{R}^{2n}$ by $u$. We introduce – both for $v \in \mathbb{R}^n$ and $v \in \mathbb{R}^{2n}$ – the abbreviation $(v, v)_1 := (v, v)_{A+M} = ((A+M)v, v)$, where $(\cdot,\cdot)$ denotes the Euclidean scalar product. The same notation is used for the norm.

The condition number is calculated by

$$\kappa(C^{-1}K) = \|C^{-1}K\|_1 \cdot \|(C^{-1}K)^{-1}\|_1. \tag{4.28}$$

The first factor equals

$$\|C^{-1}K\|_1 = \sup_u \frac{\|C^{-1}Ku\|_1}{\|u\|_1} = \sup_{u,v} \frac{(C^{-1}Ku, v)_1}{\|u\|_1\|v\|_1},$$

and we have

$$(C^{-1}Ku, v)_1 = ((A + M)C^{-1}Ku, v) = (Bu, v), \tag{4.29}$$

with the matrix

$$B = \frac{1}{2}\begin{pmatrix} A - M & A + M \\ A + M & M - A \end{pmatrix}.$$

Consequently, (4.29) is bounded from above by $\|u\|_1 \cdot \|v\|_1$, since

$$(Bu, v) = \frac{1}{2}\big[((A - M)u^c, v^c) + (u^s, v^c)_1 + (u^c, v^s)_1 + ((M - A)u^s, v^s)\big], \tag{4.30}$$

and because an elementary discussion shows

$$\begin{aligned}(4.30) &\le \frac{1}{2}\big[\|u^c\|_1\,\|v^c\|_1 + \|u^s\|_1\,\|v^c\|_1 + \|u^c\|_1\,\|v^s\|_1 + \|u^s\|_1\,\|v^s\|_1\big] \\ &\le \Big[\|u^c\|_1^2 + \|u^s\|_1^2\Big]^{\frac{1}{2}} \cdot \Big[\|v^c\|_1^2 + \|v^s\|_1^2\Big]^{\frac{1}{2}} = \|u\|_1 \cdot \|v\|_1.\end{aligned}$$

So we have $\|C^{-1}K\|_1 \le 1$. Remains to analyze the second term in (4.28):

$$\|(C^{-1}K)^{-1}\|_1 = \sup_u \frac{\|u\|_1}{\|C^{-1}Ku\|_1}, \tag{4.31}$$

and

$$\|C^{-1}Ku\|_1 = \sup_v \frac{(C^{-1}Ku, v)_1}{\|v\|_1} = \sup_v \frac{(Bu, v)}{\|v\|_1} \ge \frac{\big(B\binom{u^c}{u^s}, \binom{u^s}{u^c}\big)}{\|u\|_1}.$$

Simple calculation yields $\big(B\binom{u^c}{u^s}, \binom{u^s}{u^c}\big) = \frac{1}{2}\|u\|_1^2$ and consequently (4.31) $\le$ 2. So altogether we have the result

$$\kappa(C^{-1}K) = \|C^{-1}K\|_1 \cdot \|(C^{-1}K)^{-1}\|_1 \le 1 \cdot 2 = 2.$$

□

As mentioned above, for non-symmetric problems the condition number is not fully sufficient to illustrate the convergence properties of iterative solvers. Consequently, we also demonstrate the quality of the preconditioner (4.27) for the solution of the system

$$\text{Find } u = \begin{pmatrix} u^c \\ u^s \end{pmatrix} \in \mathbb{R}^{2n}: \quad Ku = \begin{pmatrix} A & M \\ -M & A \end{pmatrix}\begin{pmatrix} u^c \\ u^s \end{pmatrix} = \begin{pmatrix} f^c \\ f^s \end{pmatrix}, \tag{4.25}$$

by numerical computations: We solve the non-symmetric linear system (4.25) by the quasi-minimal residual method (QMR) [17] with the preconditioner (4.27). Table 4.1 presents the number of steps needed to reach a relative accuracy $\epsilon = 10^{-6}$ for different parameter settings and dimensions of the finite element space.

All these examples are test cases of the shielding problem that is described in Section 6.3 on page 69. The parameter $\sigma_{Fe}$ denotes the conductivity in the iron plate (measured in $\frac{\mathrm{C}^2}{\mathrm{Nm}^2\mathrm{s}}$), $\epsilon$ refers to the regularization parameter – we use the conductivity $\epsilon \cdot \sigma_{Fe}$ for the non-conducting regions – and $\omega$ means the angular frequency $2\pi f$. In all these cases, the reluctivity $\nu$ is set to $\nu_{Fe} = \frac{1}{\mu_0\,\mu_{Fe}} = \frac{1}{4\pi\cdot 10^{-4}} \sim 8 \cdot 10^2\,\frac{\mathrm{m}}{\mathrm{H}}$ in the iron domain and to $\nu_0 = \frac{1}{\mu_0} = \frac{1}{4\pi\cdot 10^{-7}} \sim 8 \cdot 10^5\,\frac{\mathrm{m}}{\mathrm{H}}$ in the coil and the surrounding air.
As can be seen in Table 4.1, the number of QMR iterations is independent of both dimension of the FE-space and choices of the parameters.

| Parameters $n$ | 1627 | 4942 | 19407 | 44306 | 68363 | 105225 |
|---|---|---|---|---|---|---|
| $\sigma_{Fe} = 10^4$, $\epsilon = 10^{-7}$, $\omega = 10^2\pi$ | 10 | 10 | 12 | 12 | 12 | 12 |
| $\sigma_{Fe} = 10^5$, $\epsilon = 10^{-7}$, $\omega = 10^2\pi$ | 14 | 11 | 12 | 12 | 13 | 13 |
| $\sigma_{Fe} = 10^5$, $\epsilon = 10^{-7}$, $\omega = 10^3\pi$ | 16 | 14 | 14 | 14 | 14 | 14 |
| $\sigma_{Fe} = 10^5$, $\epsilon = 10^{-7}$, $\omega = 10^4\pi$ | 14 | 14 | 14 | 14 | 14 | 16 |
| $\sigma_{Fe} = 10^6$, $\epsilon = 10^{-7}$, $\omega = 10^3\pi$ | 14 | 14 | 14 | 14 | 14 | 16 |
| $\sigma_{Fe} = 10^6$, $\epsilon = 10^{-9}$, $\omega = 10^3\pi$ | 14 | 14 | 14 | 14 | 16 | 16 |
| $\sigma_{Fe} = 10^6$, $\epsilon = 10^{-11}$, $\omega = 10^3\pi$ | 15 | 15 | 14 | 14 | 14 | 14 |

Table 4.1: QMR steps for the solution of the linear problem, for different dimensions and parameter settings.

## 4.4 Newton's Method for the Solution of the Non-linear Problem

Newton's method and variants seem to be the most widely used iterative procedures for the solution of nonlinear problems. The widespread use of this technique is due to its fast convergence: Newton's method is locally superlinearly (or even quadratically) convergent.

### 4.4.1 Introduction

We briefly describe and motivate the general procedure before we turn to our special problem.

Assume we have two Banach spaces $X$ and $Y$ and a general nonlinear map $F : X \to Y$ that is Fréchet-differentiable (at least in some set $D \subset X$). We want to solve the nonlinear problem

$$F(x) = y, \tag{4.32}$$

for some $y \in Y$.
We denote the exact solution by $x^*$ and suppose that we have some approximation $x_k$. Since $F$ is Fréchet-differentiable, we know

$$F(x) = \underbrace{F(x_k) + F'(x_k)(x - x_k)}_{=:L(x)} + o(\|x - x_k\|).$$

Consequently, we expect to get a better approximation of the solution $x^*$ by solving

$$L(x_{k+1}) = y,$$

i.e. by the assignment

$$x_{k+1} = x_k + F'(x_k)^{-1}(y - F(x_k)). \tag{4.33}$$

The question whether and how fast the iterates $x_k$ converge to the solution $x^*$ is answered in the following lemma:

**Lemma 4.10 ([15]).** *Let $X$ and $Y$ be Banach spaces, let $D \subset X$ be non-empty and open. Suppose the map $F : D \to Y$ is Fréchet-differentiable in $D$, and let $x^* \in D$ be a solution of $F(x) = y$ with regular derivative $F'(x^*)$.*
*Then,*

- *if $F'$ is continuous in $x^*$, the Newton iteration*

$$x_{k+1} = x_k + F'(x_k)^{-1}(y - F(x_k)), \quad k = 0, 1, \ldots \tag{4.33}$$

  *is locally, i.e. for a sufficiently good initial guess $x_0$, superlinearly convergent.*

- *if there exists a constant $\gamma > 0$ such that*

$$\|F'(x) - F'(x^*)\| \leq \gamma \|x - x^*\|, \quad \forall\, x \in U(x^*) \subset D,$$

  *the Newton iteration* (4.33) *is locally quadratically convergent.*

### 4.4.2 The Fréchet Derivative

In order to implement Newton's method for the nonlinear multiharmonic eddy current problem (3.21), we need to calculate the Fréchet derivative of the operators $A$ and $M$ that are defined as follows (cf. (3.21)):

$$\langle A(\boldsymbol{u}), \boldsymbol{v}\rangle := \int_\Omega \boldsymbol{H}(\mathbf{curl}\,\boldsymbol{u}) \cdot \mathbf{curl}\,\boldsymbol{v}\,\mathrm{d}\boldsymbol{x}, \qquad \forall\, \boldsymbol{u}, \boldsymbol{v} \in \boldsymbol{H}_0(\mathbf{curl})^{N+1}, \tag{4.34}$$

$$\langle M\boldsymbol{u}, \boldsymbol{v}\rangle := \int_\Omega \omega\sigma_\epsilon \boldsymbol{D}\boldsymbol{u} \cdot \boldsymbol{v}\,\mathrm{d}\boldsymbol{x}, \qquad \forall\, \boldsymbol{u}, \boldsymbol{v} \in \boldsymbol{H}_0(\mathbf{curl})^{N+1}, \tag{4.35}$$

where an element $\boldsymbol{v} \in \boldsymbol{H}_0(\mathbf{curl})^{N+1}$ is a vector of Fourier coefficients $\boldsymbol{v} = (\boldsymbol{v}_1^c, \boldsymbol{v}_1^s, \boldsymbol{v}_3^c, \ldots \boldsymbol{v}_N^c, \boldsymbol{v}_N^s)^T$. Here $N$ is the (odd) number of harmonics, and the superscripts $c$ and $s$ indicate the coefficient of cosine and sine, respectively. $\boldsymbol{D}$ is the matrix defined in (3.20), i.e.

$$\boldsymbol{D} = \begin{pmatrix} 0 & 1 & & & \\ -1 & 0 & & & \\ & & \ddots & & \\ & & & 0 & N \\ & & & -N & 0 \end{pmatrix},$$

and $\boldsymbol{H}(\mathbf{curl}\,\boldsymbol{u})$ denotes the Fourier coefficients of the magnetic field $\boldsymbol{H}(\mathbf{curl}\,\boldsymbol{u}(t))$.

As in Chapter 3, we mean by $\boldsymbol{u}$ the vector of Fourier coefficients, and by $\boldsymbol{u}(t)$ the multiharmonic function that is determined by these coefficients. So we have, for example,

$$\mathbf{curl}\,\boldsymbol{u}(t) = \sum_l \left(\mathbf{curl}\,\boldsymbol{u}_l^c \cos(l\omega t) + \mathbf{curl}\,\boldsymbol{u}_l^s \sin(l\omega t)\right).$$

Additionally, we mention that the coefficients $\boldsymbol{H}(\mathbf{curl}\,\boldsymbol{u})$ can be calculated by Fourier transformation in the following way:

$$\boldsymbol{H}_k^c(\mathbf{curl}\,\boldsymbol{u}) = \frac{2}{T}\int_0^T \nu(|\mathbf{curl}\,\boldsymbol{u}(t)|) \cdot \mathbf{curl}\,\boldsymbol{u}(t) \cdot \cos(k\omega t)\,\mathrm{d}t, \tag{4.36}$$

$$\boldsymbol{H}_k^s(\mathbf{curl}\,\boldsymbol{u}) = \frac{2}{T}\int_0^T \nu(|\mathbf{curl}\,\boldsymbol{u}(t)|) \cdot \mathbf{curl}\,\boldsymbol{u}(t) \cdot \sin(k\omega t)\,\mathrm{d}t. \tag{4.37}$$

Now we turn to the calculation of the Fréchet derivative of the operators $A$ and $M$. This is easy for $M$ since it is a linear operator – the derivative is just $M$ again. For the nonlinear operator $A$, we first calculate the Gateaux differential:

$$\begin{aligned}\langle \delta_{\boldsymbol{w}} A(\boldsymbol{u}), \boldsymbol{v}\rangle &= \lim_{t\to 0} \frac{1}{t} \int_\Omega \left[\boldsymbol{H}(\mathbf{curl}\,(\boldsymbol{u}+t\boldsymbol{w})) - \boldsymbol{H}(\mathbf{curl}\,\boldsymbol{u})\right] \cdot \mathbf{curl}\,\boldsymbol{v}\,\mathrm{d}\boldsymbol{x} = \\ &= \int_\Omega \left[\frac{\partial \boldsymbol{H}}{\partial \boldsymbol{B}}(\mathbf{curl}\,\boldsymbol{u}) \cdot \mathbf{curl}\,\boldsymbol{w}\right] \cdot \mathbf{curl}\,\boldsymbol{v}\,\mathrm{d}\boldsymbol{x}. \end{aligned}\tag{4.38}$$

Remains to clarify what we mean by the derivative $\frac{\partial \boldsymbol{H}}{\partial \boldsymbol{B}}$:

$$\frac{\partial \boldsymbol{H}_k^c}{\partial \boldsymbol{B}_l^c}(\boldsymbol{B}) = \frac{\partial}{\partial \boldsymbol{B}_l^c}\left(\frac{2}{T}\int_0^T \underbrace{\nu(|\boldsymbol{B}(t)|)\boldsymbol{B}(t)}_{=\boldsymbol{H}(\boldsymbol{B}(t))} \cos(k\omega t)\,\mathrm{d}t\right) =$$

$$= \frac{2}{T}\int_0^T \frac{\partial \boldsymbol{H}(\boldsymbol{B}(t))}{\partial \boldsymbol{B}(t)} \cos(l\omega t)\cos(k\omega t)\,\mathrm{d}t = \tag{4.39a}$$

$$= \frac{2}{T}\int_0^T \left[\nu'(|\boldsymbol{B}(t)|)\frac{\boldsymbol{B}(t)\boldsymbol{B}(t)^T}{|\boldsymbol{B}(t)|} + \nu(|\boldsymbol{B}(t)|)\boldsymbol{I}\right] \cos(l\omega t)\cos(k\omega t)\,\mathrm{d}t, \tag{4.39b}$$

with the $3 \times 3$ - identity matrix $\boldsymbol{I}$. It should be mentioned that $\boldsymbol{B}(t)\boldsymbol{B}(t)^T$ is a $3 \times 3$ - matrix as well.
We remark that for points in time with $\boldsymbol{B}(t) = 0$, the derivative

$$\frac{\partial \boldsymbol{H}(\boldsymbol{B}(t))}{\partial \boldsymbol{B}(t)},$$

in (4.39a) actually reduces to

$$\lim_{|\boldsymbol{B}| \to 0} \frac{\boldsymbol{H}(|\boldsymbol{B}|) - \boldsymbol{H}(0)}{|\boldsymbol{B}| - 0} = \lim_{|\boldsymbol{B}| \to 0} \frac{\boldsymbol{H}(|\boldsymbol{B}|)}{|\boldsymbol{B}|} = \nu(0)\boldsymbol{I}.$$

So the integrand in the explicit calculation of the derivative (4.39b) is meant as $\nu(0)\boldsymbol{I}$ for $\boldsymbol{B}(t) = 0$.

Similarly, the other derivatives $\frac{\partial \boldsymbol{H}_k^c}{\partial \boldsymbol{B}_l^s}$, $\frac{\partial \boldsymbol{H}_k^s}{\partial \boldsymbol{B}_l^c}$ and $\frac{\partial \boldsymbol{H}_k^s}{\partial \boldsymbol{B}_l^s}$ can be calculated. Note that all of them exist, since the $\boldsymbol{B}$-$\boldsymbol{H}$-curve is differentiable.

*Example.* For better understanding what the complete matrix $\frac{\partial \boldsymbol{H}}{\partial \boldsymbol{B}}$ in (4.38) looks like, we quote the example of one harmonic. In this case we have

$$\boldsymbol{u} = (\boldsymbol{u}^c, \boldsymbol{u}^s)^T, \quad \boldsymbol{H} = (\boldsymbol{H}^c, \boldsymbol{H}^s)^T.$$

The derivative then is the matrix

$$\frac{\partial \boldsymbol{H}}{\partial \boldsymbol{B}}(\mathbf{curl}\,\boldsymbol{u}) = \begin{pmatrix} \frac{\partial \boldsymbol{H}^c}{\partial \boldsymbol{B}^c}(\mathbf{curl}\,\boldsymbol{u}) & \frac{\partial \boldsymbol{H}^c}{\partial \boldsymbol{B}^s}(\mathbf{curl}\,\boldsymbol{u}) \\ \frac{\partial \boldsymbol{H}^s}{\partial \boldsymbol{B}^c}(\mathbf{curl}\,\boldsymbol{u}) & \frac{\partial \boldsymbol{H}^s}{\partial \boldsymbol{B}^s}(\mathbf{curl}\,\boldsymbol{u}) \end{pmatrix},$$

with each of its entries being calculated as derived in (4.39).

Clearly, the Gateaux differential $\delta_{\boldsymbol{w}} A(\boldsymbol{u})$ (4.38) is linear and continuous in $\boldsymbol{w}$, so $A$ is Gateaux differentiable in $\boldsymbol{u}$ with Gateaux derivative $A'(\boldsymbol{u})$ defined by

$$A'(\boldsymbol{u})\boldsymbol{w} := \delta_{\boldsymbol{w}} A(\boldsymbol{u}). \tag{4.40}$$

Since the Gateaux derivative $A'(\boldsymbol{u})$ exists for all $\boldsymbol{u}$ and obviously is continuous in $\boldsymbol{u}$ ($\nu \in C^1$), $A'$ as defined in (4.40) is the Fréchet derivative.

**The algorithm** Recapitulating, the whole Newton iteration for the multiharmonic eddy current problem reads as follows:

> Let some initial solution $\boldsymbol{u}^0$ be given. This initial guess can be, for example, the solution of the linear problem, or – in the case of a multigrid iteration, see Chapter 5 – the prolongated solution of a coarser level.
>
> For $k = 0, 1, \ldots$

- Calculate the defect

$$D^k = F - (A(\boldsymbol{u}^k) + M\boldsymbol{u}^k) \quad \text{in} \ \left(\boldsymbol{H}_0(\mathbf{curl})^{N+1}\right)^*.$$

- Solve the variational problem

$$\left\langle \left(A'(\boldsymbol{u}^k) + M\right) \boldsymbol{w}^k, \boldsymbol{v}\right\rangle = \langle D^k, \boldsymbol{v}\rangle, \quad \forall\, \boldsymbol{v} \in \boldsymbol{H}_0(\mathbf{curl})^{N+1}, \qquad (4.41)$$

  where the operator $A'(\boldsymbol{u}^k)$ is defined as in (4.38) and (4.40).

- Obtain the new iterate

$$\boldsymbol{u}^{k+1} = \boldsymbol{u}^k + \boldsymbol{w}^k.$$

*Remark* 4.4. (1) We have quoted the algorithm for the continuous problem, i.e. before discretization. Of course, Newton's method could equally be stated for the discretized problem. As can easily be seen, finite element discretization after Newton linearization leads to the same problem as applying Newton's method to the discretized nonlinear problem.
(2) Since in practice we cannot guarantee that the initial guess is sufficiently close to the solution for the iteration to converge, we add a damping parameter:

$$\boldsymbol{u}^{k+1} = \boldsymbol{u}^k + \tau^k \boldsymbol{w}^k.$$

The parameter $\tau^k \in (0, 1]$ is determined by line search.
(3) As mentioned before (cf. Section 4.3), we actually solve a perturbed problem with conductivity $\epsilon > 0$ in the originally non-conducting regions. As a consequence, we can solve the linear problem (4.41) in the space $\boldsymbol{H}_0(\mathbf{curl})^{N+1}$ and do not have to restrict ourselves to the factor space of divergence-free functions.

# Chapter 5

# Multigrid

Multigrid methods are among the most efficient solvers for discretized partial differential equations. Their convergence speed does not deteriorate when the discretization is refined, whereas classical iterative methods slow down for decreasing mesh size. More precisely, their complexity is optimal – the computational work is proportional to the number of unknowns –, and furthermore the constant of proportionality is so small that other methods can hardly outperform the efficiency of multigrid algorithms.

The ideas of multigrid rely on the observation that low and high frequency parts of the error function should be treated by two different methods: Many classical iterative methods (e.g. damped Jacobi, Gauss-Seidel) have smoothing effects, i.e. quickly reduce the oscillating parts of the error. Low frequency components on the other hand can already be approximated well on coarser grids. So the essence of multigrid is *smoothing* and *coarse grid correction*.

In this chapter, we provide a short introduction to multigrid methods and point out the sufficient conditions for convergence of the two-grid iteration. Furthermore, we quote a result on convergence of the multigrid V-cycle. Thereafter, we describe smoothers for an $\boldsymbol{H}(\mathbf{curl})$-problem with Nédélec edge discretization and show that they satisfy the required smoothing property for convergence.

For further details on the topic, we refer to [10, 13, 22, 34, 51]. A short, comprehensive overview can also be found in [9]. The special case of multigrid methods for Maxwell's equations, to wit the correct choice of the smoother, is treated in [4] and [25].

## 5.1 Introduction to Multigrid Methods

### 5.1.1 Smoothing Effects of Classical Iterations

Many classical iterative methods for solving systems of linear equations

$$Au = f, \tag{5.1}$$

quickly reduce oscillating components of the error, but have problems when dealing with slowly varying functions. This rapid convergence with respect to the high frequencies is called *smoothing effect*, because the error is *smoother* after the iteration.

*Example.* In order to clarify what we mean by that, we consider the one-dimensional model problem

$$-u''(x) = f(x), \quad \text{in } (0,1), \qquad u(0) = u(1) = 0.$$

Let $A_l$ be the matrix arising from its discretization by finite differences on a uniform grid. $f_l$ is the discretization of $f(x)$.
Figure 5.1 shows the smoothing effect of the damped Jacobi iteration

$$u_l^{j+1} = u_l^j - \theta D_l^{-1}(A_l\, u_l^j - f_l), \tag{5.2}$$

for $\theta = \frac{1}{2}$, where $D_l$ is the diagonal of $A_l$. In the figure, $u_l$ denotes the exact discrete solution, and $u_l^j$ $(j = 0, 1, 2)$ are the iterates of the Jacobi iteration. The meaning of the function $u_l^3$, which signifies the result of the coarse-grid correction, will become clearer in the following paragraphs.

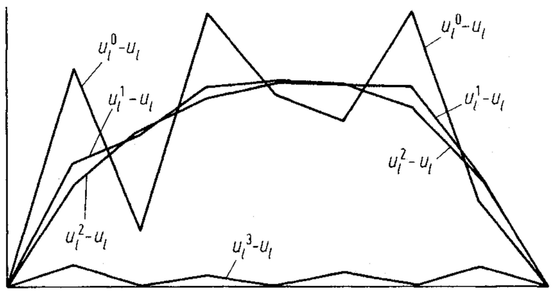


Figure 5.1: Smoothing effect of the damped Jacobi iteration.[1]

The figure plots the initial error $u_l^0 - u_l$ and illustrates the increasing smoothness of $u_l^j - u_l$ after $j = 0, 1, 2$ steps of the damped Jacobi iteration. Apparently, the error $u_l^2 - u_l$ is *smoother* than $u_l^0 - u_l$; therefore, the iteration (5.2) serves as a *smoothing iteration.*

### 5.1.2 Idea and Algorithm

The simple damped Jacobi iteration (5.2) reduces high-frequency components of the error quite efficiently. Convergence is only lacking with respect to smooth components. These, however, can be approximated well on a coarser grid, where the problem is easier to solve. This leads to the following idea:
Given some initial guess, apply some smoothing steps in order to damp oscillating components of the error. Then restrict the problem to a coarser grid and calculate the

[1]Source: W. Hackbusch, *Multi-Grid Methods and Applications* [22], page 20.

remaining smooth part. This information can now be used to update the approximate solution on the fine grid.

Although smoothing iteration and coarse-grid correction by themselves converge slowly or not at all, the combination of both components is rapidly convergent. Compare again Figure 5.1, where the fourth graph shows the error after coarse grid correction, $u_l^3 - u_l$, that has been significantly reduced by two smoothing steps and the coarse-grid correction.

Clearly, the system on the coarser grid is already easier to solve because of the smaller number of unknowns. However, in general the procedure of smoothing and restriction to a coarser grid is repeated recursively several times.

### The Algorithm

Finally we turn to the algorithm of a multigrid method with several levels. A precise formulation is easiest for conforming finite elements with nested grids.
We consider the problem

$$\text{Find } u \in V : \; a(u,v) = \langle F, v \rangle, \quad \forall\, v \in V, \tag{5.3}$$

for bilinear, continuous and elliptic $a(\cdot,\cdot)$, and discretize it by means of conforming finite elements.
Choose nested triangulations $\mathcal{T}_0, \mathcal{T}_1, \ldots \mathcal{T}_{l_{\max}}$ of the domain $\Omega$, where $\mathcal{T}_0$ is the coarsest and $\mathcal{T}_{l_{\max}}$ the finest grid. Let the finite element spaces $V_l$ correspond to the triangulations $\mathcal{T}_l$:

$$V_0 \subset V_1 \subset \ldots \subset V_{l_{\max}}. \tag{5.4}$$

The actual goal is the calculation of the finite element solution $u_l$ for the finest grid.

We denote the smoothing operator by $\mathcal{S}$, and the subscript $l$ always indicates the level number. The superscript $k$ is the iteration counter.

**Multigrid - Algorithm MGM$_l$** ($k$-th cycle at level $1 \le l \le l_{\max}$)

Let $u_l^k$ be a given approximation in $V_l$.

1. *Pre-smoothing.* Apply $\nu_1$ smoothing steps:

$$\bar{u}_l^k = \mathcal{S}^{\nu_1} u_l^k.$$

2. *Coarse-grid correction.* Let $w_{l-1}$ denote the solution of the defect problem on level $l-1$, i.e. of

$$a(w_{l-1}, v) = \langle F, v \rangle - a(\bar{u}_l^k, v), \quad \forall\, v \in V_{l-1}. \tag{5.5}$$

   - If $l = 1$, calculate the exact solution of (5.5), set $\hat{w}_{l-1} = w_{l-1}$.

- If $l > 1$, determine an approximation $\hat{w}_{l-1}$ of $w_{l-1}$ by applying $\mu$ steps of $\mathbf{MGM}_{l-1}$ with the initial value $u_{l-1}^0 = 0$.

Set

$$\tilde{u}_l^k = \bar{u}_l^k + \hat{w}_{l-1}. \tag{5.6}$$

3. *Post-smoothing.* Apply $\nu_2$ smoothing steps:

$$u_l^{k+1} = \mathcal{S}^{\nu_2} \tilde{u}_l^k.$$

*Remark* 5.1. (1) In the case of only 2 levels, the coarse-grid correction is always calculated exactly. With more than 2 levels, the solution on the coarse grid is determined only approximately, and in convergence theory a multigrid iteration is often treated as a perturbed two-grid iteration.
(2) The parameter $\mu$, which determines the effort for coarse-grid correction, is usually chosen to be 1 or 2. The case $\mu = 1$ is called V-cycle, $\mu = 2$ is the W-cycle.
(3) The multigrid iteration can of course be written in matrix-vector-form as well. For this task (and for the actual implementation) one needs restriction- and prolongation-matrices for the transition between $\mathbb{R}^{N_l}$ and $\mathbb{R}^{N_{l-1}}$, where $N_l$ and $N_{l-1}$ are the dimensions of $V_l$ and $V_{l-1}$, respectively.

### 5.1.3 Convergence of the Two-Grid Iteration

A multigrid iteration is called *convergent*, if the error is reduced by a factor $\rho < 1$ in each iteration cycle, and if $\rho$ is independent of the grid size $h$. The factor $\rho$ is called *contraction number*.

Many proofs of convergence have a very similar structure: They combine a *smoothing property*

$$\|\mathcal{S}^\nu v_l\|_X \leq c h^{-\beta} \frac{1}{\nu^\gamma} \|v_l\|_Y, \tag{5.7}$$

with an *approximation property*

$$\|v_l - v_{l-1}\|_Y \leq c h^\beta \|v_l\|_X, \tag{5.8}$$

where $v_{l-1}$ is the coarse-grid approximation of $v_l$, i.e. $v_{l-1}$ is the solution of

$$a(v_{l-1}, w) = a(v_l, w), \quad \forall\, w \in V_{l-1}.$$

The product of both factors then does not depend on the mesh size $h$ and is smaller than 1 for sufficiently large $\nu$.
These two properties lead to convergence in the norm $\|\cdot\|_Y$, as can be seen in the following theorem. For a specific problem, it remains to choose the norms $\|\cdot\|_X$ and $\|\cdot\|_Y$ and to show the properties (5.7) and (5.8).

**Theorem 5.1 ([9],[22]).** *Let $\mathcal{S}$ be a linear smoother with $\|\mathcal{S}\|_Y \leq 1$ and $\mathcal{S}u = u$ for the solution $u$, assume that the smoothing property* (5.7) *and the approximation property* (5.8) *are satisfied.*
*Then the two-grid iteration $\boldsymbol{MGM}_1$ is convergent in the norm $\|\cdot\|_Y$ for sufficiently large $\nu_1$, more precisely the estimate*

$$\|u_1^{k+1} - u_1\|_Y \leq \frac{c}{\nu_1}\|u_1^k - u_1\|_Y,$$

*holds, where $u_1$ is the exact solution on level $l = 1$, i.e. on the fine grid. Here $c$ is a constant independent of $h$, and $\nu_1$ is the number of pre-smoothing steps.*

For a proof of convergence in the case of more levels, the algorithm is mostly regarded as a two-grid iteration with non-exact, i.e. perturbed coarse-grid correction. Consequently, an additional requirement for this proof is an estimate of the magnitude of the perturbation.

### 5.1.4 Convergence of the Multigrid V-Cycle

For details on convergence of the general multigrid method, the reader is referred to one of the standard works [10, 13, 22, 51].
At this place, we only quote a result on convergence of the multigrid V-cycle that will be needed in Section 5.2 for the analysis of the smoothers for $\boldsymbol{H}(\mathbf{curl})$-problems.

Again, let $V_0 \subset V_1 \subset \ldots \subset V_{l_{\max}}$ be a sequence of nested finite element subspaces of the Hilbert space $V$ as in (5.4), and let $a(\cdot,\cdot)$ be a symmetric positive definite bilinear form. Our goal is to solve or precondition equation (5.3) by a multigrid iteration.

On each level $j$, we define the operator $A_j : V_j \to V_j$ by

$$(A_j u, v) = a(u, v), \quad \forall\, u, v \in V_j.$$

Equally we define $A : V \to V$ by the equation $(Au, v) = a(u, v)$.
Let $\mathcal{S}_j : V_j \to V_j$ denote the smoother on level $j$, and denominate the $a$-orthogonal projection onto $V_j$ by $P_j$, i.e. define $P_j : V \to V_j$ by the relation

$$a(u, v) = a(P_j u, v), \quad \forall\, u \in V, \forall\, v \in V_j. \tag{5.9}$$

We define $\Theta : V_{l_{\max}} \to V_{l_{\max}}$ by the standard multigrid V-cycle with $\nu$ pre- and post-smoothing steps. This means that in the multigrid algorithm $\mathbf{MGM}_{l_{\max}}$ (page 60) we choose $\nu_1 = \nu_2 = \nu$ and perform a V-cycle by the choice $\mu = 1$. Thus we have $\Theta = (I - M_{l_{\max}})A_{l_{\max}}^{-1}$ with the multigrid iteration operator $M_{l_{\max}}$.

With the above definitions, we have the following theorem on convergence of the V-cycle:

**Theorem 5.2 ([3, 4, 10]).** *Suppose that for each $j = 1, 2, \ldots, l_{\max}$, the smoother $\mathcal{S}_j$ is symmetric and positive semidefinite and satisfies the conditions*

$$a([I - \mathcal{S}_j A_j]v, v) \geq 0, \quad \forall\, v \in V_j, \tag{5.10}$$

*and*

$$(\mathcal{S}_j^{-1} v, v) \leq \alpha\, a(v, v), \quad \forall\, v \in (I - P_{j-1})V_j, \tag{5.11}$$

*for some constant $\alpha$. Then*

$$0 \leq a([I - \Theta A_{l_{\max}}]v, v) \leq \frac{\alpha}{\alpha + 2\nu} a(v, v), \quad \forall\, v \in V_{l_{\max}}. \tag{5.12}$$

This means that for $\nu \geq 1$ the multigrid V-cycle is convergent.

We remark that – although the assumptions of Theorem 5.2 do not exactly fit into the scheme presented by (5.7) and (5.8) – we have again a smoothing and an approximation property: Condition (5.11) describes the interaction between smoothing and coarse-grid correction, while condition (5.10) is a smoothing property.

## 5.2 A Multigrid Method designed for Problems in $\boldsymbol{H}(\mathbf{curl})$

Unfortunately, some of the simplest and most frequently used smoothers for elliptic problems do not yield efficient multigrid iterations when applied to the problem considered here. Compare Arnold, Falk and Winther [4], who note that this failure is due to a basic difference between the operator

$$\Lambda(\boldsymbol{u}, \boldsymbol{v}) = \rho^2 (\boldsymbol{u}, \boldsymbol{v})_{\boldsymbol{L}_2} + \kappa^2 (\mathbf{curl}\, \boldsymbol{u}, \mathbf{curl}\, \boldsymbol{v})_{\boldsymbol{L}_2}, \tag{5.13}$$

on the one hand and elliptic operators on the other: The point is that the eigenspace associated with the smallest eigenvalue of the operator $\Lambda$ contains many eigenfunctions which cannot be represented well on a coarse mesh. (For standard elliptic operators, however, low eigenvalue functions are always slowly varying.)
This property of $\Lambda$ follows from the fact that the operator reduces to the identity when applied to gradient fields (because $\mathbf{curl}\,\mathbf{grad}\,\phi = 0$, $\forall\,\phi$), although it behaves like a second order elliptic operator when applied to solenoidal, i.e. divergence-free vector fields. Hence, it is not surprising that the Helmholtz decomposition of an arbitrary vector field into irrotational and solenoidal components plays an important role in the understanding and analysis of this problem.

We mostly follow Arnold, Falk and Winther [4] in this section, who propose additive and multiplicative Schwarz smoothers based on a decomposition of the Nédélec edge space. They suggest to break down the finite element space into local patches consisting of all elements surrounding a vertex, or to use a decomposition arising from the Helmholtz decomposition, as is proposed by Hiptmair [25] as well.

### 5.2.1 Additive and Multiplicative Schwarz Smoothers

In order to obtain smoothers which satisfy the prerequisites of Theorem 5.2, we consider Schwarz smoothers. To describe these, we assume that for each level $j$, there exists a decomposition of $V_j$ into spaces $V_j^k \subset V_j$, such that each $v \in V_j$ can be written in the form

$$v = \sum_{k=1}^{K} v^k, \qquad \text{with } v^k \in V_j^k.$$

We denote the $a$-orthogonal projection onto the space $V_j^k$ by $P_j^k$, just as in (5.9). Now we can define the unscaled additive Schwarz smoother by

$$\mathcal{S}_j^a := \sum_{k=1}^{K} A_j^{-1} P_j^k, \tag{5.14}$$

and the smoother $\mathcal{S}_j := \eta\, \mathcal{S}_j^a$ for some scaling factor $\eta$.
Moreover, we denote the usual multiplicative Schwarz smoother associated with the spaces $V_j^k$ by $\mathcal{S}_j^m$. This means, for $f \in V_j$, $\mathcal{S}_j^m f$ is defined by the iteration

$$\begin{aligned} u^0 &= 0, && \\ u^k &= u^{k-1} + A_j^{-1} P_j^k (f - A_j u^{k-1}), && k = 1, \dots, K, \\ u^k &= u^{k-1} + A_j^{-1} P_j^{2K+1-k} (f - A_j u^{k-1}), && k = K+1, \dots, 2K, \\ \mathcal{S}_j^m f &= u^{2K}. && \end{aligned}$$

We have the following theorem, which gives conditions on the decompositions of the spaces $V_j$ under which the Schwarz smoothers fulfill the assumptions of Theorem 5.2 and consequently lead to a convergent multigrid iteration.

**Theorem 5.3 ([4]).** *Suppose that we have*

$$\sum_{k=1}^{K} \sum_{l=1}^{K} |a(u^k, v^l)| \le \left[\sum_{k=1}^{K} a(u^k, u^k)\right]^{\frac{1}{2}} \left[\sum_{l=1}^{K} a(v^l, v^l)\right]^{\frac{1}{2}}, \quad \forall u^k \in V_j^k, v^l \in V_j^l, \tag{5.15}$$

*and*

$$\inf_{\substack{v^k \in V_j^k \\ v = \sum v^k}} \sum_{k=1}^{K} a(v^k, v^k) \le \gamma\, a(v, v), \quad \forall\, v \in (I - P_{j-1}) V_j, \tag{5.16}$$

*for some constants $\beta > 0$, $\gamma > 0$. Then,*

- *if $\eta \le \frac{1}{\beta}$, the scaled additive smoothers $\mathcal{S}_j = \eta\, \mathcal{S}_j^a$ satisfy the hypotheses of Theorem (5.2) with $\alpha = \frac{\gamma}{\eta}$.*
- *the multiplicative smoothers $\mathcal{S}_j = \mathcal{S}_j^m$ satisfy the hypotheses of Theorem (5.2) with $\alpha = \beta^2 \gamma$.*

### 5.2.2 Decomposition of the Nédélec FE-Space

Eventually, we return to the $\boldsymbol{H}(\mathbf{curl})$-problem with the general bilinear form $\Lambda(\cdot,\cdot)$ as defined in (5.13). In this section we propose a decomposition of the spaces $\boldsymbol{V}_j$ in order to define the Schwarz smoothers.
For the moment, we consider a fixed level $j$. Suppose we have a triangulation $\mathcal{T}_j$ of the domain $\Omega$, and let the finite element space $\boldsymbol{V}_j$ be the Nédélec edge discretization of $\boldsymbol{H}(\mathbf{curl})$ as introduced in Section 4.2.

We denote by $\mathcal{V}_j$ and $\mathcal{E}_j$ the sets of vertices and edges of the mesh $\mathcal{T}_j$, respectively. For each vertex or edge $\nu \in \mathcal{V}_j \cup \mathcal{E}_j$, we define subdomains

$$\mathcal{T}_j^\nu := \{T \in \mathcal{T}_j : \nu \subset T\}, \quad \overline{\Omega_j^\nu} := \bigcup \mathcal{T}_j^\nu. \tag{5.17}$$

The splitting of $\Omega$ into subdomains $\Omega_j^\nu$ leads to a decomposition of the finite element space $\boldsymbol{V}_j$ in a natural way: Define

$$\boldsymbol{V}_j^\nu := \{\boldsymbol{v} \in \boldsymbol{V}_j : \operatorname{supp} \boldsymbol{v} \subset \overline{\Omega_j^\nu}\}, \quad \nu \in \mathcal{V}_j \cup \mathcal{E}_j. \tag{5.18}$$

By means of these subspaces $\boldsymbol{V}_j^\nu$ that are supported in a small patch of elements, we can decompose the space $\boldsymbol{V}_j$:

$$\boldsymbol{V}_j = \sum_{v \in \mathcal{V}_j} \boldsymbol{V}_j^v. \tag{5.19}$$

This decomposition of the finite element space was proposed by Arnold, Falk and Winther [4]; we will see in Lemma 5.4 that it defines an efficient Schwarz smoother.

A second possibility to decompose the space $\boldsymbol{V}_j$ into a sum of subspaces, which also leads to a convergent multigrid iteration, is due to Hiptmair [25]. For this second idea, which is inspired by the Helmholtz decomposition of a vector field into gradient fields and solenoidal components, we need to define another finite element space $W_j$ as the space of continuous piecewise polynomials. If $\boldsymbol{V}_j$ is the Nédélec edge discretization of index $k$, the elements of $W_j$ should be polynomials of degree at most $k+1$ in each element $T \in \mathcal{T}_j$.
As in (5.18), we define

$$W_j^v := \{\boldsymbol{v} \in W_j : \operatorname{supp} \boldsymbol{v} \subset \overline{\Omega_j^v}\}, \quad v \in \mathcal{V}_j. \tag{5.20}$$

We can then decompose the space $\boldsymbol{V}_j$ as follows:

$$\boldsymbol{V}_j = \sum_{e \in \mathcal{E}_j} \boldsymbol{V}_j^e + \sum_{v \in \mathcal{V}_j} \mathbf{grad}\, W_j^v. \tag{5.21}$$

In a triangulation by means of tetrahedra, no point belongs to more than six of the edge patches $\Omega_j^e$ or four of the vertex patches $\Omega_j^v$. Consequently, both of the proposed decompositions satisfy the condition (5.15) of Theorem 5.3 with $\beta$ independent of the mesh size $h_j$ and the parameters $\rho$ and $\kappa$ ($\beta$ never exceeds 10).
The following lemma states that both decompositions (5.19) and (5.21) also fulfill condition (5.16) and thus lead to an efficient multigrid algorithm. For this lemma we require only the bounded refinement hypothesis $h_{j-1} \le c\, h_j$.

**Lemma 5.4 ([4]).** *Assume that* $h_{j-1} \leq c\, h_j$ *and that* $\boldsymbol{v} \in (\boldsymbol{I} - \boldsymbol{P}_{j-1})\boldsymbol{V}_j$ *be given. Then there exists a decomposition* $\boldsymbol{v} = \sum_{v \in \mathcal{V}_j} \boldsymbol{v}^v$ *and a constant* $\gamma$ *depending on* $c$ *but independent of* $h_j$*,* $\rho$ *and* $\kappa$ *such that*

$$\sum_{v \in \mathcal{V}_j} \Lambda(\boldsymbol{v}^v, \boldsymbol{v}^v) \leq \gamma\, \Lambda(\boldsymbol{v}, \boldsymbol{v}).$$

*Similarly, a decomposition* $\boldsymbol{v} = \sum_{e \in \mathcal{E}_j} \boldsymbol{v}^e + \sum_{v \in \mathcal{V}_j} \mathbf{grad}\, w^v$ *and a constant* $\tilde{\gamma}$ *exist such that the estimate* (5.16) *is satisfied.*

We summarize this lemma and the preceding discussion in the following theorem.

**Theorem 5.5.** *Assume that we have* $h_{j-1} \leq c\, h_j$, $\forall\, j$ *for some* $c$ *independent of the level* $j$*.*
*Then for both decompositions of the finite element spaces* (5.19) *and* (5.21)*, the multiplicative and – for* $\eta \leq \frac{1}{10}$ *– the additive Schwarz smoother lead to convergent multigrid V-cycles.*

# Chapter 6

# Numerical Results

In this chapter we present results of simulations of diverse eddy current problems. We start with some notes on eddy current problems and on our implementation. Then we proceed with calculations on a comparatively simple problem, where we also present some results on the solution of the linearized problems and on convergence of the Newton iteration. Moreover, we compare low and high order approximation and we show the results for different numbers of harmonics in the multiharmonic ansatz.
Finally we turn to the challenging task of the eddy current welding problem in Section 6.4 and present the results of our simulation on this subject.

## 6.1 A Note on the Penetration Depth

A remarkable feature of eddy current problems is the fact that both magnetic field and eddy currents scarcely penetrate into conducting materials. The skin depth depends on permeability and conductivity of the material and on the frequency of the source current. This phenomenon is described by the following formula for the penetration depth, which gives the depth where the magnetic field will have declined to an $e^{-1}$-th of its original value, i.e. by more than 60 % (see e.g. [18], page 151):

$$\delta = \sqrt{\frac{2}{\omega\mu\sigma}}. \tag{6.1}$$

For usual ferromagnetic materials we face conductivities of approximately $\sigma \sim 10^6\,\frac{\mathrm{C}^2}{\mathrm{Nm}^2\mathrm{s}}$ and – at least for small inductions, where $\nu(|\boldsymbol{B}|) = \mu^{-1}(|\boldsymbol{H}|) \sim \mathrm{const}$ – permeabilities $\mu \sim 4\pi \cdot 10^{-4}\,\frac{\mathrm{H}}{\mathrm{m}}$. Already in the case of a frequency $f = 50$ Hz, i.e. $\omega = 100\pi$, this results in a penetration depth of

$$\delta \sim 0.00225\mathrm{m}.$$

This means that even for low frequencies we can observe the formation of a skin at the boundaries of conducting materials. The situation is even more dramatic for the problem of eddy current welding, where we usually are concerned with a source current of 200 kHz. In this case a skin of approximately $\delta \sim 0.0000356$ meters occurs, or even worse, since in the realistic setup we have a conductivity of $\sigma = 9.3 \cdot 10^6$, what leads to

$$\delta \sim 1.17 \cdot 10^{-5} \text{ m}.$$

As it is obviously necessary to mesh this skin adequately, we will have to face a substantial number of unknowns. However, we are able to keep their amount at an acceptable level by adaptive refinement of this small layer and by increasing the degree of the basis functions in the finite element space.
A two-dimensional sketch of a mesh in such a boundary layer is depicted in Figure 6.1.

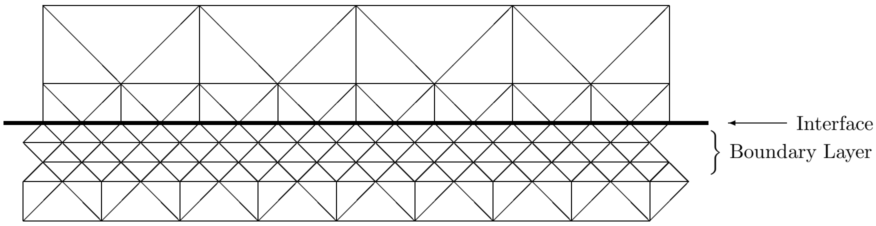


Figure 6.1: Sketch of adaptively refined mesh at a boundary layer.

## 6.2 Remarks Concerning Implementation

The mesh for discretization is generated by the Advancing Front Mesh Generator NETGEN [46] that has been developed at the University of Linz. The whole solver is implemented as an enhancement of the finite element solver NGSolve [47] (developed at the University of Linz as well).

As we have seen in Chapter 4, in each step of the Newton iteration a linear problem with system matrix $A'(\boldsymbol{u}) + M$ has to be solved. $A'(\boldsymbol{u})$ consists of entries

$$\frac{\partial \boldsymbol{H}_k^c}{\partial \boldsymbol{B}_l^c}(\mathbf{curl}\,\boldsymbol{u}) = \frac{2}{T}\int_0^T \frac{\partial \boldsymbol{H}(\mathbf{curl}\,\boldsymbol{u}(t))}{\partial \boldsymbol{B}(t)} \cos(l\omega t)\cos(k\omega t)\,\mathrm{d}t,$$

that have to be calculated for the assembly of the linearized matrix. We evaluate these integrals numerically by Simpson's integration rule, although a faster integration based on fast Fourier transformation could be envisaged. This, however, seems to be of secondary importance, since the solution of the linear systems is much more time consuming than their assembly.

The linearized problem in each Newton step is solved by a QMR iteration [17] which is preconditioned by a multigrid preconditioner. More precisely, we use the non-symmetric preconditioner that was proposed for the linear problem in (4.27). Obviously, this choice is suboptimal since the linearized matrices slightly differ from the linear system. For example, the $\nu'$-term

$$\frac{2}{T}\int_0^T \left[\nu'(|\boldsymbol{B}(t)|)\frac{\boldsymbol{B}(t)\boldsymbol{B}(t)^T}{|\boldsymbol{B}(t)|}\right]\cos(l\omega t)\cos(k\omega t)\,\mathrm{d}t, \tag{6.2}$$

is not considered in the preconditioner (4.27). Consequently, the QMR iteration for the solution of the linearized problems somewhat slows down. However, computations showed that the increase in the number of QMR steps is acceptable, cf. Table 6.1.

For the general procedure of solution, we apply a so-called *nested iteration* (cf. [22]). This means we start on the coarse grid and calculate an approximate solution $u_0$ of the nonlinear problem on this level. Then the mesh is refined adaptively and the prolongation of $u_0$ to the next level yields a good initial guess for $u_1$, the approximate solution on level 1. This algorithm is continued until a sufficiently fine level is reached. Since the approximations on the coarser grids are only used as initial guesses for the Newton iteration on the finer levels, it suffices to solve the corresponding problems with less accuracy. For instance, we have achieved good results for a relative accuracy $\epsilon_l = 10^{-2}\cdot 10^{-l}$ in the Newton iteration on level $l$. Other attempts such as $\epsilon_l = 10^{-3}$ for $l < l_{\max}$ and $\epsilon_{l_{\max}} = 10^{-8}$ seem even more promising.
We mention that the adaptive refinement is done by means of the Zinkiewicz-Zhu error estimator [58, 59]. In this context we additionally refer to other works on a-posteriori error estimation and adaptive refinement, e.g. [8, 53].

These remarks about QMR-convergence and nested iteration are concretized in the following section on the basis of numerical computations for several parameter settings. Moreover, we present results for different numbers of harmonics and different polynomial degrees of the basis functions.

## 6.3 A Shielding Problem

In this section, we analyze the efficiency of our solver at the example of a shielding problem, the geometry of which is depicted in Figure 6.2. For given current in the coil, we calculate the induction and the eddy currents in coil, iron plate and surrounding air. Here the iron plate works as a shield that hinders the magnetic field from entering the region behind it (or – for our geometrical layout – below the plate).
Unless mentioned otherwise, we use the following parameter setting: conductivity of the iron plate $\sigma_{Fe} = 10^6\frac{\mathrm{C}^2}{\mathrm{Nm}^2\mathrm{s}}$, in the rest of the domain $\sigma = \epsilon\cdot\sigma_{Fe}$ with $\epsilon = 10^{-9}$, frequency $f = 50$ Hz.
For the current in the coil, we use different values in order to obtain results with variable maximal induction $|\boldsymbol{B}|$. For reaching a saturated layer (i.e. a layer with $\nu(|\boldsymbol{B}|)\sim\nu_0$, what means $|\boldsymbol{B}|$ close to 2 Tesla), an extremely strong current of approximately $5\cdot 10^5$ Ampere is required. Since we are mainly interested in the influences of the nonlinearity, we mostly consider currents of this order of magnitude.

[1] In the figure, the domains are colored as follows: coil = red, iron = green, air = blue (transparent).

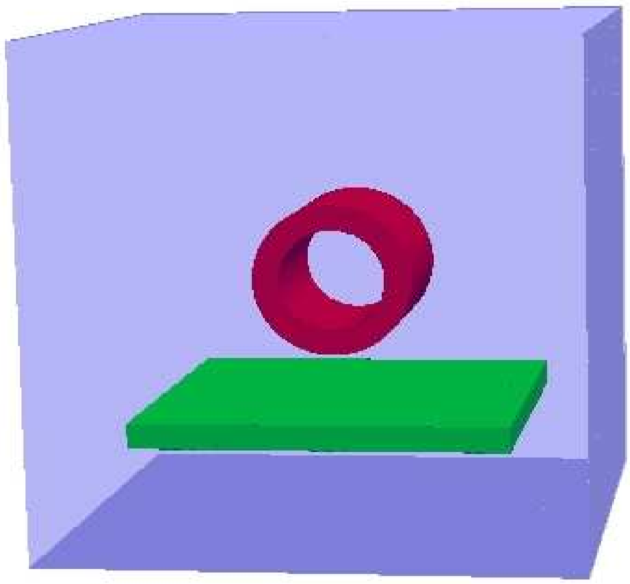

Figure 6.2: Geometry of the shielding problem.[1]

**Convergence of the QMR iteration** We have noted in the previous section that the preconditioner (4.27) for the QMR solver still has room for improvement, especially since we neglect the influence of the $\nu'$-term (6.2). However, our choice is justifiable, because the number of steps for the iterative solution of the linearized problems stays fairly small. Even when $\nu'$ reaches large values, i.e. for $|\boldsymbol{B}| \sim 1.5$ (cf. Figure 2.3 on page 15), we observe fairly good convergence properties of the QMR iteration. This fact is illustrated in Table 6.1, where we depict the number of steps needed to reach a relative accuracy of $\epsilon = 10^{-6}$ for three different meshes and various strength of the source current, i.e. for different induction in the solution.
The second column in the table shows the iterative solution of the linear problem, while the subsequent columns display the Newton iteration and the number of QMR steps for the solution of the linearized problems. In these columns we also quote the maximal induction $|\boldsymbol{B}|$ in the point of linearization, because this value reveals information about the impact of the nonlinearity.
The table demonstrates again that the iterative solution of the linear problem is not influenced neither by the dimension[2] nor by the right hand side. However, the number of steps for solving the Newton systems slightly depends on the induction $|\boldsymbol{B}|$ of the point of linearization.
Although in Table 6.1, we present results for the shielding problem with the aforesaid parameter setting, we remark that other examples and different choices of the parameters have shown similar QMR convergence.

[2]The number $n$ in Table 6.1 refers to the number of unknowns per Fourier coefficient. For the case of one harmonic, for instance, the dimension of the complete system would then be $2 \cdot n$, because we have the coefficients $\boldsymbol{u}_1^c, \boldsymbol{u}_1^s$.

| | | lin. | Newton 1 | 2 | 3 | 4 | 5 | 6 | 7 |
|---|---|---|---|---|---|---|---|---|---|
| $n = 44306.$ | Steps: | 14 | 18 | 16 | | | | | |
| | $\max \lvert \boldsymbol{B} \rvert$ | | 0.31 | 0.3 | | | | | |
| | Steps: | 14 | 21 | 19 | 17 | 17 | | | |
| | $\max \lvert \boldsymbol{B} \rvert$ | | 1.54 | 1.39 | 1.38 | 1.38 | | | |
| | Steps: | 14 | 65 | 34 | 33 | 32 | 31 | 31 | |
| | $\max \lvert \boldsymbol{B} \rvert$ | | 2.3 | 1.7 | 1.94 | 1.64 | 1.62 | 1.61 | |
| | Steps: | 14 | 125 | 48 | 54 | 49 | 47 | 40 | 38 |
| | $\max \lvert \boldsymbol{B} \rvert$ | | 2.76 | 1.72 | 2.39 | 1.77 | 1.76 | 1.76 | 1.76 |
| $n = 68363.$ | Steps: | 14 | 18 | 17 | | | | | |
| | $\max \lvert \boldsymbol{B} \rvert$ | | 0.44 | 0.41 | | | | | |
| | Steps: | 14 | 19 | 18 | 16 | | | | |
| | $\max \lvert \boldsymbol{B} \rvert$ | | 1.32 | 1.21 | 1.2 | | | | |
| | Steps: | 14 | 52 | 35 | 31 | 31 | 28 | 28 | |
| | $\max \lvert \boldsymbol{B} \rvert$ | | 2.2 | 1.65 | 1.73 | 1.69 | 1.68 | 1.68 | |
| | Steps: | 14 | 116 | 60 | 50 | 42 | 43 | 41 | 43 |
| | $\max \lvert \boldsymbol{B} \rvert$ | | 2.64 | 1.78 | 2.16 | 1.79 | 1.75 | 1.75 | 1.75 |
| $n = 105225.$ | Steps: | 14 | 18 | 18 | | | | | |
| | $\max \lvert \boldsymbol{B} \rvert$ | | 0.39 | 0.39 | | | | | |
| | Steps: | 14 | 19 | 19 | 17 | | | | |
| | $\max \lvert \boldsymbol{B} \rvert$ | | 1.38 | 1.33 | 1.33 | | | | |
| | Steps: | 14 | 42 | 28 | 28 | 27 | 27 | | |
| | $\max \lvert \boldsymbol{B} \rvert$ | | 1.97 | 1.69 | 1.68 | 1.67 | 1.67 | | |
| | Steps: | 14 | 86 | 47 | 45 | 38 | 40 | 40 | 35 |
| | $\max \lvert \boldsymbol{B} \rvert$ | | 2.37 | 1.74 | 2.11 | 1.77 | 1.74 | 1.74 | 1.74 |

Table 6.1: QMR steps for the solution of the linearized problems in the Newton iteration.

Moreover, we note that these results were achieved for only one harmonic. Since in the linear problem – and thus in the preconditioner – the harmonics are completely independent of each other, the results shown in Table 6.1 cannot be immediately transferred to the case of more modes. Given that the nonlinearity couples the different harmonics, one would expect the preconditioner to worsen, if we consider three or more modes in the multiharmonic ansatz. However, as long as the induction $|\boldsymbol{B}|$ stays small, the coupling between the modes is almost negligible. Consequently this case does not show any remarkable differences in QMR convergence for different numbers of modes. Anyhow, one can observe a minor slowdown in convergence when $|\boldsymbol{B}|$ and with it the influence of the nonlinearity increases. This pejoration is displayed in Table 6.2, where we present results of computations on a mesh with 44306 unknowns per Fourier coefficient (compare the first rows in Table 6.1) for three harmonics.

| | lin. | Newton 1 | 2 | 3 | 4 | 5 | 6 | 7 | 8 | 9 |
|---|---|---|---|---|---|---|---|---|---|---|
| Steps: | 14 | 18 | 18 | | | | | | | |
| $\max\lvert\boldsymbol{B}\rvert$ | | 0.3 | 0.3 | | | | | | | |
| Steps: | 14 | 26 | 19 | 21 | 21 | | | | | |
| $\max\lvert\boldsymbol{B}\rvert$ | | 1.54 | 1.37 | 1.36 | 1.36 | | | | | |
| Steps: | 14 | 95 | 57 | 43 | 37 | 35 | 30 | 30 | | |
| $\max\lvert\boldsymbol{B}\rvert$ | | 2.3 | 1.79 | 1.67 | 1.74 | 1.66 | 1.6 | 1.57 | | |
| Steps: | 14 | 198 | 100 | 82 | 62 | 67 | 65 | 60 | 61 | 50 |
| $\max\lvert\boldsymbol{B}\rvert$ | | 2.76 | 1.92 | 1.77 | 1.73 | 2.11 | 1.81 | 1.73 | 1.73 | 1.73 |

Table 6.2: QMR steps for the solution of the linearized problems, three harmonics.

**Multigrid preconditioner** In practice, we do not calculate the inverse of $(A+M)$ (cf. (4.27) on page 51) for the application of the preconditioner, but we approximate it by a multigrid V-cycle. Consequently, we have exact inversion only for the lowest order degrees of freedom on the coarse grid; the higher order degrees of freedom are not inverted in our implementation, but only smoothed. So for higher order and on finer levels, the non-symmetric preconditioner (4.27) is constructed by an approximation of $(A+M)^{-1}$ and thus might deteriorate.

For low order finite element spaces, the multigrid iteration yields a very good preconditioner

$$\tilde{C}_{MG}^{-1} \sim (A+M)^{-1}.$$

As a consequence, the QMR iteration with the non-symmetric preconditioner

$$C^{-1} = \frac{1}{2} \begin{pmatrix} \tilde{C}_{MG}^{-1} & 0 \\ 0 & \tilde{C}_{MG}^{-1} \end{pmatrix} \begin{pmatrix} I & I \\ I & -I \end{pmatrix}, \tag{4.27}$$

converges (almost) as fast as on the coarse grid. Unfortunately, in higher order FE-spaces already the multigrid preconditioner for the symmetric system degrades, and with it (4.27) as well.

Table 6.3 presents the number of QMR steps needed to reach a relative accuracy $\epsilon = 10^{-6}$ in the solution of the linear problem on some levels. These results were achieved for the shielding problem with a multigrid V-cycle with 3 pre- and post-smoothing steps.

The table shows iteration numbers for different parameter settings and various indices of the Nédélec finite element space, combined with the condition number of the symmetric preconditioned system $\kappa(\tilde{C}_{MG}^{-1}(A+M))$.

The abbreviations *t.1* and *t.2* in the first column of Table 6.3 refer to the linear Nédélec FE-space of type 1 and 2, respectively. Linear elements of *type 1* have exactly one degree of freedom per edge, namely the tangential component of a function along this edge. By *type 2* we mean the finite element space with linear basis functions that have two degrees of freedom per edge.

Since already for second order basis functions the quasi-minimal residual method converges fairly slowly, we mostly employ the linear Nédélec FE-space of type 2.

| Order | | Level 0 | Level 1 | Level 2 | Level 3 |
|---|---|---|---|---|---|
| **1 (t.1)** | (P1), Steps: | **15** [1] | **18** [1.15] | **16** [1.19] | **17** [1.31] |
| | $n =$ | 1627 | 12168 | 43343 | 81480 |
| | (P2), Steps: | **14** [1] | **16** [1.53] | **16** [1.42] | **18** [1.54] |
| | $n =$ | 1627 | 12255 | 43735 | 86545 |
| **1 (t.2)** | (P1), Steps: | **16** [1.28] | **17** [1.46] | **19** [1.52] | **24** [2.1] |
| | $n =$ | 3254 | 24568 | 82246 | 148404 |
| | (P2), Steps: | **18** [1.77] | **30** [2.29] | **32** [2.46] | **28** [2.49] |
| | $n =$ | 3254 | 24726 | 87412 | 166436 |
| **2** | (P1), Steps: | **71** [5.28] | **92** [7.81] | **108** [8.19] | **124** [8.18] |
| | $n =$ | 5244 | 41499 | 102330 | 111312 |
| | (P2), Steps: | **75** [6.18] | **86** [7.58] | **110** [7.57] | **145** [11.16] |
| | $n =$ | 5244 | 41499 | 102024 | 139632 |

Parameters: (P1) $\ldots \sigma_{Fe} = 10^6, \epsilon = 10^{-11}, \omega = 10^3\pi$
(P2) $\ldots \sigma_{Fe} = 10^5, \epsilon = 10^{-7}, \omega = 10^2\pi$

In square brackets []: $\kappa(\tilde{C}_{MG}^{-1}(A+M))$

Table 6.3: QMR steps for the solution of the linear problem, for different polynomial degree of the basis functions.

**Convergence of the Newton iteration** As mentioned previously, we solve the nonlinear problem iteratively by Newton's method. The convergence speed of this iteration obviously is influenced by the properties of the nonlinear reluctivity $\nu$. Since the relation between $\boldsymbol{B}$ and $\boldsymbol{H}$ is close to linear for small inductions $|\boldsymbol{B}|$ (cf. Figure 2.3), the iteration converges faster in this case. When the maximal induction in the solution approaches 2 Tesla, the method moderately slows down. Figure 6.3 shows the convergence of the iteration for different maximal $|\boldsymbol{B}|$ at the example of the shielding problem. The figure also shows that, even with strong influences of the nonlinearity, the Newton method converges very fast.

**Nested iteration** Actually, we are not interested in the solution on the coarser levels but only need them as an initial guess for the Newton iteration on the finest grid, plus for the adaptive refinement. Consequently, it seems excessive to solve the problem exactly on each level. In this context, different strategies of adaptive refinement can be considered – inexact solution on each of the coarse levels, while the fine level is solved more accurately, for example, or a consistent increase in accuracy after each refinement step. Another idea that crosses one's mind is to solve the linearized systems less exactly, since for achieving a Newton accuracy of $10^{-3}$, for instance, it is unnecessary to push the QMR iteration to a relative accuracy of $10^{-6}$.
In the following, we compare the strategies of nested iteration that are described in Table 6.4, where, when we proceed according to (S0), we do not use the prolongated solution of the coarser level as initial guess for the Newton iteration, but the solution

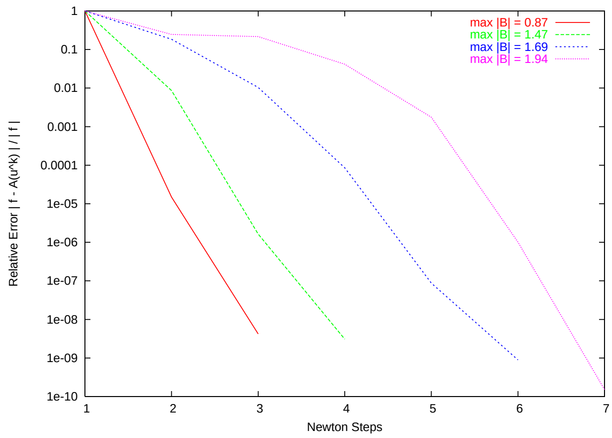


Figure 6.3: The Newton convergence depends on the maximal induction $|\boldsymbol{B}|$.

of the linear problem. So (S0) is actually not a nested iteration.

| Strategy: | Newton accuracy on level $l$ | QMR accuracy on level $l$ |
|---|---|---|
| (S0) non-nested | $\epsilon_l^N = \epsilon^N = 10^{-8}$ | $\epsilon_l^Q = \epsilon^Q = 10^{-6}$ |
| (S1) | $\epsilon_l^N = \epsilon^N = 10^{-8}$ | $\epsilon_l^Q = \epsilon^Q = 10^{-6}$ |
| (S1') | $\epsilon_l^N = \epsilon^N = 10^{-8}$ | $\epsilon_l^Q = \epsilon^Q = 10^{-4}$ |
| (S2) | $\epsilon_l^N = 10^{-2} \cdot 10^{-l}$, for $l < l_{\max}$, $\epsilon_{l_{\max}}^N = 10^{-8}$ | $\epsilon_l^Q = \max\{\epsilon_l^N, 10^{-6}\}$ |
| (S3) | $\epsilon_l^N = 10^{-3}$, for $l < l_{\max}$, $\epsilon_{l_{\max}}^N = 10^{-8}$ | $\epsilon_l^Q = \max\{\epsilon_l^N, 10^{-6}\}$ |
| (S4) | $\epsilon_0^N = 10^{-6}$, $\epsilon_l^N = 10^{-3}$, for $0 < l < l_{\max}$, $\epsilon_{l_{\max}}^N = 10^{-8}$ | $\epsilon_l^Q = \max\{\epsilon_l^N, 10^{-6}\}$ |

Table 6.4: Different strategies of nested iteration.

Table 6.5 compares the accumulated number of QMR iterations on each level together with the time needed for the solution. Again, we consider a current of $5 \cdot 10^5$ A in the coil, i.e. we observe a maximal induction $|\boldsymbol{B}| \sim 1.83$ T in the solution. Although this table presents results for one harmonic, we emphasize that we observe analogous results for a different number of modes. We remark that the computations which are shown in Table 6.5 are achieved by lowest order Nédélec edge discretization. Anyhow, even though the results for higher order basis functions differ slightly from those in the table, the general superiority of inexact solution on coarser levels is exactly the same.

For Table 6.5, we begin with a coarse grid with $n = 4942$ degrees of freedom, and then adaptively refine the mesh. The different strategies of nested iteration yield comparable sequences of grids – strategies (S0), (S1), (S1)', (S3) and (S4) yield $n = 31255$ on level 1, $n = 78665$ on level 2, $n = 91851$ on level 3 and finally with 92211 degrees of freedom on the finest mesh, level 4, while (S2) results in the sequence $n = 31264$ / 78631 / 91823 / 92013.

| **Strategy** $n =$ | **Level 0** 4942 | **Level 1** 31255 | **Level 2** 78665 | **Level 3** 91851 | **Level 4** 92013 | **Total Time** |
|---|---|---|---|---|---|---|
| (S0) | 46<br>14.32 s | 134<br>334.08 s | 630<br>3841.21 s | 638<br>6619.52 s | 619<br>9084.26 s | 19893.39 s |
| (S1) | 46<br>14.37 s | 131<br>346.15 s | 594<br>3651.97 s | 356<br>3727.81 s | 166<br>2468.43 s | 10208.73 s |
| (S1') | 34<br>12.28 s | 93<br>284.58 s | 442<br>2813.37 s | 235<br>2563.32 s | 105<br>1591.22 s | 7264.77 s |
| (S2) | 4<br>1.33 s | 44<br>167.82 s | 349<br>2229.77 s | 236<br>2543.37 s | 100<br>1490.21 s | 6432.5 s |
| (S3) | 17<br>6.43 s | 44<br>167.29 s | 240<br>1580.31 s | 90<br>1006.59 s | 174<br>2582.48 s | 5343.1 s |
| (S4) | 30<br>8.71 s | 44<br>166.8 s | 235<br>1535.77 s | 84<br>949.58 s | 172<br>2515.76 s | 5176.62 s |

Table 6.5: Total number of QMR steps per level and solution time for various strategies of nested iteration.[3]

The table impressively demonstrates the superiority of nested iterations over the non-nested strategy (S0), as well as the preeminence of procedures that solve less accurately on the coarser levels. A comparison of (S3), where we solve fairly inexactly on all the coarse levels, with the approach (S4) displays that more effort on the first comparably coarse grid pays off in the end.
In Figure 6.4, we compare the relative residuals $\frac{|f-A(u^k)|}{|f|}$ of the strategies (S1), (S2) and (S4). The plots show for example that – even for inexact solution of the linearized systems – we have superlinear convergence of the Newton iteration. Moreover, we observe that even for very exact solution, the relative residual grows considerably due to the prolongation.

**Number of harmonics needed for the multiharmonic ansatz** We have seen in Chapter 3 that the solution of the eddy current problem can be represented by means of a Fourier series. However, in the actual calculation we truncate this series

[3]The computations were done on an AMD$^{\text{TM}}$ Athlon$^{\text{TM}}$ CPU with 1800 MHz.

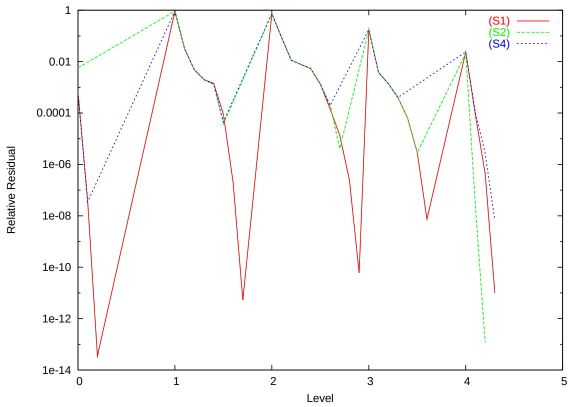


Figure 6.4: Relative residuals of three approaches of nested iteration.

and only consider the first few harmonics. Clearly, now the question arises how many harmonics we have to consider in the computations. For small inductions $|\boldsymbol{B}|$, the relation between $\boldsymbol{B}$ and $\boldsymbol{H}$ is close to linear, so we expect that in this case the base harmonic of the solution already contains significant information. For $|\boldsymbol{B}|$ approaching 2 Tesla in some part of the iron domain, the influence of the nonlinearity grows stronger and more harmonics are required. These thoughts are validated in Figure 6.5, where we depict the eddy current density

$$\int_{\Omega_{Fe}} \boldsymbol{E} \cdot \boldsymbol{J}_e \, \mathrm{d}\boldsymbol{x} = \int_{\Omega_{Fe}} \sigma \left| \frac{\partial \boldsymbol{u}(t)}{\partial t} \right|^2 \mathrm{d}\boldsymbol{x},$$

for different maximal induction $\max_{\boldsymbol{x},t} |\boldsymbol{B}|$ and for computation with seven harmonics, where in each case the influence of the different modes is plotted separately. We emphasize that the even harmonics are not needed in the calculation due to Theorem 3.2.

Figure 6.5 presents results for the shielding problem, but the general tendency can immediately be transferred to other examples, as we will see for example in Section 6.4.

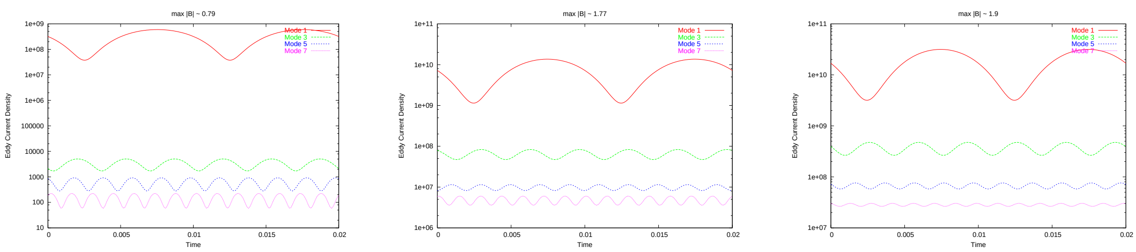


Figure 6.5: Eddy current density for different $\max |\boldsymbol{B}|$, analyzed by the first seven harmonics.[4]

[4]Note the logarithmic scale in the figures!

Especially in the right plot in Figure 6.5 the higher harmonics might seem to have great influence on the result. In order to emphasize that a small number of harmonics in the multiharmonic ansatz is sufficient, we present the results for computations with several numbers of modes in Figure 6.6. Here, the parts of each harmonic are not depicted separately as in Figure 6.5, but we show the eddy current density for various $N$ in the ansatz (3.18).

The figure conspicuously demonstrates that – even for strong influences of the non-linearity – very accurate results can actually be achieved with a small number of harmonics: 3 or 5 harmonics are often sufficient.

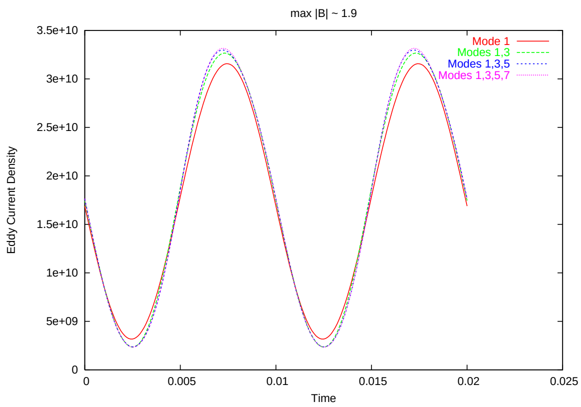


Figure 6.6: Eddy current density for different numbers of harmonics.

**Results** Finally, we present some results for the shielding problem, where we concentrate on changes in the parameter setting that imply various depths of the boundary layer.

In Figure 6.7, we show the eddy currents and their absolute value in a clipping plane, for time $t = 0$. We also present a zoom of the currents in the iron plate at this clipping plane in Figure 6.8. The result in both figures clearly demonstrates the boundary layer, which was mentioned in Section 6.1 – we observe strong eddy currents only in a small skin at the edge of the iron plate.

We remark that the results depicted in Figures 6.7 and 6.8 were achieved on a fine grid with 81750 edges and by Nédélec discretization of order 1, type 2, i.e. by a total amount of 163500 unknowns per Fourier coefficient.

It is worth mentioning that – as long as the boundary layer is properly discretized – a smaller number of unknowns is by far sufficient. Calculations on a comparatively coarse grid with only 11060 edges for the same Nédélec elements of order 1, type 2 have shown practically the same result. This is affirmed in the second picture in Figure 6.9, where we plot the absolute value of eddy currents for this FE-space with only 22120 unknowns per Fourier coefficient; there is practically no visible difference between this picture and Figure 6.7.

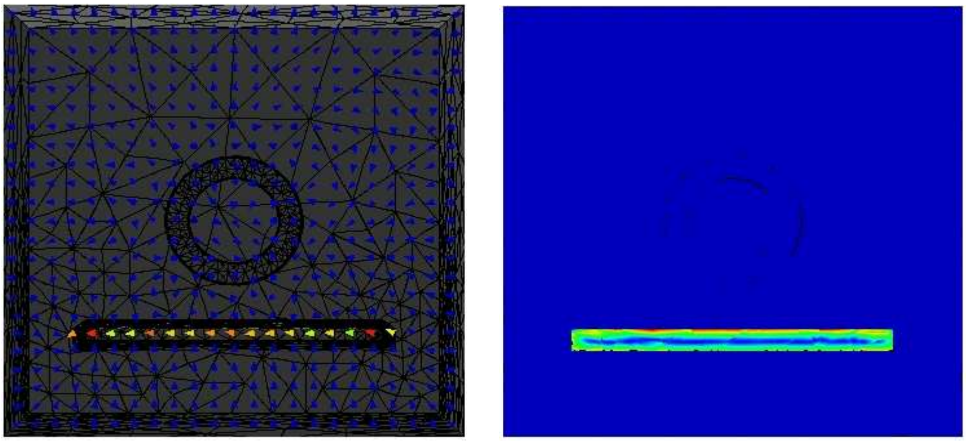

Figure 6.7: Eddy currents and their absolute value (at $t = 0$).

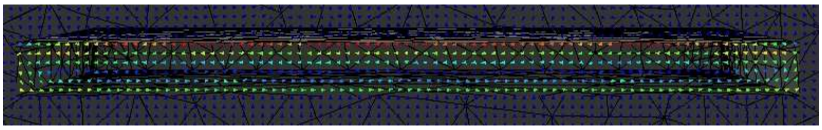

Figure 6.8: Eddy currents in a clipping plane, zoomed (at $t = 0$).

The computations for Figures 6.7 and 6.8 were done with the standard parameter setting $\sigma_{Fe} = 10^6$, $\epsilon = 10^{-9}$, frequency $f = 50$ Hz and a current of $5 \cdot 10^5$ A in the inductor. In the following, we show results for the same conductivity and current, but for different frequencies, what implies different thickness of the boundary layer.
Recall from the formula for the penetration depth (6.1) that an increase in the frequency decreases the skin depth. Figure 6.9 shows results for the frequencies $f = 12.5$ Hz, $f = 50$ Hz and $f = 200$ Hz. Since in the last case we multiply the frequency by 4 with respect to the original setup (Figure 6.7 and the central picture of Figure 6.9), we expect the layer to shrink to $\frac{1}{2}$ of the size that is depicted in the central image, while in the first picture we expect a doubling of the saturated layer. This effect can be observed quite conspicuously in Figure 6.9.
We should mention that the same current of $5 \cdot 10^5$ A generates eddy currents of different magnitude in dependence on the frequency: In Figure 6.7 and in the middle of Figure 6.9, the maximal value is $3.8 \cdot 10^6 \, \frac{\mathrm{A}}{\mathrm{m}^2}$, while in the right part of Figure 6.9, the scale reaches $1.5 \cdot 10^7 \, \frac{\mathrm{A}}{\mathrm{m}^2}$, and with a frequency of 12.5 Hz (left part of Figure 6.9), we observe eddy currents of $4.5 \cdot 10^5 \, \frac{\mathrm{A}}{\mathrm{m}^2}$ at the most.

## 6.4 Eddy Current Welding

In this section, we present the results of our computations on the eddy current welding problem, whose geometry has already been illustrated in Figure 2.1 on page 11. For this setup with the slitted iron tube, the eddy currents can only close around the tip

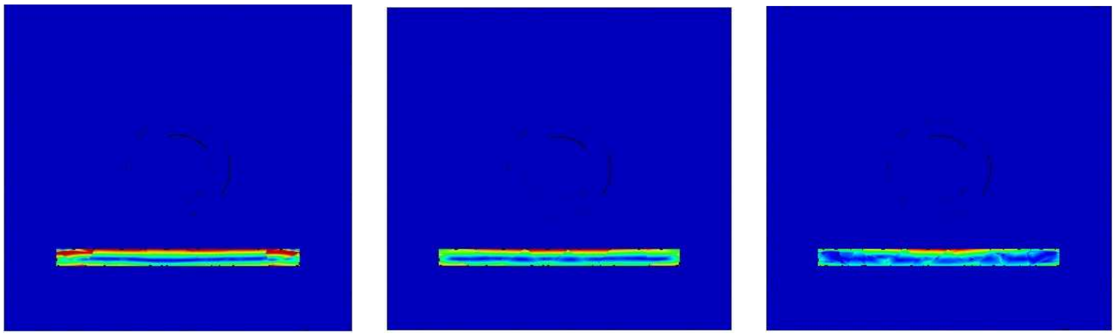

$f = 12.5$ Hz $f = 50$ Hz $f = 200$ Hz

Figure 6.9: Absolute value of eddy currents for various frequencies.

of the cut, where they considerably rise the temperature of the material.
As mentioned previously, the penetration depth is extremely small in the real life application – with a conductivity $\sigma = 9.3 \cdot 10^6$ and a frequency $f = 2 \cdot 10^5$ Hz, we face a skin depth of approximately $10^{-5}$ meters (cf. Section 6.1). Consequently, we expect to observe large currents only at the edges of the slit and around the tip of the cut.
In our calculations, we were able to solve the problem with the aforesaid realistic parameter setting; for the right hand side, we always consider a current of 2000 Ampere, which is used in the practical application as well.

Before illustrating our results by some figures, we underline that all the conclusions of Section 6.3 are equally valid for the welding problem – we observe analogous (or even better) convergence of the QMR iteration, for example. Furthermore, a nested nonlinear iteration that approximates the solution on intermediate levels only fairly inexactly seems best suited for this problem as well. As far as the number of harmonics is concerned, we conclude that three or five modes are sufficient, just as in the previous section.

For documenting these conclusions, we first present the number of QMR steps for the solution of the linearized problems in the Newton iteration, just as in Table 6.1 on page 71. The results are summarized in Table 6.6, where we also quote the maximal induction $|\boldsymbol{B}|$ in the respective point of linearization. We are interested in the maximal induction because it hints on the influence of the nonlinearity.
The computations for Table 6.6 were effectuated in a finite element space with $n = 73033$ degrees of freedom per Fourier coefficient, and for only one harmonic; we considered a relative accuracy of $\epsilon = 10^{-6}$ for the QMR iteration, just as in Table 6.1.

In contrast to Table 6.1, we observe in Table 6.6 that the preconditioned QMR iteration almost does not deteriorate even for large contributions of $\nu'$. This seemingly astonishing fact can be attributed to the higher frequency in eddy current welding problems: In conducting regions we have $\omega\sigma \sim 10^{13}$, while the reluctivity $\nu$ is bounded by $\nu_0 \sim 8 \cdot 10^5$ and – for the $\boldsymbol{B}$-$\boldsymbol{H}$-curve shown in Figure 2.3 – $\nu'$ is of the same order of magnitude. Consequently, the mass term (cf. (4.35))

$$\int_{\Omega} \omega \sigma_\epsilon \boldsymbol{D} \boldsymbol{u} \cdot \boldsymbol{v} \, \mathrm{d}\boldsymbol{x},$$

is dominant even for strong influences of the nonlinearity.

| | lin. | Newton 1 | Newton 2 | Newton 3 |
|---|---|---|---|---|
| Steps: | 18 | 18 | | |
| $\max \lvert \boldsymbol{B} \rvert$ | | 0.39 | | |
| Steps: | 18 | 18 | 16 | |
| $\max \lvert \boldsymbol{B} \rvert$ | | 1.55 | 1.55 | |
| Steps: | 18 | 18 | 16 | 16 |
| $\max \lvert \boldsymbol{B} \rvert$ | | 1.94 | 1.93 | 1.93 |
| Steps: | 18 | 17 | 18 | 18 |
| $\max \lvert \boldsymbol{B} \rvert$ | | 2.33 | 2.29 | 2.29 |

Table 6.6: QMR steps for the solution of the linearized problems in the Newton iteration.

The dominance of the mass term equally accelerates QMR convergence in the case of a larger number of harmonics in the multiharmonic ansatz. As mentioned in Section 6.3, the nonlinearity couples the different harmonics. Since in the preconditioner we neglect this coupling – remember that we use the preconditioner for the linear problem –, an increase in the number of QMR steps could be expected (cf. Table 6.2). However, in the realistic eddy current welding problem the dominant mass brings about fast convergence of the QMR iteration even in the case of several modes.
This statement is underlined in Table 6.7, where we present the number of QMR steps needed to reach a relative accuracy $\epsilon = 10^{-6}$ in the solution of the linearized problems, for the case of three harmonics. Computations for this table were effectuated in the same finite element space as for Table 6.6, i.e. with 73033 degrees of freedom per coefficient.

| | lin. | Newton 1 | Newton 2 | Newton 3 |
|---|---|---|---|---|
| Steps: | 18 | 18 | | |
| $\max \lvert \boldsymbol{B} \rvert$ | | 0.44 | | |
| Steps: | 18 | 18 | 18 | |
| $\max \lvert \boldsymbol{B} \rvert$ | | 1.09 | 1.08 | |
| Steps: | 18 | 20 | 20 | 20 |
| $\max \lvert \boldsymbol{B} \rvert$ | | 2.19 | 2.15 | 2.15 |

Table 6.7: QMR steps for the solution of the linearized problems, three harmonics.

In Table 6.8, we compare some strategies of nested iteration, just as in Table 6.5 on page 75. In this table, the accumulated number of QMR steps on each level together with the solution time is depicted for the strategies (S1), (S2), (S3) and (S4) (cf. Table 6.4). These results were achieved by computations on a coarse grid with $n = 9437$ degrees of freedom for the lowest order Nédélec edge discretization. Adaptive refinement then yields the same sequence of grids for all three strategies: $n = 40832$ on level 1, $n = 82279$ for level 2, and finally we have 181779 degrees of freedom on the finest mesh (level 3).

| **Strategy** $n =$ | **Level 0** 9437 | **Level 1** 40832 | **Level 2** 82279 | **Level 3** 181779 | **Total Time** |
|---|---|---|---|---|---|
| (S1) | 32<br>33.81 s | 105<br>541.76 s | 364<br>4154.2 s | 920<br>23562.26 s | 28292.03 s |
| (S2) | 6<br>5.51 s | 35<br>235.19 s | 232<br>2563.76 s | 778<br>18375.95 s | 21180.41 s |
| (S3) | 9<br>6.99 s | 37<br>241.2 s | 167<br>2035.57 s | 814<br>19116.48 s | 21400.24 s |
| (S4) | 32<br>33.76 s | 35<br>235.44 s | 188<br>2194.29 s | 862<br>20091.89 s | 22555.38 s |

Table 6.8: Total number of QMR steps per level and solution time for various strategies of nested iteration.[5]

Table 6.8 reveals that the choice of the optimal strategy of nested iteration is not obvious for the eddy current welding problem; however, we notice that procedures that solve less accurately on the coarser levels easily outperform the approach (S1). We remark that the relatively long time needed for solution on the finest grid is largely due to the huge difference between level 2 and 3. This rise in the number of unknowns brings about a suboptimal initial guess – we need some damped Newton steps in all strategies – and a pejoration of the multigrid preconditioner for the symmetric system. Consequently, some improvements of convergence are imaginable by a better adjustment of the adaptive refinement process, for example by an intermediate mesh of approximately 120000 degrees of freedom between level 2 ($n = 82279$) and 3 ($n = 181779$).

As in Section 6.3, we present a figure that analyzes the part of the different harmonics in the eddy current density (comparable to Figure 6.5), namely Figure 6.10. The results shown in this plot were achieved by computations with seven harmonics, and for a solution with maximal induction $|\boldsymbol{B}| \sim 1.73$ Tesla.
Similar to Figure 6.5, we observe in Figure 6.10 that the contribution of the higher harmonics to the total eddy current density is of some orders of magnitude smaller than the share of the base harmonic. For this example, the difference is even more explicit than in Figure 6.5.

[5]The computations were done on an AMD™ Athlon™ CPU with 1800 MHz.

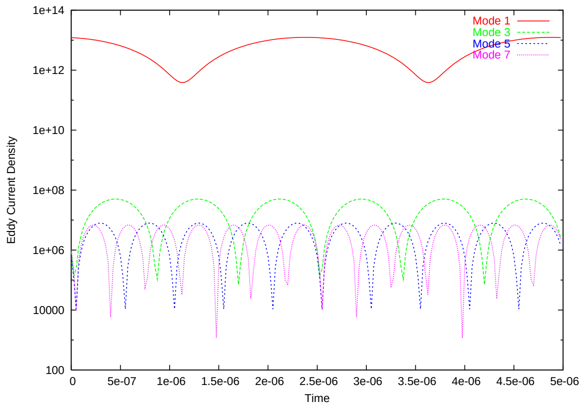


Figure 6.10: Eddy current density, analyzed by the first seven harmonics.

Now, we can finally manifest our results by some figures. In Figure 6.11 we show the absolute value of the eddy currents in a plane that clips the slitted tube, for the parameter setting mentioned previously. Due to the extremely small penetration depth, we present a zoom of the region close to the tip of the cut.
The figure depicts the currents for different time $t$, where $T$ indicates the length of the period, i.e. $T = \frac{1}{f} = 5 \cdot 10^{-6}$ s, since the frequency equals $f = 2 \cdot 10^5$ Hz.
Computations for this figure were done on a fine grid with 58907 edges, again with Nédélec discretization of order 1, type 2, i.e. with 117814 degrees of freedom per Fourier coefficient.

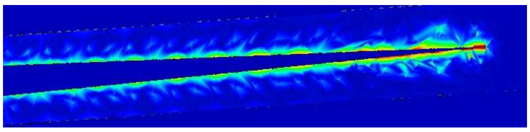

$t = 0.$

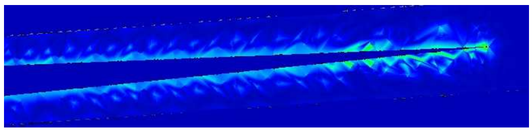

$t = \frac{T}{8}.$

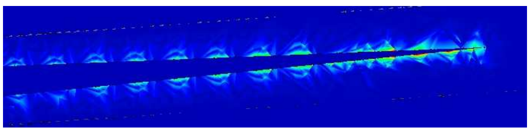

$t = \frac{T}{4}.$

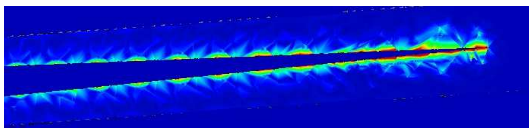

$t = \frac{3T}{8}.$

Figure 6.11: Absolute value of eddy currents in the slitted tube, for various $t$.

# Chapter 7

# Conclusions

This thesis covers the full range of mathematical problem solving at the example of eddy current welding: Starting from the electromagnetical problem formulation, we have rewritten the governing equations in the abstract mathematical framework and proven unique solvability of general eddy current problems in the subspace of divergence-free functions. This result was achieved by a combination of prior analysis for both conducting and non-conducting regions.

Then, taking into consideration that we are interested in a periodic steady state solution, we have presented the idea of Fourier series expansion, which reduces the originally time-dependent problem to a system of equations in space. Again, we have provided a proof of existence and uniqueness of such a periodic solution and have demonstrated some of its properties. In contrast to other authors who often prefer complex notation, we have chosen real Fourier coefficients and justified this choice by pointing out the difficulties that the complex problem entails.

These questions settled, we could finally apply the multiharmonic ansatz – a truncated Fourier series expansion – to the eddy current problem. The resulting system of PDEs was linearized by a Newton iteration and discretized by means of the finite element method.

In order to enforce unique solvability of the linear systems that arise in each step, we have introduced a regularization parameter, what allowed us to directly solve the variational problem instead of tackling the problem in the factor space of divergence-free functions or working with the mixed formulation. This procedure was vindicated by providing an estimate of the error that was incorporated by the perturbation.

For facilitating the faster solution of the linearized problems, a preconditioner was proposed and analyzed. The symmetric part of this preconditioner was realized by a multigrid iteration, wherefore some general results on multigrid convergence were quoted and the way to treat the peculiarities connected with electromagnetical problems was mentioned.

Finally, we have presented the results of our computations, where we were able to solve the challenging problem of eddy current welding with realistic geometry and parameters. In the extremely fine saturated layer, a sufficiently good approximation of the solution was achieved by adaptive refinement strategies.

As a matter of course, the work can still be continued into different directions. Some issues of further research are for example

- anisotropic meshing in the small layer of strong induction in order to reduce the number of unknowns even more,
- the theoretical analysis and implementation of multigrid methods for non-symmetric systems, what would accelerate the solution of the linearized problems,
- the possibility to choose higher polynomial degrees in the saturated layer than in other elements, what should again lower the total amount of unknowns,
- a complete analysis of the combined discretization error in the mesh size $h$ and the number of harmonics $N$ in the multiharmonic ansatz.

# Bibliography


[1] R. Adams. *Sobolev Spaces*, Academic Press, New York, 1975.

[2] C. Amrouche, C. Bernardi, M. Dauge, V. Girault. *Vector Potentials in three-dimensional nonsmooth domains*, Math. Meth. Appl. Sci. **21** (1998), pp. 823-864.

[3] D. N. Arnold, R. S. Falk, R. Winther. *Preconditioning in* $H(\mathrm{div})$ *and applications*, Math. Comp. **66** (1997), pp. 957-984.

[4] D. N. Arnold, R. S. Falk, R. Winther. *Multigrid in* $H(\mathrm{div})$ *and* $H(\mathrm{curl})$, Numer. Math. **85** (2000), pp. 197-218.

[5] I. Babuška, B. Q. Guo. *Approximation properties of the hp-version of the finite element method*, Comp. Meth. Appl. Mech. Engg. **133** (1996), pp. 319-346.

[6] I. Babuška, M. Suri. *The p- and hp-versions of the finite element method: an overview*, Comp. Meth. Appl. Mech. Engg. **80** (1990), pp. 5-26.

[7] F. Bachinger, M. Kaltenbacher, S. Reitzinger. *An Efficient Solution Strategy for the HBFE Method*, in: Proceedings of the IGTE '02 Symposium, Graz, Austria, 2002, pp. 385-389.

[8] R. Beck, R. Hiptmair, R. H. W. Hoppe, B. Wohlmuth. *Residual based a posteriori error estimators for eddy current computations*, M2AN Math. Model. Numer. Anal. **34** (2000), pp. 159-182.

[9] D. Braess. *Finite Elements: Theory, Fast Solvers and Applications in Solid Mechanics*, 2nd edition, Cambridge University Press, Cambridge, 2001.

[10] J. H. Bramble. *Multigrid Methods*, Longman, Harlow, 1995.

[11] S. C. Brenner, L. R. Scott. *The Mathematical Theory of Finite Element Methods*, Springer, New York, 2002.

[12] F. Brezzi. *On the existence, uniqueness and approximation of saddle-point problems arising from Lagrangian multipliers*, RAIRO Anal. Numér. **8** (1974), pp. 129-151.

[13] W. L. Briggs et al. *A Multigrid Tutorial*, Society for Industrial and Applied Mathematics (SIAM), Philadelphia, 2000.

[14] P. G. Ciarlet. *Basic Error Estimates for Elliptic Problems*, in: P. G. Ciarlet, J. L. Lions [eds]. *Handbook of Numerical Analysis II: Finite Element Methods (Part 1)*, North-Holland, Amsterdam, 1991.

[15] P. Deuflhard, G. Heindl. *Affine invariant convergence theorems for Newton's method and extensions to related methods*, SIAM J. Numer. Anal. **16** (1979), pp. 1-10.

[16] L. C. Evans. *Partial Differential Equations*, Graduate studies in mathematics, vol. 19, American Mathematical Society, Providence, Rhode Island, 1998.

[17] R. W. Freund, N. M. Nachtigal. *QMR: a quasi-minimal residual method for non-Hermitian linear systems*, Numer. Math. **60** (1991), pp. 315-339.

[18] N. Ida, P. A. Bastos. *Electromagnetics and Calculation of Fields*, Springer, New York, 1997.

[19] H. De Gersem, H. V. Sande, K. Hameyer. *Strong coupled multiharmonic finite element simulation package*, COMPEL **20** (2001), pp. 535-546.

[20] V. Girault, P.-A. Raviart. *Finite Element Methods for Navier-Stokes Equations, Theory and Algorithms*, Springer, Berlin, 1986.

[21] J. Gyselinck, P. Dular, C. Geuzaine, W. Legros. *Harmonic-Balance Finite-Element Modeling of Electromagnetic Devices: A Novel Approach*, IEEE Transactions on Magnetics **38** (2002), pp. 521-524.

[22] W. Hackbusch. *Multi-grid Methods and Applications*, Springer, Berlin, 2003.

[23] R. Hiptmair. *Multigrid Method for* $H(\mathrm{div})$ *in three dimensions*, Electronic Transactions in Numerical Analysis **6** (1997), pp. 133-152.

[24] R. Hiptmair. *Canonical Construction of Finite Elements*, Math. Comp. **68** (1999), pp. 1325-1346.

[25] R. Hiptmair. *Multigrid method for Maxwell's equations*, SIAM J. Numer. Anal. **36** (1999), pp. 204-225.

[26] B. Heise. *Analysis of a Fully Discrete Finite Element Method for a Nonlinear Magnetic Field Problem*, SIAM J. Numer. Anal. **31** (1994), no. 3, pp. 745-759.

[27] A. Jack, B. Mecrow. *Methods for magnetically nonlinear problems involving significant hysteresis and eddy currents*, IEEE Transactions on Magnetics **26** (1990), pp. 424-429.

[28] M. Jung, U. Langer. *Applications of multilevel methods to practical problems*, Surv. Math. Ind. **1** (1991), no. 3, pp. 217-257.

[29] M. Jung, U. Langer. *Methode der Finiten Elemente für Ingenieure*, Teubner, Stuttgart, 2001.

[30] M. Jung, U. Langer, A. Meyer, W. Queck, M. Schneider. *Multigrid preconditioners and their applications*, in: G. Telschow [ed.], *Third Multigrid Seminar (Biesenthal 1988)*, Karl-Weierstrass-Institut, Berlin, Report R-MATH-03/89, 1989, pp. 11-52.

[31] A. Kost. *Numerische Methoden in der Berechnung elektromagnetischer Felder*, Springer, Berlin, 1994.

[32] M. Kuhn. *Efficient Parallel Numerical Simulation of Magnetic Field Problems*, PhD thesis, Johannes Kepler University Linz, 1998.

[33] D. Lahaye. *Algebraic Multigrid for Two-Dimensional Time-Harmonic Magnetic Field Computations*, PhD thesis, Katholieke Universiteit Leuven - Faculteit Toegepaste Wetenschappen, Heverlee, 2001.

[34] S. F. McCormick [ed]. *Multigrid Methods*, Society for Industrial and Applied Mathematics (SIAM), Philadelphia, 1994.

[35] J. C. Nédélec. *A New Familiy of Mixed Finite Elements in* $\mathbb{R}^3$, Numer. Math. **50** (1986), pp. 57-81.

[36] J. T. Oden. *Optimal hp-Finite Element Methods*, Comp. Meth. Appl. Mech. Engg. **112** (1994), pp. 309-331.

[37] G. Paoli, O. Bíro, G. Buchgraber. *Complex representation in nonlinear time harmonic eddy current problems*, IEEE Transactions on Magnetics **34** (1998), pp. 2625-2628.

[38] S. Reitzinger. *Algebraic Multigrid Methods for Large Scale Finite Element Equations*, PhD thesis, Schriften der Johannes Kepler Universität Linz, Reihe C - Technik und Naturwissenschaften **36**, Universitätsverlag Rudolf Trauner, Linz, 2001.

[39] S. Reitzinger, B. Kaltenbacher, M. Kaltenbacher. *A Note on the Approximation of B-H Curves for Nonlinear Magnetic Field Computations*, Johannes Kepler Universität Linz, SFB “Numerical and Symbolic Scientific Computing”, SFB-Report No. 02-30, 2002.

[40] S. Reitzinger, U. Schreiber, U. von Rienen. *Algebraic Multigrid for Complex Symmetric Matrices: Numerical Studies*, Johannes Kepler Universität Linz, SFB “Numerical and Symbolic Scientific Computing”, SFB-Report No. 02-01, 2002.

[41] J. E. Roberts, J.-M. Thomas. *Mixed and Hybrid Methods*, in: P. G. Ciarlet, J. L. Lions [eds]. *Handbook of Numerical Analysis II: Finite Element Methods (Part 1)*, North-Holland, Amsterdam, 1991.

[42] M. Schinnerl. *Numerische Berechnung magneto-mechanischer Systeme mit Mehrgitterverfahren*, PhD thesis, Fortschritt-Berichte VDI Reihe 21 Nr. 308, VDI Verlag, Düsseldorf, 2001.

[43] J. Schöberl. *Robust Multigrid Methods for Parameter Dependent Problems*, PhD thesis, Johannes Kepler Universität Linz, 1999.

[44] J. Schöberl. *Multigrid methods for a parameter-dependent problem in primal variables*, Numer. Math. **84** (1999), pp. 97-119.

[45] J. Schöberl. *Commuting Quasi-Interpolation Operators for Mixed Finite Elements*, Preprint ISC-01-10-MATH, Texas A&M University, 2001.

[46] J. Schöberl. *NETGEN - An advancing front 2D/3D-mesh generator based on abstract rules*, Comput. Visual. Sci. **1** (1997), pp. 41-52.

[47] J. Schöberl. *NGSolve - 3D Finite Element Solver*, http://www.hpfem.jku.at/ngsolve/index.html

[48] C. Schwab. *p- and hp-Finite Element Methods, Theory and Applications in Solid and Fluid Mechanics*, Oxford University Press, Oxford, 1998.

[49] C. Schwab, M. Suri. *The p- and hp-version of the finite element method for problems with boundary layers*, Math. Comp. **65** (1996), pp. 1403-1429.

[50] G. Strang. *Variational crimes in the finite element method*, in: A. K. Aziz [ed]. *The Mathematical Foundations of the Finite Element Method with Applications to Partial Differential Equations*, Academic Press, New York, 1972.

[51] U. Trottenberg et al. *Multigrid*, Academic Press, San Diego, 2001.

[52] L. Vandevelde, J. Gyselinck, J. Melkebeek. *Steady-state finite element analysis in the frequeny domain of squirrel-cage induction motors*, in: Proceedings of the SPEEDAM '94 Symposium, Taormina, Italy, 1994, pp. 29-34.

[53] R. Verfürth. *A Review of A Posteriori Error Estimation and Adaptive Mesh-Refinement Techniques*, Wiley-Teubner, Chichester, 1996.

[54] S. Yamada, K. Bessho. *Harmonic field calculation by the combination of finite element analysis and harmonic balance method*, IEEE Transactions on Magnetics **24** (1988), pp. 2588-2590.

[55] S. Zaglmayr. *Eigenvalue Problems in SAW-Filter Simulations*, Diploma thesis, Johannes Kepler Universität Linz, 2002.

[56] E. Zeidler. *Nonlinear Functional Analysis and its Applications II/A: Linear Monotone Operators*, Springer, New York, 1990.

[57] E. Zeidler. *Nonlinear Functional Analysis and its Applications II/B: Nonlinear Monotone Operators*, Springer, New York, 1990.

[58] J. Z. Zhu, O. C. Zinkiewicz. *Adaptive techniques in the finite element method*, Commun. Appl. Numer. Methods **4** (1988), pp. 197-204.

[59] O. C. Zinkiewicz, J. Z. Zhu. *A simple error estimator for practical engineering analysis*, Int. J. Numer. Meth. Engg. **24** (1987), pp. 337-357.

# Eidesstattliche Erklärung

Ich, Florian Bachinger, erkläre an Eides statt, dass ich die vorliegende Diplomarbeit selbstständig und ohne fremde Hilfe verfasst, andere als die angegebenen Quellen und Hilfsmittel nicht benutzt bzw. die wörtlich oder sinngemäß entnommenen Stellen als solche kenntlich gemacht habe.

Linz, Oktober 2003

Florian Bachinger

# Curriculum Vitae

| | |
|---|---|
| **Name:** | Florian Bachinger |
| **Date of Birth:** | July 29, 1978 |
| **Place of Birth:** | Ried i. I., Austria |
| **Citizenship:** | Austria |

| | | |
|---|---|---|
| **Education:** | 1984 - 1988 | Elementary School in Taiskirchen |
| | 1988 - 1996 | Comprehensive Secondary School in Ried i. I. |
| | 1997 - 2003 | Studies of Applied Mathematics at the Johannes Kepler University Linz, Branch of study: Mathematics in Computer Sciences |
| | 09/1999 - 06/2000 | Studies at the Saint Petersburg State Technical University, Russia |

**Internships and Practical Experience:**

| | |
|---|---|
| 08/2000 - 09/2000 | Internship at the Instituto Nacional de Tecnología Industrial in Buenos Aires, Argentina |
| 07/2001 | Internship at Siemens Austria, Linz |
| 09/2001 | ECMI Modeling Week in Klagenfurt, Austria |
| 09/2002 | Internship at the Czech Technical University in Prague, Czech Republic |

**Alternative Service:** October 1996 - August 1997